JYU DISSERTATIONS 533

Shuai Shao

The Visualization and Analysis of Cell Polarity Based on Dynamic Fluorescence Images

UNIVERSITY OF JYVÄSKYLÄ
FACULTY OF INFORMATION TECHNOLOGY

JYU DISSERTATIONS 533

Shuai Shao

The Visualization and Analysis of Cell Polarity Based on Dynamic Fluorescence Images

Esitetään Jyväskylän yliopiston informaatioteknologian tiedekunnan suostumuksella
julkisesti tarkastettavaksi yliopiston vanhassa juhlasalissa S212
kesäkuun 2. päivänä 2022 kello 12.

Academic dissertation to be publicly discussed, by permission of
the Faculty of Information Technology of the University of Jyväskylä,
in Seminarium, auditorium S212, on June 2, 2022 at 12 o'clock noon.

JYVÄSKYLÄN YLIOPISTO
UNIVERSITY OF JYVÄSKYLÄ

JYVÄSKYLÄ 2022

Editors
Timo Tiihonen
Faculty of Information Technology, University of Jyväskylä
Ville Korkiakangas
Open Science Centre, University of Jyväskylä

ISBN 978-951-39-9314-6 (PDF)
URN:ISBN:978-951-39-9314-6
ISSN 2489-9003

Permanent link to this publication: http://urn.fi/URN:ISBN:978-951-39-9314-6

ABSTRACT

Shao, Shuai
The visualization and analysis of cell polarity based on dynamic fluorescence images
Jyväskylä: University of Jyväskylä, 2022, 69 p.
(JYU Dissertations
ISSN 2489-9003; 533)
ISBN 978-951-39-9314-6 (PDF)

Biosensors fused with fluorescent proteins can now track the dynamics of proteins and protein-protein interactions in living cells. The live-cell imaging with these biosensors enables monitoring cellular processes in real-time, opening possibilities to reveal hitherto hidden information about cellular processes if processing the images effectively.

This thesis develops methods to analyze dynamic fluorescence images for visualizing the cell polarity dynamics upon shear stress by pipelining the analysis to the preprocessing and the formal polarity analysis. The preprocessing section utilizes a two-step segmentation combining Otsu's method with a high-pass filter to rapidly obtain refined cell edge. It proposes a new algorithm based on k-means clustering to identify focal adhesions stably, which extracts the potential polarity regions accurately and reliably and reduces the defects due to human factors in the earlier methods. The polarity analysis section applies to different forms of polarity. It quantifies the analysis by normalizing the cell with zones to analyze the polarity distributed in the whole cell and defining upstream/downstream based on the incident angle between the cell edge and the external forcing to detect the polarity occurring on subcellular structures, enlarging the application range of cell polarity analysis. The analysis results show a pathway to sense and transduce the extracellular mechanical signals to intracellular force and transmit the force to the remote sites through membrane fluidity and cytoskeleton to activate signaling proteins and establish cell polarity.

In summary, the thesis considers polarity analysis based on dynamic fluorescence images as an independent issue for the first time, establishes an integrated pipeline to obtain polarity information at both cellular and subcellular scales, improves the accuracy and reliability of polarity analysis, and further provides an efficient tool to analyze different forms of polarity. It promotes the application of fluorescent proteins related techniques in exploring cellular processes, offers new insights to explain the establishment of cell polarity, and further advances how mechanotransduction occurs in cells.

Keywords: fluorescent protein, live-cell images, cell polarity, mechanotransduction, image processing

TIIVISTELMÄ (ABSTRACT IN FINNISH)

Shao, Shuai
Solujen polaarisuuden visualisointi ja analysointi fluoresenssikuvantamisen avulla
Jyväskylä: University of Jyväskylä, 2022, 69 p.
(JYU Dissertations
ISSN 2489-9003; 533)
ISBN 978-951-39-9314-6 (PDF)

Fluoresoituviin proteiineihin perustuvat biosensorit pystyvät seuraamaan elävän solun proteiinien dynamiikkaa. Tämä mahdollistaa solun sisäisten prosessien monitoroinnin ja avaa näkymiä tähän asti tuntemattomiin mekanismeihin, mikäli biosensorien signaaleja osataan tulkita luotettavasti.

Työssä kehitettiin menetelmiä soveltaa fluoresenssiin perustuvaa dynaamista kuvantamista solujen polarisoitumismekanismeihin. Menetelmiä kehitettiin sekä kuvien esikäsittelyyn että itse polarisoitumisdynamiikan tunnistamiseen. Esikäsittelyn tavoite on tunnistaa tarkasti solun reunat ja edelleen solun fokaaliset liitokset. Kuvat segmentoidaan Otsun menetelmällä, reunoja korostetaan ylipäästösuotimilla ja fokaaliset liitokset tunnistetaan K-means klusteroinnilla. Näin saadaan sekä solun muodosta että liitosten paikoista luotettavampi ja toistettavampi tieto kuin aiemmilla asiantuntijan silmämääräiseen arvioon perustuvilla menetelmillä. Polaarisuuden analyysimenetelmät perustuvat solujen vyöhykejakoon, jolla normalisoidaan solujen kokovaihtelu solujen sisäisessä polaarisuudessa. Solun reunalla puolestaan polaarisuus suhteutetaan solun reunan ja ulkoisen kuormituksen kohtauskulmaan, mikä mahdollistaa solujen muotovaihtelujen paremman huomioinnin. Menetelmien avulla voitiin tunnistaa, miten solut tunnistavat ulkoisen kuormituksen ja välittävät sen mekaanisesti ja biokemiallisesti solun eri osiin. Solukalvon joustavuuden ja sisäisen tukirangan osuudesta solun polaarisuudessa ja signaaliproteiinien aktivoinnissa saatiin näin uutta tietoa.

Yhteenvetona, työssä käsitellään ensimmäistä kertaa solun polaarisuuden analyysiä dynaamisen fluoresenssikuvauksen avulla omana tutkimusongelmanaan. Polaarisuuden havainnointiin kehitettiin menetelmäkokonaisuus, joka soveltuu sekä solutason että solun alarakenteiden polarisoitumismekanismien analyysiin, parantaa tarkkuutta ja luotettavuutta suhteessa aiempiin menetelmiin ja soveltuu niin solun sisäisen kuin solun pintarakenteisiin liittyvän polaarisuuden analysointiin. Työ tukee fluoresoituvien proteiinien hyödyntämistä solutason prosessien tutkimuksessa, lisää ymmärrystä solun polaarisuuden syntymekanismeista ja yleisemminkin mekaanisten voimien vaikutuksesta soluihin.

Avainsanat: fluoresoituvat proteiinit, solujen kuvantaminen, solujen polaarisuus, mekanotransduktio, kuvan käsittely

Author

Shuai Shao
Faculty of Information Technology
University of Jyväskylä
Finland

Supervisors

Bo Liu
School of Biomedical Engineering
Dalian University of Technology
China

Fengyu Cong
Faculty of Information Technology
University of Jyväskylä
Finland

Timo Tiihonen
Faculty of Information Technology
University of Jyväskylä
Finland

Tapani Ristaniemi
Faculty of Information Technology
University of Jyväskylä
Finland

Reviewers

Jin-Yu Shao
Department of Biomedical Engineering
Washington University in Saint Louis
USA

Yonggang Lv
Mechanobiology and Regenerative Medicine laboratory
Bioengineering College
Chongqing University
China

Opponent

Jussi Parkkinen
Faculty of Science and Forestry
University of Eastern Finland
Finland

ACKNOWLEDGEMENTS

It has been more than four years since I arrived in Finland and started my doctoral study in Jyväskylä. I still remember the first day I arrived in Finland. It was in November, so the temperature was very low, and it got dark early. Everything seemed different from my hometown. On the bus to Jyväskylä, the traveller I met told me that my destination was a quiet, clean and friendly city and my study in Jyväskylä would be a great experience. Now, I would like to say that it is really a fantastic journey in which there have been individuals who have helped me a lot. I thank all of you from the bottom of my heart.

First of all, I would like to extend my sincere gratitude to my supervisor, Prof. Bo Liu. I met Prof. Liu in the summer of 2012 when he arrived at Dalian University of Technology to start his new job, and I was experiencing my second year in college. Prof. Liu is humble and knowledgeable, and always gives me guidance patiently and constructively. He leads me in the way of doing research. It is an honour for me to study with him for such a long time. I also thank the valuable advice he gave to me sincerely when I was facing a crossroads in my life and had to make choices for myself.

I would like to express my sincere thanks to my supervisor Prof. Tapani Ristaniemi who gave me diligent guidance and general support in my study. It is really challenging for me to revisit the familiar work from an unfamiliar perspective due to that I majored in biomedical engineering during my bachelor's and master's studies, instead of information technology. Fortunately, Tapani discussed my study with me patiently and gave me inspiring suggestions, pulling me through the toughest phase of my study. This thesis is to memorize Prof. Tapani Ristaniemi for his help and encouragement to me.

Meanwhile, I wish to give special thanks to Prof. Timo Tiihonen, who is my supervisor at the end of my PhD study, for his enthusiastic support to me. Although he is not so familiar with the theme of my work and the time is constrained, he still discusses my work repeatedly with me and gives me constructive suggestions. These suggestions inspire me a lot and provide ideas for my future work.

I also would like to give my thanks to Prof. Fengyu Cong. I will never forget the day I received a phone call from him in Chongqing, asking if I would like to study in Finland for a doctoral degree. Also, with his help, I determined the theme of my doctoral study. Although his comments are sometimes harsh, he has always been ready to assist me.

Special thanks to the external reviewers of the thesis, Professor Jin-Yu Shao and Professor Yonggang Lv, and the opponent Professor Jussi Parkkinen. They devoted valuable time and effort to reviewing my thesis. Their comments and suggestions have helped me improve my thesis greatly.

Besides, I would like to thank Fei Xie, Sha Deng and Qingyun Jiang, who provided part of the data in this thesis, and my friend Ruijiao Dai, Rui Yan and many others who stand by my side and always support me. There are also many

friends online who listen to my distress and comfort me. I also would like to say thank you to them.

Finally, I would like to thank my parents. They support my decisions, tolerate my capriciousness, and never ask for anything in return. I love them so much.

Jyväskylä 16.5.2022
Shuai Shao

LIST OF ACRONYMS

ATP	Adenosine triphosphate
BA	Benzyl alcohol
BAECs	Benzyl alcohol
CHO	Cholesterol
CtyoD	Cytochalasin D
DAC	The distance to the cell centroid
DAE	The distances to the nearest edge
ECM	Extracellular matrix
ECs	Endothelial cells
FAK	Focal adhesion kinase
FAs	Focal adhesions
FPs	Fluorescent proteins
FRET	Fluorescence resonance energy transfer
GFP	Green fluorescent protein
ML-7	The myosin light chain kinase inhibitor
MSCs	Multipotent stromal cells
NOCO	Nocodazole
PAK1	P21-activated kinase 1
PBD	The p21-binding domain
RhoGDIα	Rho GDP-dissociation inhibitor α
ROI	Regions of interest
SNR	Signal-to-noise ratio

FIGURES

FIGURE 1 Schematic diagram for basic cell structure (organelles not shown) 16
FIGURE 2 Schematic representation for FRET 21
FIGURE 3 Possible errors in ROI chosen during cell deformation and migration, scale bar: 10 μm 32
FIGURE 4 System providing laminar flow or disturbed flow: (A) Whole system; (B) Flow chamber structure; (C) Vertical step structure .34
FIGURE 5 Polarized Rac activation by laminar flow: (A, B) Live-cell images, scale bar: 10 μm; (C) Spatiotemporal map of averaged single-cell images; (D) Laminar and disturbed flow logistic curves 39
FIGURE 6 Model of Rac activation under laminar flow and disturbed flow: (A) Static condition before applying shear stress; (B) Case of laminar flow; (C) Case of disturbed flow 40
FIGURE 7 Schematic sketch of image analysis, scale bar: 10 μm....42
FIGURE 8 Polar distribution of the affinity between RhoGDIα and Rho GTPases upon shear stress: (A) Live-cell images upon shear stress with drug treatment, Scale bar: 10 μm; (B) Distribution of affinity between RhoGDIα and Rho GTPases under shear stress; (C) Ratio of upstream and downstream averages of the control group and other drug treatment groups; (D) Effect of zone number on upstream and downstream measurements in the control group.43
FIGURE 9 Proposed mechanism of shear stress induced-RhoGDIα activation 44
FIGURE 10 Image processing of FAs segmentation and FRET ratio generation, scale bar: 20 μm 46
FIGURE 11 Tension across paxillin upon shear stress: (A) Live-cell images from ECFP channel of PaxTS biosensor under shear stress and the segmentation results (control group), scale bar: 20 μm; (B) Partial enlargement of Region 1 (R1) and Region 2 (R2) from (A), scale bar: 10 μm; (C) Time series of the FRET ratio of the control group....47
FIGURE 12 Tension across paxillin upon shear stress with different drug treatment: (A, B) Time series of FRET ratio of control group and drug treatment groups after normalization, scale bar: 20 μm; (C) Bar graph of the FRET ratio in control group and drug treatment groups after 10 min of shear stress; (D) Bar graph of the FRET ratio in the upstream and downstream regions of the control group and drug treatment groups....48
FIGURE 13 Process of FAs quantified analysis, scale bar: 20 μm 49
FIGURE 14 Cell body detection on a live-cell image, scale bar: 20 μm: (A) Detected cell body by the Otsu's threshold (*red*); (B) Refined cell body (*green*) 53

FIGURE 15 Clustering results with different clustering numbers: (A) Live-cell image, scale bar: 20 μm; (B) Clustering results with different clustering numbers (CN); (C) Number of identified FAs in the image and the mean fluorescence intensity at the FA sites 54

TABLES

TABLE 1 Overview of involved biosensors in the included articles.....35
TABLE 2 Overview of the drugs used in the included articles.....36
TABLE 3 Parameters from fitting curve in different groups.....38

CONTENTS

ABSTRACT
TIIVISTELMÄ (ABSTRACT IN FINNISH)
ACKNOWLEDGEMENTS
LIST OF ACRONYMS
FIGURES AND TABLES
CONTENTS
LIST OF INCLUDED ARTICLES

1 INTRODUCTION 15
1.1 Basic cell structures 15
1.1.1 Plasma membrane 16
1.1.2 Cell cytoskeleton 17
1.1.3 Organelles 18
1.2 Mechanical force and cell polarity 18
1.2.1 Cell polarity and cancer metastasis 19
1.2.2 Potential mechanism of cell polarity upon shear stress 19
1.3 Live-cell imaging with fluorescent protein 20
1.3.1 Fluorescent proteins 20
1.3.2 Fluorescence Resonance Energy Transfer 21
1.3.3 Dynamic fluorescence images 22
1.4 Goal and structure of the thesis 23

2 VISUALIZATION AND ANALYSIS OF CELL POLARITY 25
2.1 Preprocessing of fluorescence images 25
2.1.1 Improving the signal-to-noise ratio 26
2.1.2 Cell body detection 26
2.1.3 Focal adhesions identification 27
2.2 Generation of FRET index 28
2.3 Analysis of cell polarity 29
2.4 Research objectives 30
2.4.1 Detection of the cell body 30
2.4.2 Identification of FAs 30
2.4.3 Definition of upstream/downstream 31

3 OVERVIEW OF INCLUDED ARTICLES 33
3.1 Article I 36
3.2 Article II 40
3.3 Article III 44
3.4 Article IV 49

4 DISCUSSION 52
4.1 Contributions 52
4.1.1 Improvement of preprocessing 52

4.1.1.1 Refinement of the cell body 53
4.1.1.2 Identification of FAs 53
4.1.2 Quantitative definition of upstream/downstream 54
4.1.3 Biological contribution 55
4.2 Limitations and future research 56

5 CONCLUSION 58

YHTEENVETO (SUMMARY IN FINNISH) 59

REFERENCES 61

APPENDIX: IMPLEMENTATION OF OTSU'S METHOD 68

ORIGINAL PAPERS

LIST OF INCLUDED ARTICLES

I Shuai Shao, Cheng Xiang, Kairong Qin, Aziz Ur Rehman Aziz, Xiaoling Liao, and Bo Liu. 2017. "Visualizing the spatiotemporal map of Rac activation in bovine aortic endothelial cells under laminar and disturbed flows." *PLoS One* 12(11): e0189088; DOI: 10.1371/journal.pone.0189088.

II Shuai Shao, Xiaoling Liao, Fei Xie, Sha Deng, Xue Liu, Tapani Ristaniemi and Bo Liu. 2018. "FRET biosensor allows spatio-temporal observation of shear stress-induced polar RhoGDIα activation." *Communications Biology* 10(1):224; DOI: 10.1038/s42003-018-0232-2.

III Shuai Shao, Sha Deng, Qingyun Jiang, Hangyu Zhang, Zhengyao Zhang, Na Li, Fengyu Cong, Timo Tiihonen, and Bo Liu. 2021. "A DNA-encoded FRET biosensor for visualizing the tension across paxillin in living cells upon shear stress." *Analysis & Sensing* 1: e202100061; DOI: 10.1002/anse.202100061.

IV Shuai Shao, Sha Deng, Fengyu Cong, Timo Tiihonen, and Bo Liu. "Mapping the distribution of tension across paxillin upon shear stress with FRET-based biosensor." Submitted to *EMBO Journal*.

Author's contribution

Taking into account the suggestions and comments of co-authors, the author of this thesis made the following contributions to the attached four publications are listed as follows:

Article I: Shuai Shao analyzed the data under the guidance of Xiaoling Liao and Bo Liu; wrote the draft with Cheng Xiang, Kairong Qin, Aziz ur Rehman Aziz and Bo Liu; reviewed and edited the paper with Bo Liu.

Article II: Shuai Shao designed the research of this paper under the guidance of Bo Liu; performed research with Fei Xie and Sha Deng; analyzed data with the assistance of Bo Liu and Tapani Ristaniemi; wrote the draft with Xue Liu, Xiaoling Liao, Tapani Ristaniemi and Bo Liu; further reviewed and edited the paper with Bo Liu.

Article III: Shuai Shao analyzed the data under the guidance of Timo Tiihonen, Bo Liu and Fengyu Cong; wrote the draft with Hangyu Zhang, Zhengyao Zhang, Na Li and Bo Liu. Sha Deng and Bo Liu designed the research for this paper; Sha Deng and Qingyun Jiang performed the experiments.

Article IV: Shuai Shao analyzed the data under the guidance of Timo Tiihonen, Bo Liu and Fengyu Cong; wrote the draft with Bo Liu. Sha Deng and Bo Liu designed the research for this paper; Sha Deng performed the experiments.

1 INTRODUCTION

Cells are the basic structural and functional units of all living organisms, from bacteria to humans. Although cells may look widely different, they share similar cellular structures, functions, and properties. Many works prove that cells can respond to mechanical surroundings in function (Zalba & Ten Hagen, 2017). This chapter begins with a short overview of the essential cell structures, then discusses the effect of mechanical force on cells, and finally introudce to a new imaging technique to visualize the signaling events in live cells.

1.1 Basic cell structures

A cell is an individual unit that can give substance and energy to itself by metabolism, synthesize fundamental molecules of life, and replicate itself to produce generations depending on its structure. Generally, it is easy to think of a eukaryote as a house to understand the classic cell structure model. The plasma membrane is the wall of the house to separate the cell from the external environments, the cytoplasm fills the inside of the cell like the house full of air, and the organelles perform various jobs like furniture in the house. There also lies an intricate cytoskeleton network within the cytoplasm to keep the cell shape. These basic cell structures support the cell in performing its functions (Figure 1).

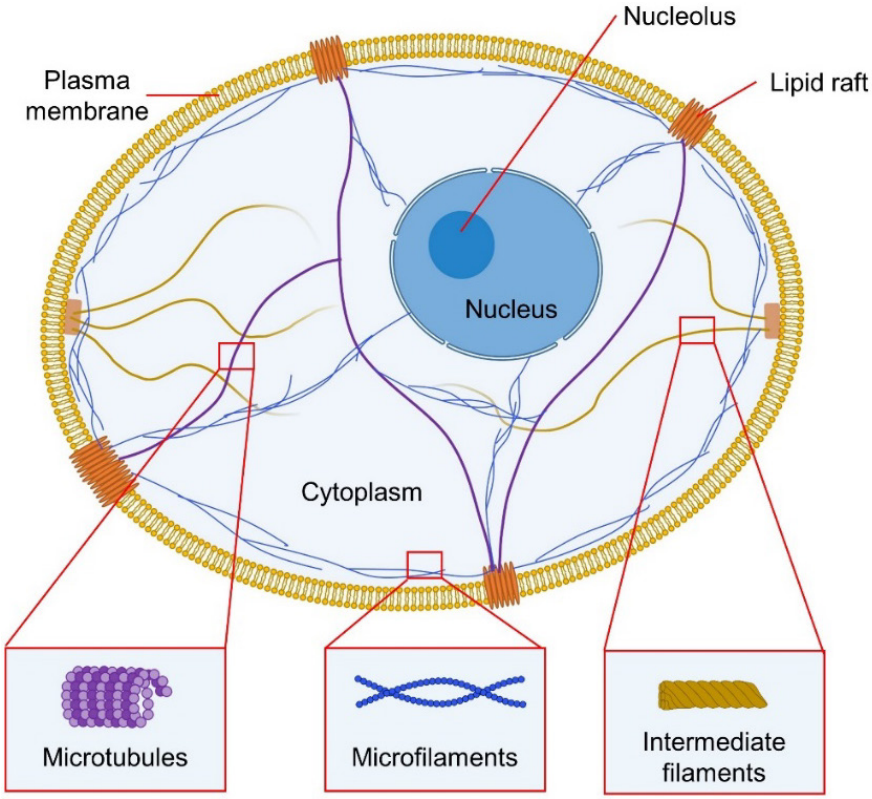

FIGURE 1 Schematic diagram for basic cell structure (organelles not shown)

1.1.1 Plasma membrane

The plasma membrane is a dynamic entity composed of lipids and proteins. It serves as the outer barrier to separate the cell from its external surrounding (Head et al., 2014) and is an essential structure for cells to communicate with their environments (Nicolson & Ferreira de Mattos, 2021; Singer & Nicolson, 1972). The fluid-mosaic model is the most accepted model to describe the membrane organization (Le Roux et al., 2019). In the model, the plasma membrane is described as a bilayer of lipids with some proteins embedding in. Lipids are in a liquid-disordered state at body temperature. Hence, the lipids can rotate, move laterally, and exchange between bilayers. This mobility of lipids provides the foundation for membrane fluidity affected by cholesterol and unsaturated lipids content. Unsaturated lipids can improve membrane fluidity, while cholesterol enrichment leads the fluidity to decrease (Zalba & Ten Hagen, 2017).

The proteins embedded in the membrane are related closely to the interaction between cells and the environment involving adhesion and signaling. The membrane proteins are organized nonrandomly and regulated by various membrane organizers. One of the membrane-organizers is lipid rafts which are microdomains presenting an enrichment in cholesterol and particularly saturated acyl lipids on the membrane (Head et al., 2014). The lipid rafts are highly dynamic structures interacting with the cytoskeleton, which contributes to lipid rafts and the cytoskeleton dynamics (Pralle, 2020; Suzuki et al., 2011).

1.1.2 Cell cytoskeleton

The cytoskeleton is a vital cell component showing high complexity and dynamics and participates in a large amount of fundamental cellular processes, such as cell shape and deformation, growth, migration, and division (Ruggiero & Lalli, 2021). The three primary functions carried by the cytoskeleton are organizing the contents in cells in space, establishing physical and biochemical connections between the cells and extracellular surroundings, and generating forces to coordinate the cell movement and deformation (Fletcher & Mullins, 2010; Gould et al., 2021). The three components of the cytoskeleton (actin, microtubules, and intermediate filaments) play different roles in the network.

Actins are the most dynamic component of the three cytoskeletal members and are present in two distinct states, the monomeric G-actin and the filamentous F-actin. Monomeric G-actin, whose full name is globular actin, can polymerize into filamentous F-actin (Hohmann & Dehghani, 2019; Sept et al., 1999). The balance between these two states is the key regulator of the modulation of the actin cytoskeleton (Rotty & Bear, 2014). The filamentous actin can be bundled with both parallel and anti-parallel orientation. Those parallel actin bundles usually exist in actin structures like filopodia. In contrast, the anti-parallel actin bundles mainly serve as a composition of stress fibers pulled by the myosin II motor to generate cell contractility. The various forms of actin are linked to a contractile network that is beneath the plasma membrane (actin cortex), linked to focal adhesions and runs across the cell (Hohmann & Dehghani, 2019). Focal adhesions are the sites where cells adhere to the substrate. Taken together, the actin filaments are closely associated with the cell movement, adhesions, and the maintaining and changing of cell shape.

Microtubules are hollow filaments formed by α- and β-tubulin heterodimers, displaying dynamic instability (Ohi & Zanic, 2016). The dynamic instability can be understood as a switch from growing to stopping and rapid depolymerization; finally, a new cycle begins (Ohi & Zanic, 2016). Microtubules connect to actin by some across-linkers physically and co-regulate with actin directly. However, microtubules are stiffer when compared to actin, which results in a higher magnitude of force (3-4 pN) generated during polymerization (Janson et al., 2003). In brief, microtubules are associated with actin from structure to function closely and, consequently, are usually considered as a coupled system.

Besides actin and microtubules, the third elastic component of the cytoskeleton is intermediate filaments which are grouped into five classes. Four of the five classes can be regarded as cytoplasmic intermediate filaments, while the fifth types are the nuclear filaments (Hohmann & Dehghani, 2019). From the view of the structure, the four types of cytoplasmic intermediate filaments mainly occur around the nucleus and reach the cortex to further communicate with subcellular structures, such as focal adhesions, to maintain the adhesions (Kreis et al., 2005; Tsuruta & Jones, 2003). In addition, intermediate filaments link to actin, microtubules, nuclear, and other intermediate filaments. This network structure of intermediate filaments anchoring different subcellular locations

provides a scaffold for organelles (Biskou et al., 2019; Matveeva et al., 2015; Nekrasova et al., 2011). Based on the structure and the property of elastic, intermediate filaments are considered mechanical buffers and anchors to organelle, playing essential roles in cell adhesion and migration (Hohmann & Dehghani, 2019).

1.1.3 Organelles

Besides the plasma membrane and cytoskeleton, there are also multiple organelles in cells. The cell *nucleus* is regarded as the largest and stiffest organelle to protect and organize the genetic material enclosed in the nucleus (Janota et al., 2020; Stephens et al., 2019). *Ribosomes* are in charge of protein synthesis (Emmott et al., 2019). They are attached to the *endoplasmic reticulum*, which plays a role in lipid metabolism and calcium storage besides protein synthesis (Schwarz & Blower, 2016). The newly synthesized proteins are trafficked, processed, and sorted on the *Golgi apparatus* (Kulkarni-Gosavi et al., 2019). Compared to these factories for producing and processing proteins, the *lysosome* works as a highly dynamic organelle dedicated to disposing and recycling cellular waste (Ballabio & Bonifacino, 2020). *Mitochondria* supply adenosine triphosphate (ATP) as energy for all the cellular needs and function in many biochemical processes (Roger et al., 2017). There is also *chloroplast* in plant cells which serves as a metabolic factory to provide fuels for the life of cells (Kirchhoff, 2019).

1.2 Mechanical force and cell polarity

As the minimum units in our bodies, cells experience mechanical stimuli every moment. Mechanical stimuli are closely related to several physiologies closely (Tschumperlin, 2011), such as the morphogenesis and physiology of the vascular system (Garoffolo & Pesce, 2021), the shaping of bones (Uda et al., 2017), and even our hearing, touch, and breath (Martinac & Poole, 2018). The ability of cells to respond to mechanical stimulation specifically is called mechanosensitivity, a common property shared by the cells and hard to be explained only by several mechanosensors (Orr et al., 2006). The mechanical stimulation to which cells are exposed contains multiple extrinsic mechanical forces and affects cells differently (Steward & Kelly, 2015). For example, fluid flow applies shear stress to cells, which plays an important role in the signaling pathways related to cytoskeleton, the cytoskeletal stress and reorganization, and focal adhesions (FAs) remodeling (Verma et al., 2015). In these abundant physiological processes based on mechanosensitivity, the abnormal responses of cells to mechanical force will lead to various diseases, especially cancers (Panciera et al., 2017). A considerable feature of cancer cells is the abnormality of cell polarity.

1.2.1 Cell polarity and cancer metastasis

The cancer cells break away from the primary focus by migration and adhere to other organs through blood, lymph, and extravasate. Hence, cell migration is a vital stage and the precondition to cancer invasion and metastasis (Duff & Long, 2017; Trepat et al., 2012; Zanotelli et al., 2021). Generally, the cancer cells experience various mechanical forces directly during the migration.

The cycle of cell migration contains multiple processes. Firstly, the stimuli induce the intracellular factors related to migration to establish an asymmetric distribution in space; and then, the lamellipodia extend at the leading edge of the cell along the migration direction and adhere to forward ECM; finally, the cell body migrates, and the trailing edge is pulled to dissociate from ECM. During this process, the asymmetric distribution of factors relevant to migration (e.g., proteins, organelles, and cytoskeleton) is known as cell polarity. Cell polarity is usually front-to-back to migrating cells. However, apical-basal polarity also exists in epithelial cells, which is caused by the interactions between cells and cells and cells to ECM (Piroli et al., 2019).

The metastasis of cancer cells is a kind of abnormal migration for which the loss of epithelial polarity is considered an essential requirement. As mentioned above, the target of metastasis is establishing a new focus at a remote site. The epithelial polarity loses from the cell-cell junction and the front-to-back polarity recovers subsequently (Yang et al., 2004). Researchers have found that many polarity genes are amplified in cancers (e.g., PARD6B, SCRIB, PRKCI, Dlgs, and Lgls), supporting the point that the related polarity proteins promote cancer development (Katoh, 2005).

1.2.2 Potential mechanism of cell polarity upon shear stress

Since cell polarity is so essential to understanding the mechanism of cancer development, a large number of studies have been focusing on it. There are signaling proteins comprising Rho family GTPases with their downstream and upstream effectors to construct polarity in the leading edge of migrating cells and are influenced by mechanical force, especially shear stress applied by fluid flow (Collins & Tzima, 2014; Nelson, 2009). For instance, Rac, a member of Rho family GTPases, is activated locally at the downstream regions along the direction of shear stress (Kraynov et al., 2000). As another member of the Rho family GTPases, Cdc42 shows polarity with a preferential activation downstream relative to the shear stress direction (Tzima et al., 2003). In addition, the activation of proteins related to Rho signaling pathways, including Src and focal adhesion kinase (FAK), also occurs in a directionally polarized manner upon shear stress (Liu et al., 2014). This case questions how mechanical force is transduced into biological signals in cells.

To answer this question, the previous studies provide a view. The intracellular signaling proteins are activated by the responses of stress-sensitive structures on the plasma membrane (e.g., integrins, G Protein-Coupled Receptors, and ion channels) to mechanical signals since the stress is applied to the plasma

membrane first. In brief, mechanotransduction begins on the plasma membrane with physical force. Then, the mechanical signals are transduced into biological signals and participate in different signaling pathways, further affecting the expression of genes and proteins. The assumed mechanism is adequate to explain the cell function changes induced by mechanical force in most cases. However, it is insufficient in cell polarity during the direct migration. The experimental evidence indicates that the establishment of cell polarity upon shear stress is more rapid than the translocation of diffusive molecules in the cytoplasm from the locations on which the local force acts to the remote sites (Na et al., 2008; Poh et al., 2009). Therefore, some researchers propose a new assumption considering the cell polarity induced by mechanical factors due to direct force transmission. In this assumption, a force-cell interface (e.g., FAs) and a tensed cytoskeleton are essential in the model to describe the underlying mechanism of rapid mechanotransduction. The mechanical force can be sensed on the force-cell interface and propagated much further in the cytoskeleton, which causes long-distance deformation at remote sites to activate signaling proteins for transduction (Chowdhury et al., 2021; Na et al., 2008). There is accumulating experimental data to support the assumption. However, the details of the underlying mechanism of mechanotransduction are still not clear at present.

1.3 Live-cell imaging with fluorescent protein

As mentioned in the last section, understanding mechanosensitivity and mechanotransduction is crucial to finding out the nosogenesis of cancer. For decades, researchers have been obtaining knowledge on mechanobiology via traditional biochemical methods, such as western blotting based on the lysate of a great collection of cells and immunofluorescence with fixed cells. However, those methods have their shortcomings. It is difficult to detect some low abundant or substantial molecular or post-translation modified proteins in western blotting (Mishra et al., 2017). The fixation and immunostain in immunofluorescence kill the cell, making the dynamic observation in the same living cell impossible.

In recent years, a new approach combining fluorescent proteins (FPs) and microscopy technologies has been used more and more widely due to its advantages of visualizing the signaling events in live cells with high resolutions in both spatial and temporal dimensions (Wang et al., 2008). It offers an effective tool in mechanobiology studies.

1.3.1 Fluorescent proteins

The wild-type green fluorescent protein (GFP) was first discovered in the jellyfish Aequorea Victoria in the 1960s and cloned in the 1990s (Lu et al., 2019; Shimomura et al., 1962). GFP is a kind of endogenous companion protein to aequorin and is able to emit green fluorescence upon excitation. It is considered

a fluorescent marker due to its superior performance in producing fluorescence in vivo without any other cofactors (Wang et al., 2008). The core motif of the wild-type GFP is the chromophore which is composed of Ser/Thr65-Tyr66-Cly67 and encapsulated centrally by a shell. The shell consists of 11 strands of β-barrels and short segments of α-helix, different from other known proteins (Yang et al., 1996). The unique structure highly protects the chromophore and ensures its formation.

Based on the wild-type GFP, a series of variants have been developed by site-directed mutation technique, increasing the brightness, quantum yield, stability, photostability, and expanding the colour map from violet with an emission peak at 424 nm to far-red at 650 nm (Lu et al., 2019). The multi-coloured FPs make it possible to target more than one molecular signal in the same live cell with distinct colours. Those improvements further broaden the application of FPs as an invaluable tool to observe the cellular structures and visualize the cellular process.

1.3.2 Fluorescence Resonance Energy Transfer

The development of FPs promotes new imaging technologies used in mechanobiology. One of the developed technologies utilizing FPs is fluorescence resonance energy transfer (FRET), a quantum mechanics concept involving the non-radiative energy transfer between the molecules with different levels of energy (Figure 2) (Jares-Erijman & Jovin, 2003). Specifically, suppose there is a fluorophore with an emission spectrum overlapping the excitation spectrum of another fluorophore. In that case, it can be regarded as a FRET donor, and the other fluorophore serves as an acceptor. When the distance between the donor and the acceptor is low enough, and the orientations are favourable, then the emission of the acceptor can be induced by energy transfer which is elicited by the excitation of the donor (Wang et al., 2008).

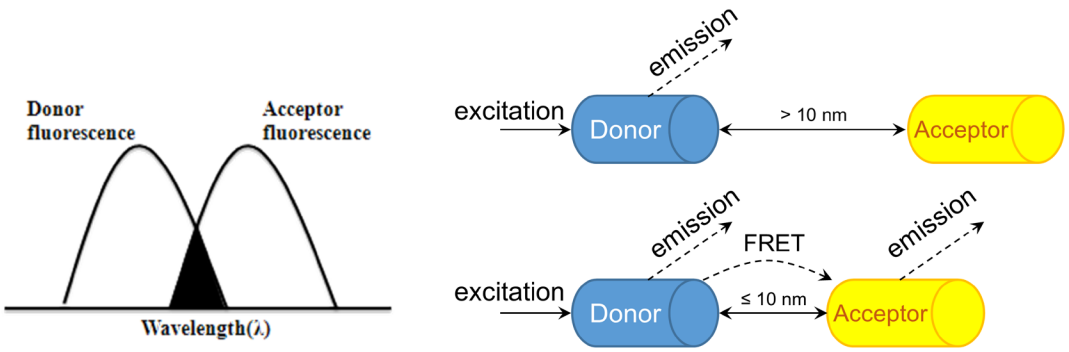

FIGURE 2 Schematic representation for FRET

The FRET theory states the efficiency of energy transfer (E) as

$$E = \frac{R_0^6}{R^6 + R_0^6} \quad (1)$$

where "R" is the actual distance between donor and acceptor, while "R_0" is the FRET distance which is defined as the distance when the energy transfer is 50%. It can be known from (1) that the energy transfer efficiency shows an inverse relationship with the 6th power of the separation between donor and acceptor (Edelhoch et al., 1967; Qiao et al., 2021). Hence, FRET is a photophysical process highly dependent on distance. The donor-acceptor separation ranges over $1-10$ nm, a distance of which the scale is near biological interactions. Thus FRET can provide the details on the molecule level (Chen et al., 2015).

1.3.3 Dynamic fluorescence images

The central manner for the FRET technique visualizing and measuring biological signals in bioimaging applications is to utilize genetically encoded biosensors, also called indicators or probes. They are chimeric proteins fused with FPs and show sensibility to physiological or biomolecular stimuli through fluorescence (Lu et al., 2019). There are two essential elements in most genetically encoded biosensors, the sensing domains and FPs (Lu et al., 2019). The sensing domains are usually the derivatives from endogenous proteins or peptides displaying the inherent ability to sense the biological activities or detect molecules of interest, and the FPs function as reporters. FPs in a biosensor may be single or a pair. In practice, a biosensor is usually a recombinant genetic construct with a gene from a molecule of interest and FPs and can be transferred into cells to realize the visualization (Chudakov et al., 2010). After transfection, the genetic construct will be expressed in the live cells, illuminated with excitation, and then observed and recorded in real-time at emission wavelength by fluorescence microscopy with continuous images at regular intervals ranging from seconds to hours. Those images are arranged in chronological order and defined as dynamic fluorescence images, which exhibit bimolecular activities with fluorescence dynamically upon stimulus. In this thesis, dynamic fluorescence images can be divided into two classes based on FPs, images based on a single FP and images based on a FRET pair. A FRET pair is a pair of two FPs between which FRET can occur.

A single FP often functions as a visual label to track the subcellular address or protein expression, localization, and translocations in live cells in time. Hence, the objects of observation are usually the intensity and distribution of fluorescence in those dynamic fluorescence images based on a single FP. For instance, transfecting DNA plasmids that encode GFP-tagged FAK (GFP-FAK) into migrating cells and imaging with time-lapse confocal microscopy display the dynamics of FAK-containing adhesions. The fluorescence distribution maps the locations of FAK, while the increase and decrease of the local fluorescence intensity show the assembly and disassembly of FAK to adhesions (Hu et al., 2014). Notably, combing FPs with different colours allows for straightforward multi-colour imaging, which simultaneously visualizes different targets in the same living cell. The co-transfection of recombinant DNA, mCherry-paxillin

(mCherry fluorescent protein tagged-paxillin) and GFP-FAK, provides the information on FAK and paxillin dynamics, respectively, by fluorescence intensity changes and the time difference of assemblies between FAK and paxillin by fluorescence intensity ratio between the two colors of fluorescence (Hu et al., 2014).

Compared to the dynamic fluorescence images obtained by a single FP, the fluorescence signals in the images based on FRET pairs have more complex meanings. Images are acquired in both donor and FRET (acceptor) channels at their emission peaks, respectively, upon the illumination at the donor excitation wavelength at the same time. The absolute FRET efficiency E, in theory, is mentioned in the last section. It represents the ratio of the energy emitted by the acceptor and the total energy during FRET. In addition, a FRET index used more widely is calculated as the ratio of fluorescence intensities between the FRET channel and donor channel due to its stability (Shrestha et al., 2015). The definition of the FRET index will be described briefly in Section 2.2.

Summing up, the genetically encoded biosensor based on FRET estimates the actual distance between the pair of FPs. The sources of distance alteration are various, such as the conformation changes within a protein and the protein-protein interactions. Consequently, the FRET ratio in dynamic fluorescence images has various meanings in different cases. A FRET-based calcium biosensor developed by Tsien's laboratory inserts a CaM-binding peptide into a FRET pair to detect Ca^{2+} considering that Ca^{2+} can cause a tightening of CaM, and further decreases the distance between the FRET pair (Palmer & Tsien, 2006). Therefore, the FRET ratio here is related to the protein conformation changes. In another case of the activation indicator for Rac1, the biosensor structure contains two sections, a GFP tagged Rac1 and a fusion. The fusion consists of a p21-binding domain (PBD) from p21-activated kinase 1 (PAK1) and Alexa 546, serving as a GFP acceptor. The PBD domain can bind activated Rac1 specifically to enable FRET to occur (Shrestha et al., 2015). The FRET ratio changes, in this case, derive from the protein-protein interactions. In addition, the differences in the FRET ratio can also originate from the physical deformation of protein upon mechanical force to indicate the tension across the protein (Grashoff et al., 2010). Generally, the dynamic fluorescence images based on FRET convert different protein behaviors to FRET ratio. The value changes of the FRET ratio with time and subcellular locations provide spatial-temporal information in cellular processes.

1.4 Goal and structure of the thesis

In this thesis, the biological interest focuses on the potential mechanism of cell polarity upon mechanical force, which draws a question of how to extract information related to polarity from dynamic fluorescence images. So far, obtaining polarity information from fluorescent protein imaging has been considered a question attached to an individual biological issue, not an

independent image processing issue. Hence, the existing methods of polarity analysis based on dynamic fluorescence images are fragmented and not systematic. The work of this thesis regards polarity analysis as an independent issue for the first time, integrates existing thoughts to establish a pipeline to obtain polarity information, develops a set of methods to complete the analysis accurately and quantitatively, and further provides an efficient and adaptive tool to analyze different forms of polarity, which contributes to the insight into the invisible intracellular mechanotransduction.

To frame the problems, Chapter 2 summarizes the current status of dynamic fluorescence image-based cell polarity analysis, including the main issues, the traditional approaches to handle the issue, and the inadequacies of the existing methods. The summary involves the preprocessing for extracting potential polarity regions and the actual polarity analysis. Also, it identifies the methodological challenges explicitly in cell body detection, subcellular structure identification (FAs), and upstream/downstream definition.

Chapter 3 summarizes the four articles included in this thesis. Each article is introduced in detail, covering the research background, the methods, and the main results. Chapter 4 further discusses the findings on how to improve the performance of preprocessing and quantify the definition of upstream/downstream for polarity analysis. It also proposes further views to answer how cell polarity is established upon shear stress. In addition, the limitations of this study and the direction of future research are also elaborate. Finally, Chapter 5 is a brief summary of the whole work.

2 VISUALIZATION AND ANALYSIS OF CELL POLARITY

With the development of FPs and microscopy techniques, there has been much research around biosensors based on FPs. However, these pay more attention to the biosensor and the biochemical processes related to the biosensors. The method to process the fluorescence images is an accessorial content that is not valued enough. In addition, after the transfection of biosensors into living cells, the patterns of biosensor expressions are various. In some cases, the biosensor locates in the cytoplasm or links to the plasma membrane, which leads to the fluorescence being distributed throughout the cell. In some other cases, the biosensor is attached to subcellular structures, such as cytoskeleton and FAs, which mostly causes the fluorescence to gather on those subcellular structures. These differences in expression pattern result in different requirements for the analysis of dynamic fluorescence images based on diverse biosensors.

Summing up, it is hard to propose a standard procedure or a systematic methodology to analyze all types of dynamic fluorescence images. This chapter summarises the main issues and existing methods related to the polarity analysis based on dynamic fluorescence images. This summary forms the basis for formulating the specific research goals for developing a complete set of methods for cell polarity analysis that is accurate, quantitative, stable, and adaptive to correct the defects of existing methods.

2.1 Preprocessing of fluorescence images

The aim of preprocessing fluorescence images is to improve the image quality, identify the potential polarity regions, and obtain the characteristics of the polarity regions. Proper preprocessing can improve the accuracy of polarity analysis. This section will discuss improving the signal-to-noise ratio and detecting cells and their substructures, as these are widely needed for fluoresce images.

2.1.1 Improving the signal-to-noise ratio

The fluorescence signals, especially in the FRET images, are usually weak, challenging signal changes detection (Piston & Kremers, 2007). In a particular experiment, various factors may affect the intensity of fluorescence, such as the state of the cell and the expression level of the biosensor. Especially to FRET images, a weak signal may also derive from the design of the biosensor. A relatively unfavorable orientation and a slightly larger distance between the FRET pair within the biosensor will impair the FRET signals (Algar et al., 2019). For weak signals, an important issue in preprocessing fluorescence images is eliminating noise and improving the signal-to-noise ratio (SNR). The potential sources of random noise include the brightness difference between the FRET pair, the camera devices, and the experiments system.

A usual approach to handle these issues is filtering. Besides, another measure to enhance SNR is the background subtraction to remove the effect of the background fluorescence. The background here refers to the wide range outside the cell in which the exposure values can be regarded as nonspecific intensity (LaCroix et al., 2015). A method to estimate the fluorescence intensity of the background is proposed based on the histogram (Lo & Puchalski, 2008). As the cells are sparse and the background covers most of the image, the value which occurs most frequently can be regarded as the fluorescence value of the background.

2.1.2 Cell body detection

Cell body detection is an important step in polarity analysis. The mistakes in detecting the cell edge probably lead to errors in the subsequent FRET measurement and polarity analysis. However, when visualizing the cell polarity by focusing on a particular protein, the observation target is usually a single cell, which indicates that it is unnecessary to consider the segmentation of clustered cells. Moreover, the background subtraction in the last step inhibits the background, enhancing the fluorescence difference between the cell body and the background. Hence, a method based on a threshold is able to segment an image into two parts, the cell body, and the background. One of the most widely used segmentation approaches is Otsu's method (Eichorst et al., 2008; Lu et al., 2011; Wu et al., 2016).

Otsu's method is a nonparametric and unsupervised means to segment an image with an automatic threshold to maximize the differences between the resultant classes in gray levels (Otsu, 1979). To a given image, supposing Otsu's method dichotomize all the pixels into two classes, C_0 and C_1, at the gray level k. Then, the implementation procedure of Otsu's method can be generalized as follows (the specific algorithm for Otsu's method is seen in the appendix):

1. Calculating the normalized distribution of the gray level of the given image with L levels, and p_i (i=1, 2, …, L) represents the components of a gray level;

2. Calculating the probabilities of C_0 and C_1 occurrence as ω_0 and ω_1;
3. Calculating the mean level of C_0 and C_1 as μ_0 and μ_1;
4. Calculating the total mean gray level of the given image as μ_T;
5. Calculating the between-class variance σ_B^2;
6. Searching the value of k to maximize σ_B^2 as the best threshold to segment the image.

The best threshold k divides the image into two classes. The class with a higher mean gray level is the cell. In practice, the threshold renews to adapt to the changes in potential fluorescence intensity in the series of dynamic fluorescence images.

2.1.3 Focal adhesions identification

In some cases, the observation target is not the cell body but some specific subcellular structures, such as organelles, cytoskeleton, and FAs. Therefore, it is required to identify those subcellular structures before the subsequent processing. The most common observation target is FAs due to the abundant proteins located in FAs. It is also necessary to identify FAs in the work of this thesis. Thus, the identification of FAs is taken as an example in this section.

FAs are the sites where the cell adheres to its substrate. In fluorescence images, the indicator based on FPs labels FAs and forms plaques with high fluorescence intensity. The detection and identification of these high fluorescence sites is the basis of studies targeted at FAs. There are two types of approaches to identifying and marking FAs. One method is to utilize some interactive software (e.g., ImageJ) to circle FAs manually or screen the high fluorescence regions during which the regions with similar high intensity but from the cytoplasm are removed by hand. After that, the FAs are saved as regions of interest (ROI) for further analysis (Legerstee et al., 2019; Verma et al., 2015). The other method is to rely on algorithms to reduce the subjective factor. The most widely accepted algorithm is the 'water' algorithm which has been used in various research (Berginski et al., 2011; Grashoff et al., 2010; Lu et al., 2014; Wu et al., 2016; Zaidel-Bar et al., 2005; Zamir et al., 1999).

The segmentation algorithm for FAs identification, named 'water', is proposed based on a modified 'lake' algorithm. The water algorithm regards an image as the topological landform in geodesy. In this analogy, the gray value of a pixel is considered as the elevation of this point. A local maxima value and the area affected by it compose a hill. Assuming that the area (the image) is completely submerged in the water, nothing can be observed above the water. However, as water declines, some peaks are gradually visible (local maxima values), and the hills where the peaks belong expand. As the water continues to decline, two disjoined hills begin to meet, and then they are considered whether to merge or remain independent based on their size (Zamir et al., 1999).

In practice, the inputs of the water algorithm include an image P, a threshold for minimum intensity $Pmin$, an area threshold for minimum patch

APmin, and a threshold determining whether to merge *AMmin*. With those inputs, the water algorithm can give a mask to identify the FAs by the routine as follows:

1. A high-pass filter is applied to the image *P*, after which the intensity sorts all pixels from *P* in decreasing order;
2. The pixels with higher intensity than *Pmin* are cycled and determined to form a new patch when it does not touch any existing patch or is subsumed to an existing patch when it touches one. There is also a case where a pixel touches more than one existing patch. In this case, the patches will be merged if at least one of them is below than *AMmin* in size. Otherwise, the pixel will be subsumed to the first pact it touches;
3. The patches smaller than *APmin* are deleted.

The reserved patches form a mask to indicate the FAs. The FAs can be characterized in area, position, orientation, and axial ratio for further analysis with the mask.

2.2 Generation of FRET index

The methods used to measure FRET can be placed into different categories, among which the simplest and most widely used approach is sensitized emission measurement. In practice, the donor in a FRET pair is excited by a light on a specific wavelength. Then, the fluorescence signals are collected on the emission wavelength of the donor (donor channel) and acceptor (FRET channel) with filters, respectively (Piston & Kremers, 2007). A sensitized emission can be detected in the FRET channel owing to the excitation energy transferred from donor to acceptor. This approach defines a value named FRET index to perform studies qualitatively or describe the relative measurements within the same study. Generally, a FRET index is a relative value that varies with the changes in energy transfer and is further related to the configuration of donor and acceptor (Berney & Danuser, 2003; Deal et al., 2020). It increases with the increase of FRET and decreases with the decrease of FRET. Although the FRET index is not a quantitative value to represent FRET efficiency, it performs more sensitively and consistently if properly defined when compared to those rigorous values for measurement. Hence, the FRET index is still attractive in many cases, for instance, when the experiment is designed to answer whether the interaction between two molecules occurs or learn the coherence of a signaling pathway in a relative term.

To a biosensor based on FRET, the relative amount of donor and acceptor is controlled in a ratio of 1:1. Thus, a FRET index can be defined as the ratio of fluorescence intensity between the FRET channel and the donor channel. This ratiometric FRET value is called FRET ratio, accepted commonly and used widely in a large amount of research since its performance is fairly consistent (Esposito, 2020; Shrestha et al., 2015). However, it must be noted that the definition of the FRET ratio ignores the multiple spectral cross-talks (such as the direct acceptor excitation when the donor is excited) and the spectral bleed-through features

(such as the direct excitation of the acceptor in the acceptor spectral mission channel) (Padilla-Parra & Tramier, 2012).

2.3 Analysis of cell polarity

After preprocessing and generating the FRET index, the dynamic fluorescence images have been prepared for polarity analysis. A crucial concept in cell polarity analysis is upstream or downstream. Here, upstream and downstream are concepts used to describe locations relative to a certain direction. The definition of direction depends on the observation target and requirements of experiments. For instance, the direction can be the migration direction to a migrating cell or the flow direction to a cell enduring shear stress provided by laminar flow. Based on the direction, the downstream region is generally defined as the location near the leading edge of a cell, while the upstream region is near the rear edge. However, the definition may vary slightly due to different analysis demands. As in the case of categorizing FAs, FAs are placed into upstream FAs and downstream FAs, relying on their orientation relative to the actin stress fibers instead of their subcellular localization (Zaidel-Bar et al., 2005).

In most cases, the determination of upstream and downstream regions depends on some commercial software coupled with the fluorescence microscope, such as MetaMorph and MetaFluor. However, polarity analysis is not a standalone function in that software. Instead, researchers use a built-in function to choose the upstream or downstream by shape tool as ROI and save ROI for further analysis. It should be noticed that the size and location of ROI cannot be changed automatically once the software determines ROI. The manual selection of ROI leads the results to be affected artificially. Hence, choosing the positions of upstream and downstream as proper as possible to avoid the potential errors caused by artificial factors is the core question waiting for an answer.

To answer this question, different researchers propose different solutions. For instance, to observe the difference in Rac activity between the leading and the rear edge of a cell, the upstream and downstream regions are defined as squares with sides of 3 μm on each side (Kraynov et al., 2000). The upstream and downstream are set as the central portion of the membrane between the leading or rear edge of the cell boundary and the nucleus, respectively, to map the spatial-temporal distribution of membrane fluidity upon shear stress (Butler et al., 2001). In the work to quantify the activation and polarity of Src and FAK, the single cell is further divided into three parts by two parallel lines perpendicular to the direction of flow and pass through the two poles of the nucleus. Then, the upstream region is from the leading edge of the cell to the top line, the middle region is between the two parallel lines, and the downstream region is from the bottom line to the rear edge of the cell. The centroids of the three regions are identified and considered as the centers of the circles covering the maximal area within each region, respectively, to represent upstream, middle, and

downstream (Liu et al., 2014). In addition, the subcellular location can also be described by its normalized distance to the assigned edge during cell migration (Lu et al., 2011).

2.4 Research objectives

With the development of FPs, the application of biosensors based on FPs is becoming widespread. However, the tools focusing on analyzing the dynamic fluorescence images and visualizing the potential polarity are still lacking. The existing methods fail to handle the issues in some cases consistently, even leading to errors. The potential problems may occur at multiple steps during the analysis.

2.4.1 Detection of the cell body

The fluorescence intensity is uneven along the cell boundary in some cases. It usually occurs where the plasma membrane is concave, which is probably related to the three-dimensional shape of the cell. On the cell profile, the concave edge leads to the thickness of the cell changing locally. Although the fluorescence microscope focuses on the basal layer and the fluorescence images only afford information on a two-dimensional surface, the difference in cell thickness still results in fluorescence interference.

In this case, a global threshold given by Otsu's method fails to detect the cell body correctly, while identifying the cell body completely and accurately is vital for the subsequent analysis. A precise cell edge allows a more accurate FRET estimation of the whole cell body. It contributes to describing the characteristics of the cell shape more concretely, which is the foundation for quantitative analysis.

2.4.2 Identification of FAs

As introduced above, a common method for FAs identification is the water algorithm which is sensitive to the abnormal local maxima. Still, the local abnormal values are hard to avoid entirely during imaging. In addition, prior knowledge of the threshold to distinguish the FAs and background is necessary to apply the water algorithm. An inaccurate elimination of the threshold will cause a part of FAs to be omitted or some background pixels to be mistaken as FAs. The estimation of the threshold is directly related to various factors.

In practice, when researchers choose a focal adhesion protein A as the observation target, sometimes they will inhibit the expression level of the endogenous A to avoid the overexpression of the exogenous A imported by biosensors. Thus, most A in the biosensors can assemble to FAs instead of retaining in the cytoplasm (Grashoff et al., 2010). This treatment minimizes the fluorescence intensity of the background and highlights the FAs, which makes the application of the water algorithm easy. However, according to the

experiment design, the exogenous *A* derived from the biosensor will compete with endogenous *A* when it is unnecessary to silence endogenous *A*. The overexpression of *A* leads *A* to exist at FA sites and in the cytoplasm concurrently, which increases the fluorescence intensity of the background and narrows the intensity difference between FAs and the background. It is hard to determine a threshold for the background in this case.

In addition, the expression level of a biosensor is decided by both its construction and the state of cells. It means that even the same biosensor can be expressed differently in different individuals and makes the background changeling to estimate, especially when the expression level of the biosensor is low or the grayscale of the whole image is narrow.

As a result, the water algorithm cannot precisely identify FAs in these cases. It leads to several issues. For instance, how to distinguish FAs from the background without eliminating a threshold, lower the difficulty of FAs identification, and improve the performance of the identification algorithm.

2.4.3 Definition of upstream/downstream

In polarity analysis, a decisive issue is how to determine the upstream and downstream regions. The current division of upstream/downstream mainly depends on delineating ROI. Indeed, ROI can be selected and saved to monitor how fluorescence intensity or FRET value changes over time at a local location by developing a software package. However, ROI cannot be altered in location and shape automatically once established, while the cells experience morphological changes due to cell growth and migration. The established ROI is unable to adapt to the cell deformation, which results in the unconformity of the ROI and regions needed to be observed, the boundary of ROI outside the cell body, and further the errors in results (Figure 3). Adjusting the location and size of ROI can reduce these errors manually but not eliminate them. Moreover, it is difficult for ROI to cover the whole region of downstream or upstream, which leads to errors. In addition to the ROI, the definition of upstream and downstream is usually qualitative and rough in the current analysis methods, not a result of numerical calculation. It may be affected by human or incidental factors. It proves that the existing methods fail to handle the polarity analysis properly. Defining upstream/downstream quantitatively from the view of processing images is still a question without an appropriate answer.

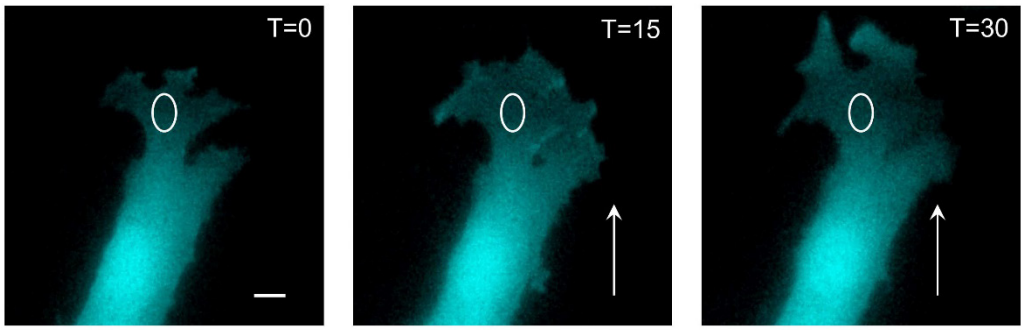

FIGURE 3 Possible errors in ROI chosen during cell deformation and migration, scale bar: 10 μm

Summing up, the existing methods for polarity analysis are not adequate. It is necessary to develop a set of methods to analyze polarity with better performance. This work aims to analyze the dynamic fluorescence images more correctly and deeply, adapt to the diverse analyzing requirements of different forms of polarity, provide more information, and visualize the results to speculate the potential pathway to activate cell polarity upon shear stress. The achievement of the objective covers multiple stages of polarity analysis, which in a nutshell contains improving accuracy, lowering the difficulty of the preprocessing, defining upstream/downstream quantitatively to identify the occurrence of cell polarity under different treatments and further describing the spatial-temporal characteristics of polarity.

To achieve these objectives, the work contains four articles covering different stages of polarity analysis. Article I analyzes the cell polarity based on dynamic fluorescence images with a single fluorescent protein, and Article II develops the polarity analysis to dynamic FRET images. These two articles propose a method to define the upstream/downstream to analyze the cell polarity which occurs in the whole cell. Ulteriorly, Article III visualizes and measures the intercellular force signals on specific subcellular structures temporally. Article IV further maps the polarized distribution of these signals in both spatial and temporal dimensions. These two articles promote the preprocessing at the steps of the cell body detection and FAs identification and propose a new method to define upstream/downstream based on FAs sites, which further gives an approach to analyze the potential polarity on specific subcellular structures and descript the spatial-temporal characteristics of polarity.

It is vital to properly excavate the polarity information hidden in dynamic fluorescence images to offer insight into intracellular processes. The tool provided in this work will advance the application of live-cell imaging techniques in cell polarity research.

3 OVERVIEW OF INCLUDED ARTICLES

This chapter summarizes the papers contained in this work. The main experimental methods to obtain dynamic fluorescence images are described briefly before introducing the included articles formally, contributing to understanding the experiments involved in the papers. For better readability of the overview, some figures are reproduced from the included articles.

The biological experiments in this work serve two main purposes, verification experiments, and live-cell imaging. The verification experiments are conducted to ensure the accuracy and reliability of the biosensor when Articles II and III introduce new biosensors. However, the significance of such experiments lies more in biology. Hence, there will be no further elaboration of the verification experiments in this thesis beyond the detailed descriptions in the papers.

In the process of live-cell imaging, DNA plasmids that contain biosensor sequences are transfected into living cells. Table 1 lists the basic information about the biosensors used in this work. After that, the use of some drug treatments alters the cell state. Table 2 lists the drugs involved in this work, containing their functions and the pretreatment used in actual experiments. The cells are exposed to the mechanical force that involves two patterns of flow in this work, shear stress due to laminar and disturbed flow. The images are recorded with a time interval of 1 min for at least 15 min, and the ground state before flow application lasts for at least 5 min to ensure that the cell is in a steady state. The images based on a single FP are captured in only one channel, while the FRET images are obtained from both donor and acceptor channels. All images are arranged in chronological order to form dynamic fluorescence images.

The flow system used in this work to provide the mechanical loading is shown in Figure 4, containing a parallel-plate flow chamber, a peristaltic pump, and two reservoirs. Cells are seeded in the flow chamber, specifically in the region where the flow is laminar. The laminar flow provides shear stress τ in the flow chamber, which can be calculated as follows:

$$\tau = \frac{6\mu Q}{H^2 W} \tag{2}$$

where μ is the flow density, Q is the average flow rate through the interface, and H and W represent the height and width of the chamber. In the system in Figure 4, changing the height difference between the two reservoirs can regulate the magnitude of the shear stress. A classic vertical-step is added in the chamber close to the entrance to provide disturbed flow. It is composed of two silicone membranes with different sizes of rectangular space. The figure is reproduced based on Article I, Fig 1.

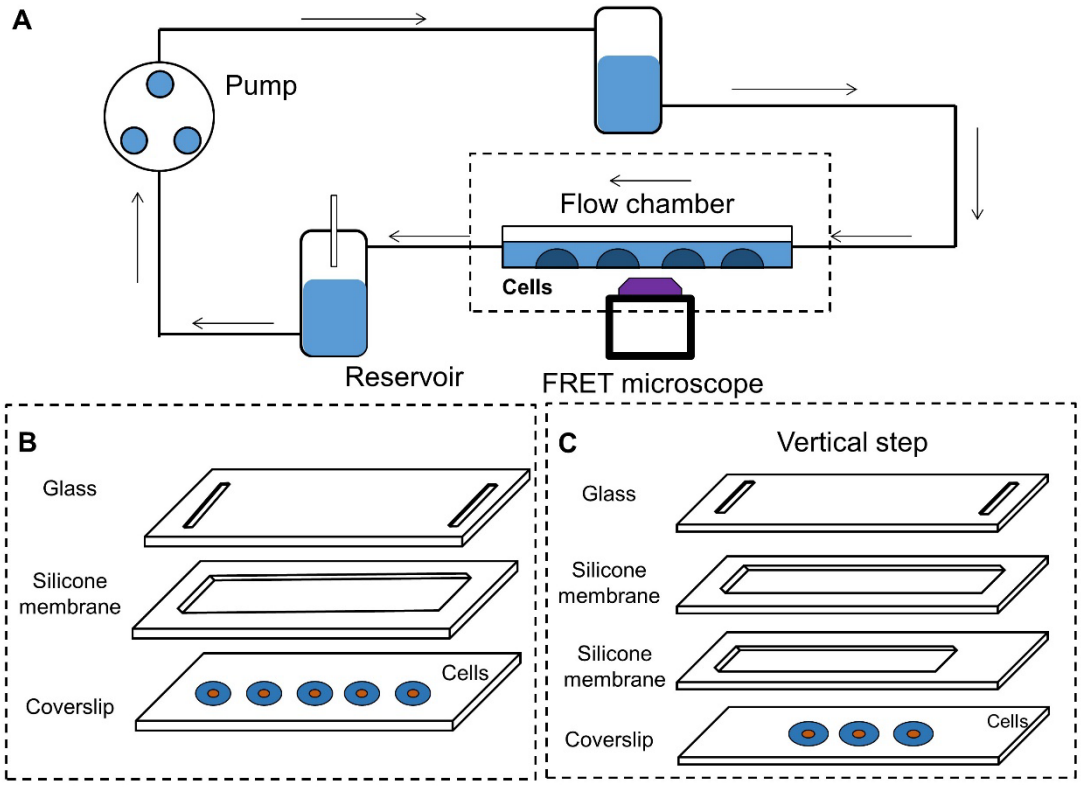

FIGURE 4 System providing laminar flow or disturbed flow: (A) Whole system; (B) Flow chamber structure; (C) Vertical step structure

TABLE 1 Overview of involved biosensors in the included articles

Name	Application	Construction	Function	Reference
PAK-PBD-GFP	Article I	PBD domain+GFP	To label the activated Rac	(Magalhaes et al., 2007; Srinivasan et al., 2003)
sl-RhoGDIα	Article II	ECFP+Switch II linker+RhoGDIα+Ypet	To visualize the affinity between RhoGDIα and Rho family GTPases (activity of RhoGDIα)	Published first in Article II
Lyn-sl-RhoGDIα	Article II	Lyn+ECFP+Switch II+linker+RhoGDIα + Ypet	To link sl-RhoGDIα biosensor to lipid rafts on the plasma membrane	Published first in Article II
Kras-sl-RhoGDIα	Article II	ECFP+Switch II+linker+RhoGDIα+Ypet+Kras	To link sl-RhoGDIα biosensor to non-lipid raft regions on the plasma membrane	Published first in Article II
s-RhoGDIα	Article II	ECFP+Switch II+RhoGDIα+Ypet	Contrast biosensor to sl-RhoGDIα biosensor to test the efficiency	Published first in Article II
nsl-RhoGDIα	Article II	ECFP+RhoGDI α+Ypet	Contrast biosensor to sl-RhoGDIα biosensor to test the accuracy	Published first in Article II
R66E-sl-RhoGDIα	Article II	ECFP+Switch II (66Arg→Glu)+linker+RhoGDIα+Ypet	Contrast biosensor to sl-RhoGDIα biosensor to test the accuracy	Published first in Article II
PaxTS	Articles III and IV	LD12+ECFP+nanospring+Ypet+LIM1234	To visualize the tension across paxillin	Published first in Article III
PaxDL	Article IV	ECFP+nanospring+Ypet+LIM1234	Contrast biosensor to PaxTS	Published first in Article III

TABLE 2 Overview of the drugs used in the included articles

Name	Pretreatment	Function
Benzyl alcohol (BA)	45 mmol/l for 45 min	Increasing the membrane fluidity
Cholesterol (CHO)	0.1 mmol/l for 3 h	Decreasing the membrane fluidity
Cytochalasin D (CytoD)	2 μmol/l for 30 min	Depolymerizing agents of actin
The myosin light chain kinase inhibitor (ML-7)	5 μmol/l for 1 h	Inhibiting the contractility of actin
Nocodazole (NOCO)	1 μmol/l for 1 h	Depolymerizing the microtubules
PP1	50 mmol/l for 30 min	Inhibiting the activity of Src

3.1 Article I

Shuai Shao, Cheng Xiang, Kairong Qin, Aziz Ur Rehman Aziz, Xiaoling Liao, and Bo Liu. 2017. "Visualizing the spatiotemporal map of Rac activation in bovine aortic endothelial cells under laminar and disturbed flows." *PLoS One* 12(11):e0189088; DOI: 10.1371/journal.pone.0189088

Background

Atherosclerosis usually occurs at the aortic arch, branch points, and vessel bifurcations where the positions are with more curvature. The atherosclerotic plaques mainly localize in the disturbed flow area where random orientations characterize the flow. It has been known that the inner surface of vessels is covered by endothelial cells (ECs). ECs endure the mechanical force and respond to diverse patterns of flow differently. Thus, the flow pattern is considered a potential pathogenic factor. Rac is a key regulator in the shear stress-mediated ECs orientation depending on its polar activation upon shear stress and probably plays a role in atherosclerosis. However, the potential mechanism is still not clear.

Methods

In this article, activated Rac was detected by the FP biosensor PAK-PBD-GFP (Table 1), and bovine aortic endothelial cells (BAECs) transfected with the biosensor were exposed to laminar flow for shear stress and disturbed flow application, respectively. The shear stress was 15 dyn/cm^2, and the same mean flow was set in disturbed flow. Table 2 summarizes the drugs used in this work.

The fluorescence distribution in the dynamic fluorescence images indicated the distribution of activated Rac upon shear stress. The direction was from right to left in the images. A Matlab package was developed to analyze the polarized

Rac activation and visualize the polarity in a spatial-temporal map. After that, the polarity was further characterized by the logistic curve.

In the software package, all the dynamic fluorescence images were filtered by a median filter to inhibit noise, pretreated to eliminate the effect of the background, and processed with a threshold that was renewed over time automatically to detect the cell body. The cell was divided into 50 zones on average and respectively on the dimension of width (along the shear stress direction) and height (vertical to the shear stress direction) to normalize the cell shape, which could be understood as grid handling. The difference between two images from two adjacent time frames highlighted fluorescence intensity changes. In the direction of the flow, the zones divided the cell into 50 cross-sections perpendicularly to form a profile to display how Rac was activated along the shear stress direction. The zones were numbered from 1 to 50 from left to right. Hence, the downstream regions were on the left, while the upstream regions were on the right. The average intensity in each zone is normalized to the average at the ground state. Gathering the intensity changes of each zone with the time displayed the shear stress-induced Rac activation spatially and temporally. The data showing the fluorescence changes with zones at the thirtieth min was fitted by a logistic curve as follows:

$$y = \frac{A_1 - A_2}{1 + e^{(x - X_0)/D}} + A_2 , \quad (3)$$

where x was the zone number, and y was the fitting value of the normalized fluorescence data. The absolute value of the difference between A_1 and A_2 measured the range of fluorescence changing. The first point of which the slope was very close to zero (<0.005) was named X′ and considered a parameter related to the position where the fluorescence began to appear. X_0 was the inflection point at which the slope measured the activation speed. The slope at X_0 was calculated as

$$y'(X_0) = \frac{A_2 - A_2}{4D}. \quad (4)$$

The differences of the same parameter between the control group and the drug treatments are detected by T-test to observe whether the drugs play roles in shear stress activating Rac polarity.

Main results

The software package provided an approach to identify a polarized distribution. The zones divided the cell equally along the flow direction, covering the whole cell without missing, instead of only considering a part of the cell by selecting ROI. Moreover, the zones were relative regions referring to the cell edge. The zone marked as 1 was always the leftmost region of the cell, ensuring that the position and width of the zone relative to the whole cell remained unchanged during cellular processes. In addition, these zones normalized the cell length along the shear stress direction, which eliminated the effect of cell size on the results. It meant that the approach of dividing the cell into zones was robust to the cell shape, cell growth, deformation, and migration. Based on the zones, the approach provided functions to visualize the distribution of shear stress-induced

Rac activation as a spatial-temporal map and fitted the data with the logistic curve. The logistic fitting gave parameters to measure the Rac activation (Table 3). The range of the curve ($|A_1-A_2|$) indicated the intensity of the polarity. The zone in which the curve slope began to increase significantly described the subcellular location of polarity began to appear (X′). The slope of the inflection point, together with X′, displayed whether the polarity distribution was gentle or sharp.

TABLE 3 Parameters from fitting curve in different groups

	$\|A_1-A_2\|$	X′	Slop	Polarization at X′ (%)	X_1
Control	1.15±0.44	12.30±5.71	-0.29±0.23	0.45±0.56	11.20±6.37
Disturbed flow	0.41±0.17*	24.25±12.39*	-0.07±0.02*	1.75±0.53*	30.00± 10.80*
ML-7	1.29±0.84	17.00±4.41	-0.22±0.14	0.38±0.19	15.25±6.95
CytoD	0.32±0.86	31.50±15.91*	-0.13±0.09	1.11±0.87	32.50± 11.45*
NOCO	0.31±0.14*	30.00±12.47*	-0.05±0.05*	10.67±9.49*	34.80± 15.93*
CHO	0.26±0.16*	22.75±11.57*	-0.01±0.07*	1.34±0.74*	22.50± 10.72*
BA	2.39±1.5*	15.17±5.27	-0.19±0.10	0.65±0.55	18.00±7.81

Notably, Table 3 also listed the polarization at X′, defined as the ratio between the fitting value at X′ and the full range ($|A_1-A_2|$). The polarization showed that the relative activation level where the polarity increased sharply was not at the same level. Compared to X′, X_1 was defined as the zone where the fitted polarization reaches 1% of the total value ($|A_1-A_2|$), functioning as another parameter to evaluate the subcellular location of polarity. The reason to choose 1% was that the polarization at X′ hovered around 1% when the polarity was not inhibited. The results demonstrated that both X′ and X1 could assess the polarity location and gave the same conclusion, but their emphasis differed. The definition of X_1 seemed more transparent to detect the potential polarity, while the slop value made X′ more sensitive to the spatial changes of the polarity distribution. Moreover, X_1 was eventually a function of X_0 and D only, even if it was defined according to a percentage of the total value ($|A_1-A_2|$). In this article, X′ was chosen as the formal parameter to determine the start location of the polarity with a more dramatic spatial difference and a bit smaller standard error. The processing results and the static analysis showed that Rac could be activated polarized at the downstream regions upon shear stress (Figure 5) but not disturbed flow. In addition, depolymerizing the structure or inhibiting the contractility of the cytoskeleton eliminated the shear stress-induced Rac polar activation. Inhibiting the membrane fluidity also inhibited the Rac polarity upon

shear stress while enhancing the fluidity promoted the polarity. These results demonstrated that the shear stress-induced Rac polar activation depended on the structural integrity of the cytoskeleton and the ability of force transmission along the cytoskeleton, and also mediated by the membrane fluidity. Figure 5A-B showed the live-cell images transfected with PAK-PBD-GFP biosensor upon the laminar flow and disturbed flow, respectively. The arrow indicated the main flow direction. The spatiotemporal map of averaged single-cell images showed an obvious Rac activation at the downstream along the direction of laminar flow but not the disturbed flow group (Fig. 5C). The data of the thirtieth min upon the laminar flow and disturbed flow were fitted by logistic curve, respectively (Fig. 5D). The figure was reproduced from Article I, Fig 3.

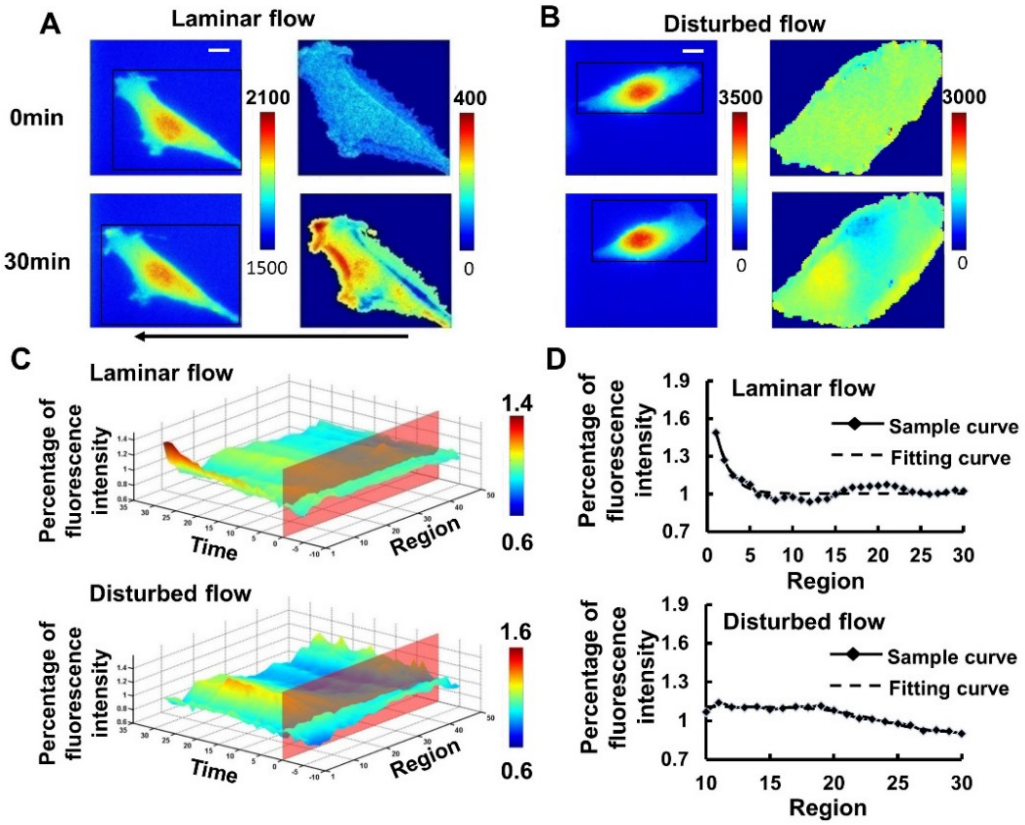

FIGURE 5 Polarized Rac activation by laminar flow: (A, B) Live-cell images, scale bar: 10 μm; (C) Spatiotemporal map of averaged single-cell images; (D) Laminar and disturbed flow logistic curves

The model of shear stress-induced Rac polarity can be described as (Figure 6): force was applied to the membrane and stretched the cytoskeleton unevenly due to the different fluidity between upstream and downstream; then, the cytoskeleton polarized in a clear direction gradually with time, which caused force transmitted to local locations through cytoskeleton network rapidly and differently; finally, the local strain at the downstream edge of the cell promoted the polar Rac activation under shear stress. Nevertheless, the membrane changed

randomly without any apparent spatial direction under disturbed flow, stretching the cytoskeleton homogeneously. The elimination of force difference between upstream and downstream regions was the determining factor because Rac was not activated upon disturbed flow. The figure was reproduced from Article I, Fig 6.

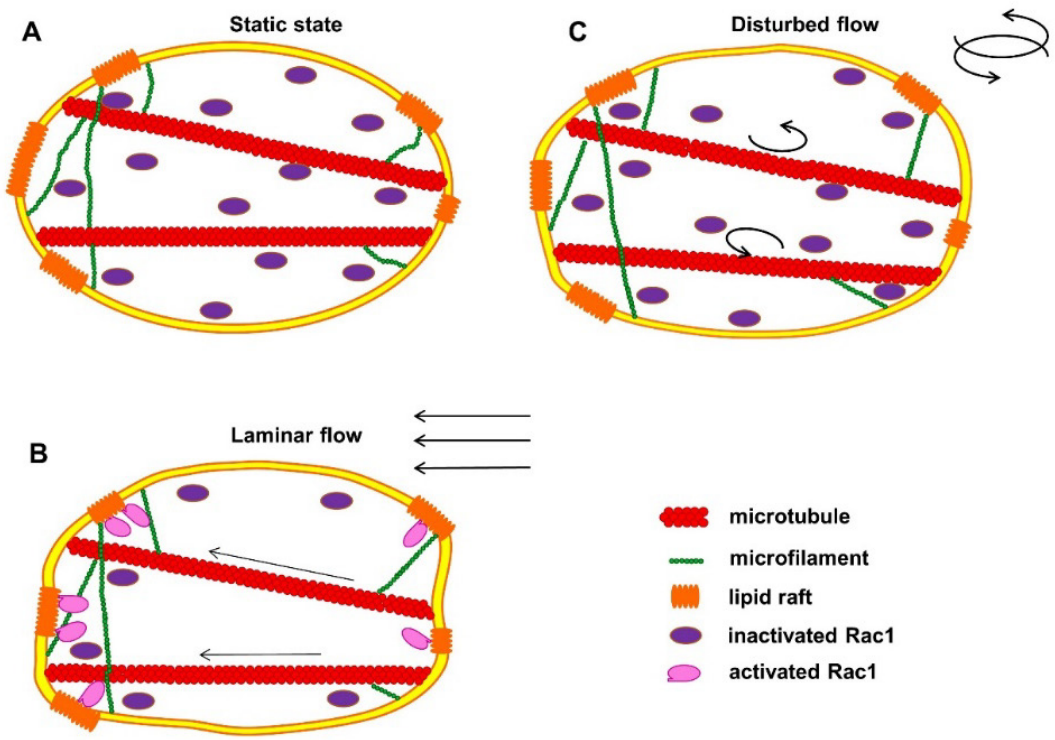

FIGURE 6 Model of Rac activation under laminar flow and disturbed flow: (A) Static condition before applying shear stress; (B) Case of laminar flow; (C) Case of disturbed flow

Contributions

Shuai Shao analyzed the data under the guidance of Xiaoling Liao and Bo Liu; wrote the draft with Cheng Xiang, Kairong Qin, Aziz ur Rehman Aziz and Bo Liu; reviewed and edited the paper with Bo Liu.

3.2 Article II

Shuai Shao, Xiaoling Liao, Fei Xie, Sha Deng, Xue Liu, Tapani Ristaniemi and Bo Liu. 2018. "FRET biosensor allows spatio-temporal observation of shear stress-induced polar RhoGDIα activation." Communications Biology 10;1:224; DOI: 10.1038/s42003-018-0232-2

Background

A crucial contributor to the establishment of cell polarity before formal cell migration is the Rho family GTPases which cycles between the GTP-bound form (active state, on the membrane) and the GDP-bound form (inactive state, in the cytoplasm) in cells. One of the central regulators of Rho family GTPases is Rho GDP-dissociation inhibitor α (RhoGDIα). RhoGDIα serves as a negative inhibitor by forming a complex with Rho family GTPases in the cytoplasm to prevent Rho family GTPases from translocating to the membrane for activation. As an essential regulator of Rho family GTPases, the expression level of RhoGDIα also mediates the invasion and metastasis of cancer. However, how RhoGDIα is activated upon shear stress is still unknown. The leading cause of this issue is the lacking tools for observing the activity of RhoGDIα effectively in living cells.

Methods

A FRET-based biosensor named sl-RhoGDIα (Table 1) was designed and constructed to observe the activity of RhoGDIα in living cells. Hela cells transfected with sl-RhoGDIα and its derivative biosensors were applied with shear stress in the flow chamber. The shear stress magnitudes were set at 5 dyn/cm^2 (low level), 20 dyn/cm^2 (control group), and 40 dyn/cm^2 (high level), respectively, and different drugs used in this work referred to Table 2.

The distribution of RhoGDIα activity was indicated as the FRET ratio distribution upon shear stress to the dynamic fluorescence images obtained in this article. The direction was from the bottom to the top in the images. A Matlab software package was developed to process the images rapidly for further polarity analysis. The analysis tool contained three sections and was developed from Article I to allow the polarity analysis to develop from only processing dynamic fluorescence images based on single FP to two-channel FRET images. A schematic sketch to process the dynamic fluorescence images is shown in Figure 7.

Firstly, the dynamic fluorescence images from two channels were pre-treated to remove the disturbance of the background. The background of each image was set as the mean fluorescence intensity from the four corners of the image. A threshold that was renewed over time automatically was utilized to detect the cell body based on the images from the ECFP channel. Next, the FRET index was defined as the FRET ratio, which was the ratio of the fluorescence intensity of FRET channels divided by the value from the ECFP channel. The overall level of the affinity between RhoGDIα and Rho family GTPases was calculated as the mean FRET ratio of a whole sample. To the two images from the same frame, the FRET ratio of each zone was simplified as the mean value in the zone and normalized by the mean value of the whole cell. After that, the cell was divided into 50 zones with equal width along the direction of shear stress, and the first five zones were regarded as the downstream according to the direction of shear stress, while the last five zones were the upstream. If the T-test confirmed a significant difference between upstream and downstream, the cell exhibited polarity. The ratio between the values from upstream and downstream was the parameter to measure the level of the polarity. A T-test detected a significant

difference in the upstream/downstream ratio between the control and drug treatment groups, indicating that drug treatment enhanced or inhibited the polarity.

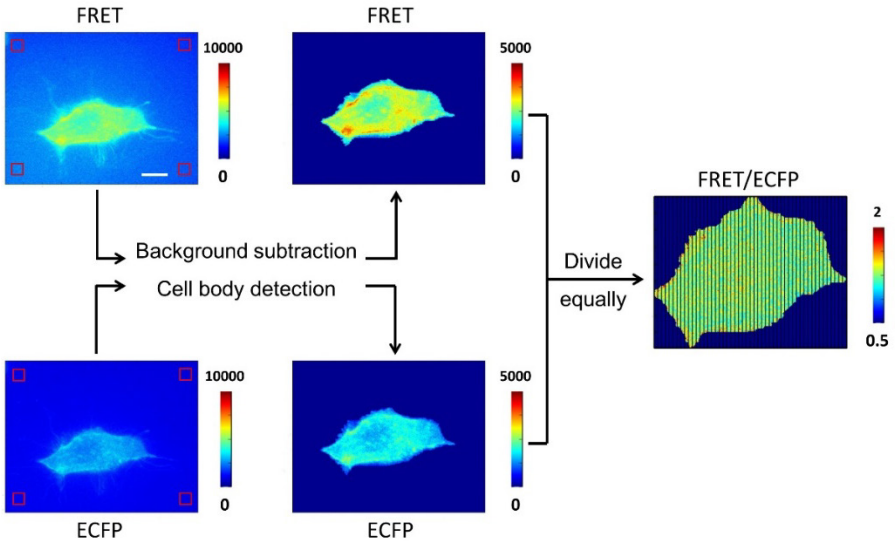

FIGURE 7 Schematic sketch of image analysis, scale bar: 10 μm

Main results

The approach in this article was developed from Article I, while it defines the downstream as the first five zones and the upstream as the last five zones, instead of the logistic fitting in Article I. The zone number is chosen as five to avoid that a single zone may not cover the polarity regions entirely, but more zones may lead to an underestimated polarity level. Controlling the number of chosen zones for upstream and downstream could change the size of upstream and downstream to adapt to different analysis requirements. Five was found as an adequate compromise for the set of experiments in this article. As shown in Figure 8D, the polarity measurement was not sensitive to the choice of zone number in a certain range. However, a zone number beyond the acceptable range would dilute the polarity and make the difference between upstream and downstream hard to detect.

The processing of the dynamic fluorescence images by the software package proved the sl-RhoGDIα biosensor efficient, accurate, and reliable in indicating the RhoGDIα activity both in vivo and vitro. In living cells, after shear stress application, the affinity between RhoGDIα and Rho family GTPases decreased, demonstrating that Rho family GTPases dissociated from RhoGDIα upon shear stress and RhoGDIα was activated. The dissociation was related to the subcellular localization of RhoGDIα and was affected by the shear stress magnitudes, the membrane fluidity, and the integrity of the cytoskeleton. Interestingly, inhibiting Src remained more RhoGDIα-Rho family GTPases complex in the cytoplasm instead of dissociating upon shear stress. Moreover, the spatial-temporal maps showed the complex of RhoGDIα and Rho family

GTPases dissociated unevenly upon shear stress in space. The polarized dissociation was related to the subcellular location, the magnitudes of shear stress, the membrane fluidity, the integrity of the cytoskeleton, and the activity of Src (Figure 8). In Figure 8, the control group was without drug treatment. Arrow represented the shear stress direction (Fig. 8A). ** denoted that there was an obvious difference between the treatment group and the control group (Fig. 8C). * denoted that there was an obvious difference between upstream and downstream. # denoted that there was an obvious difference when compared to using five zone (Fig. 8D). The figure was compiled using Fig 5, Fig 6 and Fig 7 from Article II.

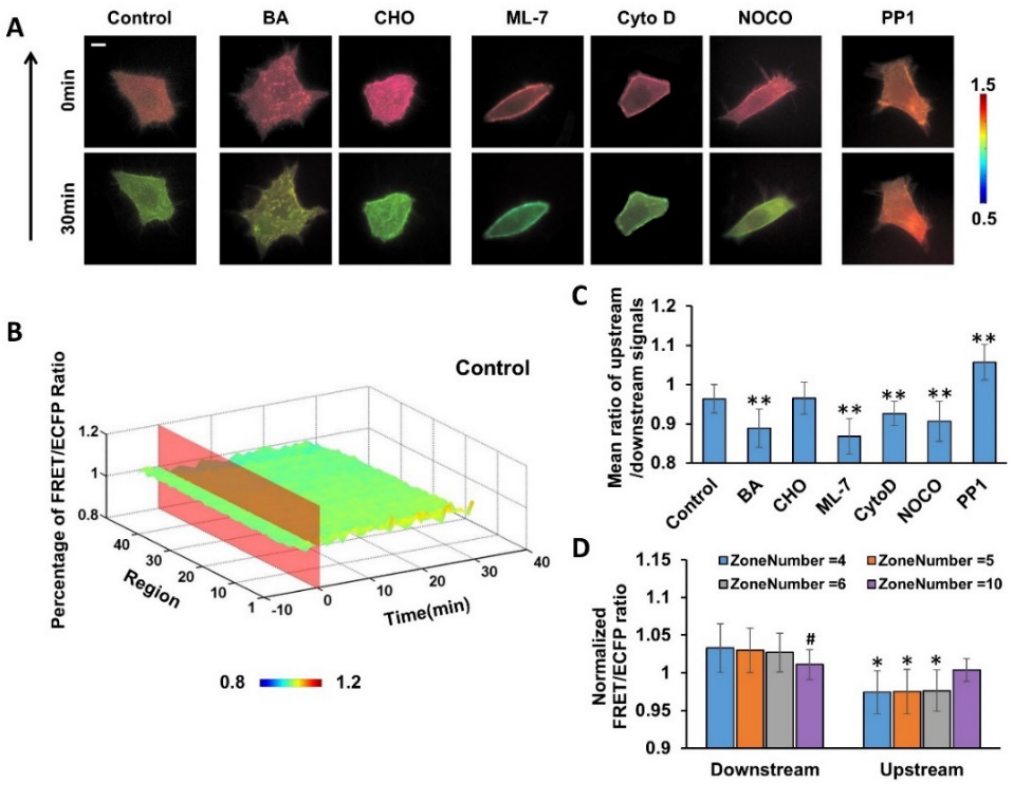

FIGURE 8 Polar distribution of the affinity between RhoGDIα and Rho GTPases upon shear stress: (A) Live-cell images upon shear stress with drug treatment, Scale bar: 10 μm; (B) Distribution of affinity between RhoGDIα and Rho GTPases under shear stress; (C) Ratio of upstream and downstream averages of the control group and other drug treatment groups; (D) Effect of zone number on upstream and downstream measurements in the control group

The visualization results showed a negative regulation in the dissociation of the RhoGDIα-Rho family GTPases complex upon shear stress. This was mediated by membrane fluidity and cytoskeleton (especially the microfilaments) with the help of Src. The findings indicated a relatively independent regulatory mechanism for RhoGDIα activation under shear stress, independent of Rho family GTPases. The model describing how the shear stress activates RhoGDIα can be simplified as follows (Figure 9): the plasma membrane deformed when

the extracellular shear stress was applied to increase the cell membrane fluidity inhomogeneously; then, the force was transferred into cells and transmitted along actin to the stress concentration point at the distal end through their contractions; some mechanosensors anchored to the actin activated Src locally, the polarized activity of Src provided the spatial guide and regulated the dissociation of RhoGDIα and Rho family GTPases by the phosphorylation of the former, or maintained the complex in its original state. The figure was reproduced from Article II, Fig 8.

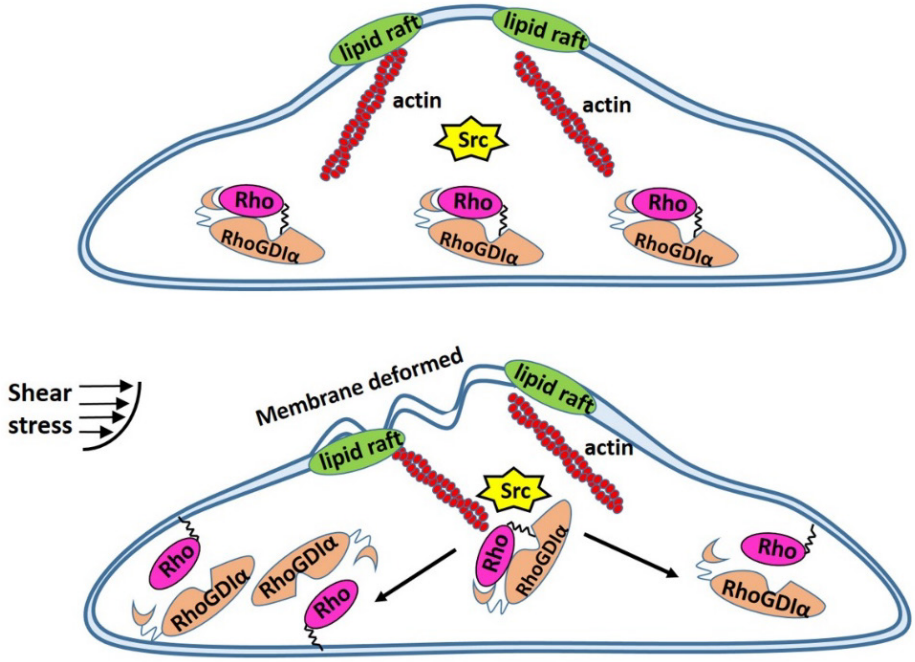

FIGURE 9 Proposed mechanism of shear stress induced-RhoGDIα activation

Contribution

Shuai Shao designed the research of this paper under the guidance of Bo Liu; performed research with Fei Xie and Sha Deng; analyzed data with the assistance of Bo Liu and Tapani Ristaniemi; wrote the draft with Xue Liu, Xiaoling Liao, Tapani Ristaniemi and Bo Liu; further reviewed and edited the paper with Bo Liu.

3.3 Article III

Shuai Shao, Sha Deng, Qingyun Jiang, Hangyu Zhang, Zhengyao Zhang, Na Li, Fengyu Cong, Timo Tiihonen, and Bo Liu. 2021. "A DNA-encoded FRET biosensor for visualizing the tension across paxillin in living cells upon shear stress." *Analysis & Sensing*; 1: e202100061. DOI: 10.1002/anse.202100061

Background

FAs are where the cells adhere to ECM and they have been proven sensitive to mechanical force by several studies. There are hundreds of proteins existing in FAs. Several of them are considered mechanosensitive, such as vinculin and talin. Paxillin, a main component of FAs, is anchored to FA sites on the plasma membrane and connected to the cytoskeleton. Various proteins require paxillin to provide docking sites for the subsequence biochemical processes. Some of the cellular processes have been verified to be able to be activated by mechanical forces like shear stress. Herein, paxillin is probably another potential participant in the process of cells responding to mechanical stimuli. However, the detection and measurement of the tension across paxillin have still not been achieved due to lacking efficient tools.

Methods

A FRET based-biosensor named PaxTS was designed and constructed to observe the force signal across paxillin in living cells. U-2 OS cells expressing PaxTS were applied with shear stress at 20 dyn/cm^2 in the flow chamber. Table 2 listed the drugs used in this article.

The tension across paxillin was visualized as the FRET ratio in this article. The direction of the shear stress applied in flow experiments was left to right in the dynamic fluorescence images. A software package implemented by Matlab was developed to analyze the tension changes on FA sites upon shear stress. Figure 10 lists a simple sketch for the analyzing procedures. First, all the dynamic fluorescence images from the two channels of the same cell were read in to remove noise by median filter and the background interference. The background of each image was defined as the mean value of the fluorescence intensity from the four corners of the image. The cell body was detected with the image from the ECFP channel by a segmentation algorithm based on Otsu's method with an adaptive detection threshold. Then, the initial image was enhanced based on a low pass filter. Applying K-means clustering to the enhanced image divided it into several clusters which contained the FAs sites. There were some cases in which the local boundary of a cell could not be segmented ideally with the global threshold due to the intensity profile around the cell was not uniform. In this case, the area marked as the cell body mistakenly could also be recognized and contained in the clusters. The clustering results detected the FA sites and renewed the cell boundary with higher accuracy.

To the FA sites, calculating the distances of each FA to its nearest edge (DAE), its distance to the cell centroid (DAC), and the ratio between the two distances (DAE/DAC) to set a standard to describe the positions of FAs. The standard divided the cell into layers. Only the FAs in the outermost layer (ratio>0.85) remained for further analysis. The FRET index was defined as the ratio between FRET and ECFP channels in this article. The tension across paxillin was regarded as the averaged FRET ratio on those final segmentation results of FAs.

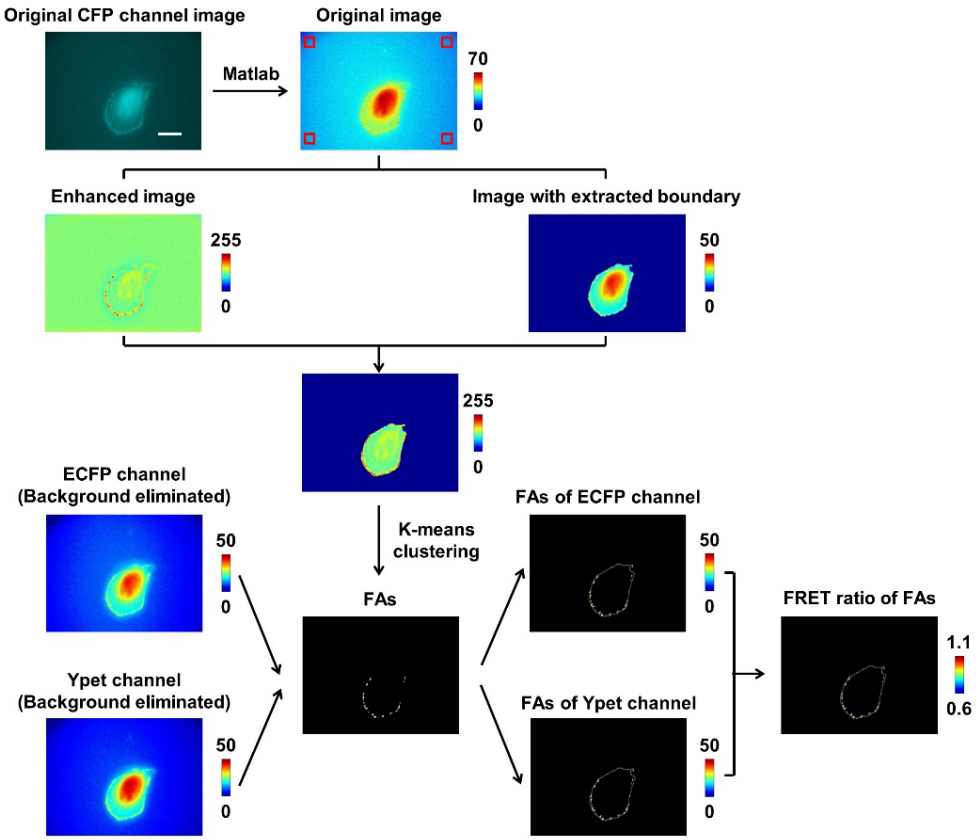

FIGURE 10 Image processing of FAs segmentation and FRET ratio generation, scale bar: 20 μm

Main results

The approach to processing the dynamic fluorescence images improved the accuracy of cell body detection when the fluorescence intensity is uneven around the cell profile with high robustness to the cell shape. In addition, there proposed a new method to identify FAs by K-means clustering. The method segmented the FAs accurately without any prior knowledge and performed well even when the grayscale of the image was narrow, overcoming the defect of the traditional water algorithm in which the estimation of the background was necessary. Generally, the approach provided a new tool to measure the FRET ratio values on FA sites efficiently and more accurately.

The analysis results proved that PaxTS detected the tension across paxillin with stability, reversibility, and accuracy. Measuring the tension across paxillin on the FAs sites in static states indicated that paxillin endured tension in living cells and the integrity of the cytoskeleton and the contractility of actin maintained the tension. The results under laminar flow demonstrated that the tension across paxillin decreased upon shear stress (Figure 11). The increase of the membrane fluidity and the depolymerization of cytoskeletal components resulted in the reduction of decline. R1 was the Regions 1, and R2 was the Regions 2 (Fig. 11A). The arrow represented the direction of shear stress. Figure 11 was compiled using Fig 3 from Article III.

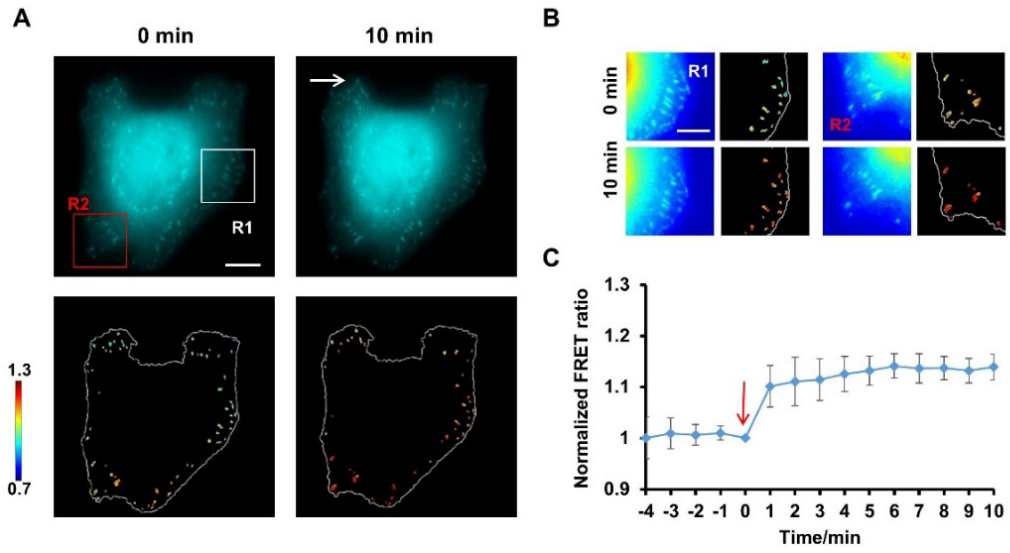

FIGURE 11 Tension across paxillin upon shear stress: (A) Live-cell images from ECFP channel of PaxTS biosensor under shear stress and the segmentation results (control group), scale bar: 20 μm; (B) Partial enlargement of Region 1 (R1) and Region 2 (R2) from (A), scale bar: 10 μm; (C) Time series of the FRET ratio of the control group

At the same time, the loss of actin contractility promoted the decrease of tension across paxillin (Figure 12, A-C). In addition, the FRET ratio leapt at the onset of flow applied and remained increasing slowly during the shear stress application. Still, the pattern of slow increase vanished when the structure of the cytoskeleton and the actin contractility were destroyed, respectively (Figure 12, A-C). It implied that the extracellular mechanical force could be transmitted to FAs with the assistance of membrane fluidity and the cytoskeleton. Actin also functioned as a 'buffer' in the tension changes mediated by shear stress to cushion the sudden impact from external mechanical stimuli rather than a simple transmitter. In Figure 12A-B, the red arrow represented shear stress applied at zero time. # represented there was an obvious difference compared to control group (Fig. 12C). * represented there was an obvious difference between upstream and downstream (Fig. 12D). Figure 12 was compiled using Fig 4, Fig 5 from Article III and Fig 3, Fig 2-4 from Article IV.

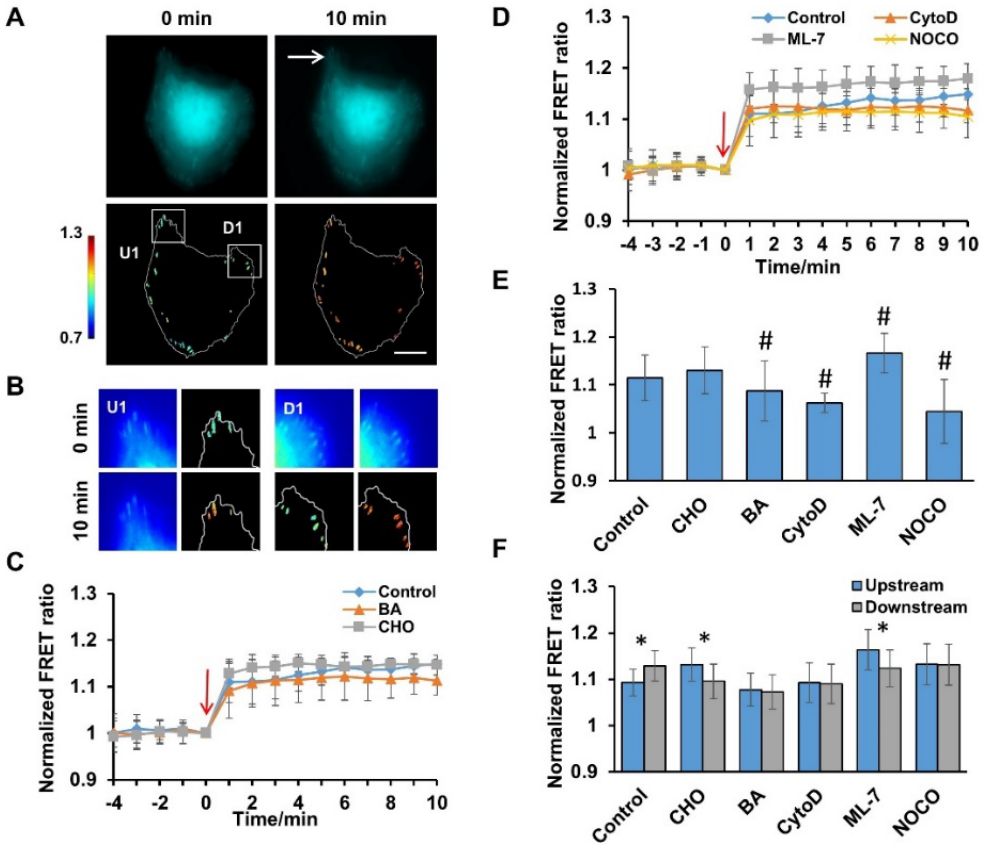

FIGURE 12 Tension across paxillin upon shear stress with different drug treatment: (A, B) Time series of FRET ratio of control group and drug treatment groups after normalization, scale bar: 20 μm; (C) Bar graph of the FRET ratio in control group and drug treatment groups after 10 min of shear stress; (D) Bar graph of the FRET ratio in the upstream and downstream regions of the control group and drug treatment groups

In summary, paxillin endured tension in living cells, regulated in a novel manner upon shear stress. In this manner, after the force was applied on the upper surface of the cell, the plasma membrane fluidity and the cytoskeleton helped the force to transmit to remote sites. The elastic network of actin served as a buffer to cushion the sudden impact caused by the extracellular mechanical force.

Contribution

Shuai Shao analyzed the data under the guidance of Timo Tiihonen, Bo Liu and Fengyu Cong; wrote the draft with Hangyu Zhang, Zhengyao Zhang, Na Li and Bo Liu. Sha Deng and Bo Liu designed the research for this paper; Sha Deng and Qingyun Jiang performed the experiments.

3.4 Article IV

Shuai Shao, Sha Deng, Fengyu Cong, Timo Tiihonen, and Bo Liu. "Mapping the distribution of tension across paxillin upon shear stress with FRET-based biosensor." Submitted to *EMBO Journal*.

Background

It has been indicated in Article III that paxillin participates in the force transferring from the extracellular to the intracellular. In addition, there is also research suggesting that cell polarity induced by mechanical factors is a result of direct force transmission. Paxillin also provides docking sites for several proteins contributing to establishing cell polarity. Taken together, it proposes a question of whether paxillin plays a role in the establishment of cell polarity. It is essential to map the tension distribution across paxillin both spatially and temporally to answer this question.

Methods

A DNA-encoded FRET biosensor named PaxTS was utilized to directly observe and measure the tension across paxillin in living cells upon shear stress. The details of the cell experiments obeyed the description in Article III. The dynamic images were analyzed by an analysis package built on the manner in Article III and further developed to characterize and track FAs to quantify the time series of force across paxillin in FAs (Figure 13). The figure was reproduced from Article IV, Fig 5.

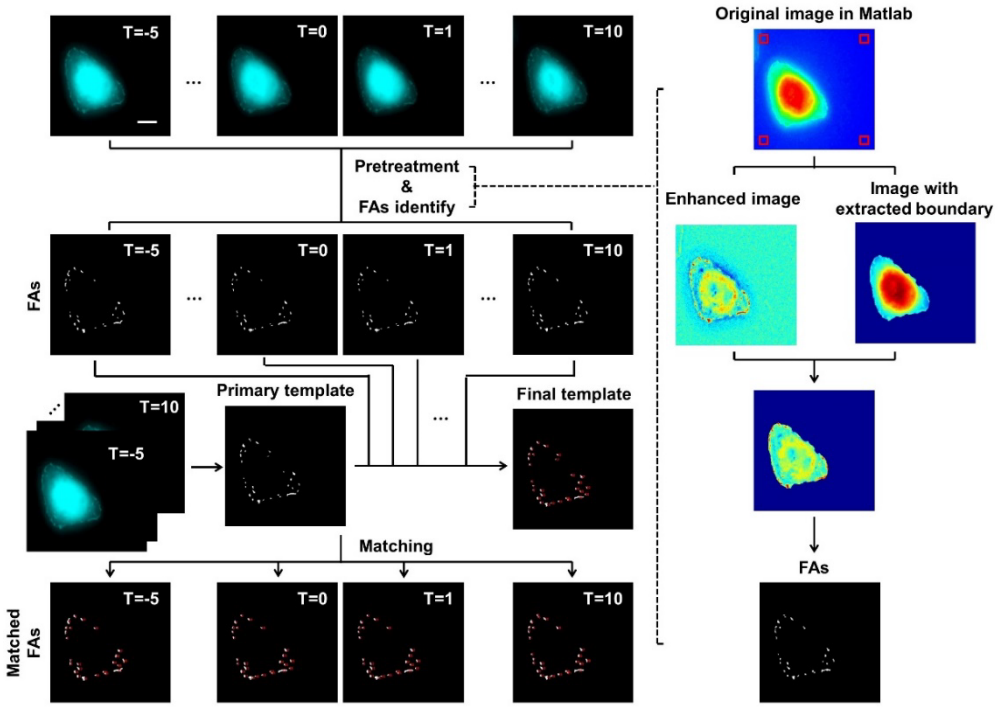

FIGURE 13 Process of FAs quantified analysis, scale bar: 20 μm

In the modified analysis method, after identifying the FA sites, the area of each FA was calculated and recorded, respectively. All the FAs were placed into two types according to their orientations. The orientation of FAs was described by classifying FAs into 'pointing' and 'parallel'. When the angle between the long axis of a FA and its closest ventral membrane edge was 90°±45°, the FA was classified as 'pointing' which was perpendicular to the edge. When the angle was 180°±45°, the FA was parallel to the edge and classified as 'parallel'. The area and orientation were considered the two parameters to characterize FAs.

After identifying FAs, FAs were tracked in the frames established by the dynamic fluorescence images. Considering the observation time was too short for dramatic cell deformation, only slight displacement would happen and could be corrected with the centroid. After position correction, the pixels contained in the corrected cell body were placed into clusters according to the intensity-time series on the pixels by K-means clustering. The intensity and characteristic of intensity changing with time were similar within FA sites and differed from the background, which contributed to the FAs identification based on the whole time series and formed a primary FA template. Each isolated FA site in the primary template was voted across the observation time to avoid the probable joining or separating effects on the time scale. If an isolated FA site were identified as several disjoint components in most frames and connected for a few frames, the site would be considered as several FAs and replaced. The time voting generated the final FA template. The FAs in one frame and the final FA template were matched according to measuring the position by Euclidean distance. If there were two or more FAs from the template matched to one FA in a frame, all these template FAs would be marked as the final match, and vice versa.

These tracked FAs were placed into two types, upstream and downstream, depending on whether the projection of a FA onto its closest ventral membrane edge belonged to the upstream membrane. The upstream membrane was defined as the part of the boundary which faced the flow directly. To determine whether a fragment of the plasma membrane was upstream or downstream, the boundary of the cell was evenly divided into zones. The length of a zone was set as 10 pixels in this work. The unit exterior normal corresponding to a zone was decomposed into two components. The component along the flow direction was regarded as the incident angle of this zone. In an ideal case, the cell boundary can be divided into two consecutive and non-overlapping parts based on the symbol of the incident angles. Considering the flow direction was from left to right in this work, the upstream membrane should be the accumulation of the zones with a positive incident angle, while the symbol of the downstream membrane was negative. However, sudden symbol changes usually occurred, which were attributed to only one zone or several consecutive zones. The probable reasons were the local branches or the discrete cell edge. Therefore, the symbol of each zone was adjusted based on the two adjacent zones until the whole cell boundary was divided into two consecutive and non-overlapping parts. When the point on the cell boundary closest to the centroid of a FA belonged to the upstream membrane,

the FA was considered an upstream FA. Otherwise, it was marked as downstream.

Main results

The results showed that the analysis approach could handle the issue of detecting and tracking FA sites when the grayscale of the image was narrow and the fluorescence intensity difference between FAs and background was small. The precise detection of the cell body and the accurate identification of FAs made it feasible to observe the relationship between the FRET ratio and the characteristics of FAs (size and orientation). Meanwhile, the analysis approach defined the upstream/downstream based on incident angles, inhibiting the effect of artificial and incidental factors on the definition of upstream/downstream.

The accurate segmentation and efficient tracking of FA sites provided the spatial and temporal information of tension distribution across paxillin. The results exhibited that the tension across paxillin does not correlate with the FA area in the static state. There was no significant tension difference between the 'pointing' FAs and the 'parallel' FA. It seemed that the tension across paxillin was not related to the inherent features of FAs.

It has been known from Article III that the tension across paxillin decreased upon shear stress. The results further showed that the tension decline occurred in a polarized manner, with a higher tension concentrated at the upstream FA sites than at the downstream sites (Figure 12D). In addition, promoting the membrane fluidity led the polar tension distribution to vanish, while inhibiting the fluidity resulted in lower tension across downstream FAs (Figure 12D). The interesting phenomenon probably contributed to the buffer of the plasma membrane to the force. Besides the membrane fluidity, destroying the cytoskeleton structure abolished the polar distribution of tension across paxillin, but inhibiting the contractility of actin led to a reversal polarity similar to decreasing the membrane fluidity (Figure 12D). It implied that the polarized manner of tension distribution across paxillin was regulated by the membrane fluidity and the cytoskeleton under shear stress application.

In summary, the model of shear stress induced-tension polarity across paxillin upon shear stress could be described as follows: once the shear stress was applied to cells, the force was sensed by the plasma membrane and transmitted to paxillin through the cytoskeleton; the upstream regions of the membrane with a gradually increasing fluidity stretched the cytoskeleton more dramatically; meanwhile, the actin filaments clustered downstream regions and buffered the force with the contractility of actomyosin; finally, the tension across paxillin upon shear stress displayed a polarized distribution with a higher tension in upstream regions and lower in downstream.

Contribution

Shuai Shao analyzed the data under the guidance of Timo Tiihonen, Bo Liu and Fengyu Cong; wrote the draft with Bo Liu. Sha Deng and Bo Liu designed the research for this paper; Sha Deng performed the experiments.

4 DISCUSSION

This work contributes to understanding how cell establishes polarity by providing an effective tool to explore the potential polarity in cells based on dynamic fluorescence images. The contributions of the thesis are summarized in this chapter from two views, mainly from the method point of view and briefly from the biological significance. Following the contributions are the research limitations and the prospects for my future research. The part related to the method will spread with the challenges in developing the tool, including how to improve the preprocessing qualify of dynamic fluorescence images and analyze different forms of polar distribution accurately and adequately.

4.1 Contributions

The thesis provides methods for analyzing and visualizing the dynamic fluorescence images to investigate the underlying pathway to activate cell polarity upon shear stress. The contributions of this work are listed in this section from the view of methodology first.

4.1.1 Improvement of preprocessing

In addition to removing interferences such as noises, the main aim of preprocessing is to extract the potential region containing the polarity information. Because of the different forms of cell polarity, the confirmation of underlying polarity regions can be summarized as two questions, how to determine the cell body for the polarity occurring in the whole cell and how to identify the specific subcellular structures for the polarity on those sites. This thesis modified the traditional means and developed new algorithms, forming two thoughts to answer these questions.

4.1.1.1 Refinement of the cell body

A two-step segmenting method is developed to determine the cell body precisely. First, Otsu's method generates a global threshold to obtain a basic cell boundary. Then, a high-pass filter processes the original image. The edge is always together with high frequency due to the sudden alteration of the grey value. The high-pass filter preserves the high-frequency component of an image to enhance the edge. The fluorescence interference along the cell profile is converted to low intensity after the high-pass filter, contrasting to the local real cell edge, which remains high intensity after filtering. K-means clustering can detect the contrast to renew the whole-cell boundary (Figure 14). The application of k-means clustering in this work will be discussed in detail later. Generally, this two-step method refines the cell edge rapidly. It also improves the accuracy in cell body detection, which is not impressed by the cell deformation and fluorescence intensity level of the image.

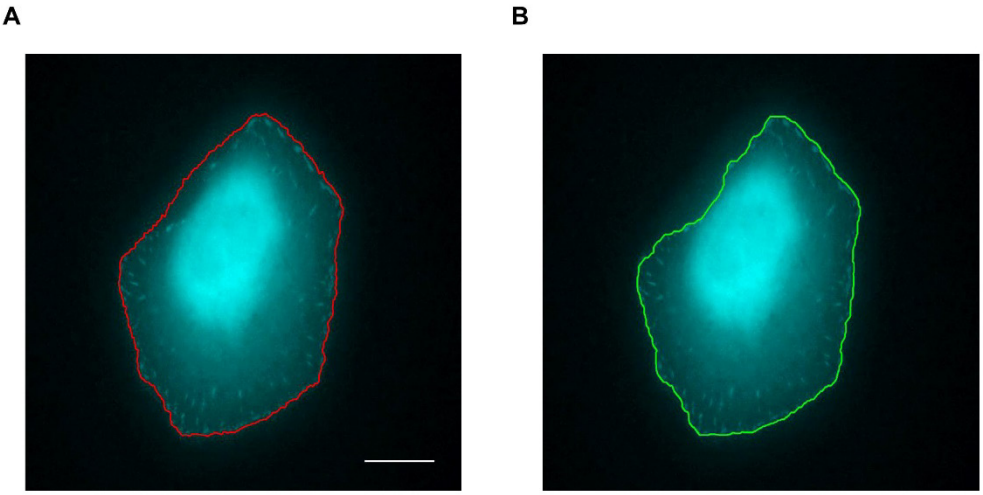

FIGURE 14 Cell body detection on a live-cell image, scale bar: 20 μm: (A) Detected cell body by the Otsu's threshold (*red*); (B) Refined cell body (*green*)

4.1.1.2 Identification of FAs

Besides improving the accuracy of cell body detection by modifying the traditional method, a new algorithm is developed to identify FAs to overcome the defects of the water algorithm, the most popular method in FA identification for now.

The essence of FAs identification can be described as finding the pixels with similar fluorescence intensity. Thus, it is appropriate for the K-means clustering to address this issue. K-means clustering is unsupervised learning, organizing the pixels in an image into groups or clusters with similar values. A high-pass filter further improves the grey difference between FAs and background, and the k-means clustering automatically organizes the pixels into clusters with similar values. The FA sites show higher fluorescence intensity and can be detected easily by k-means clustering without knowing the information about the

background. The cluster containing the FA sites is chosen as the cluster with the highest mean intensity value. Observing the clustering results is the main approach to obtaining the proper clustering number. The clustering result is not very sensitive to the clustering number within a certain range. For example, the correct clustering number for this image is considered five, while in fact, the clustering results are similar when the clustering number ranges from 4 to 7 (Figure 15).

The new algorithm to segment FAs from the background with k-means clustering simplifies the identification of FAs. It is robust for the expression level of biosensor and different practices of silencing the endogenous protein, performs well on a narrow gray scale, and lowers the difficulty to identify FAs.

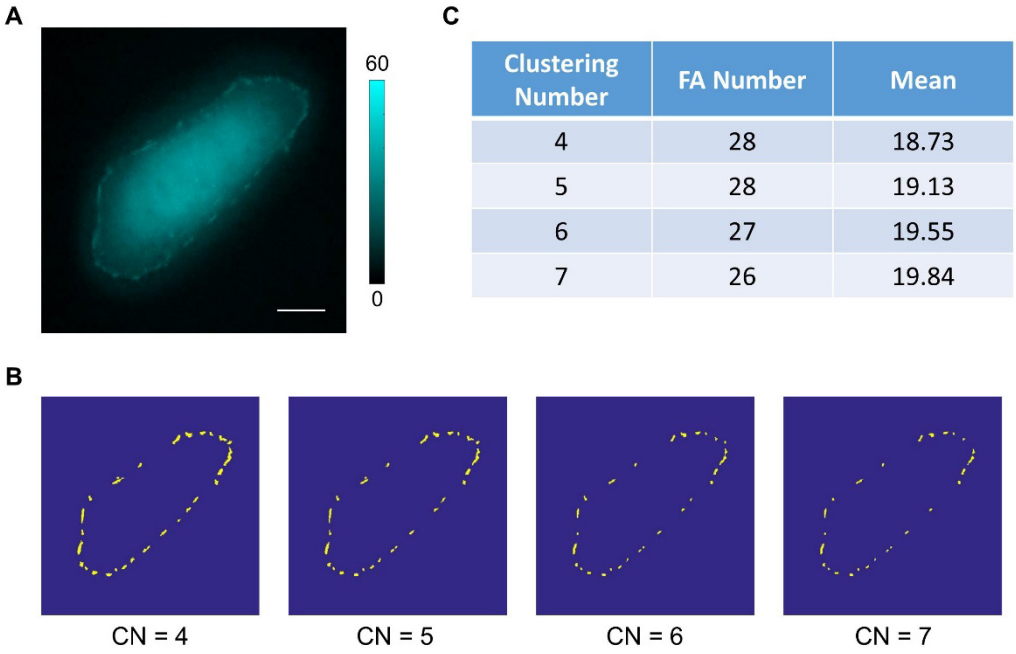

FIGURE 15 Clustering results with different clustering numbers: (A) Live-cell image, scale bar: 20 μm; (B) Clustering results with different clustering numbers (CN); (C) Number of identified FAs in the image and the mean fluorescence intensity at the FA sites

4.1.2 Quantitative definition of upstream/downstream

As mentioned in Section 2.4, the existing methods for the polarity analysis are scarce. An open problem is how to define and select the upstream and downstream regions, respectively. This thesis gives two solutions to answer the question based on different modes of cell polarity.

The first approach aims at polarity, distributing widely on the plasma membrane or in the cytoplasm upon shear stress. In this case, polarity analysis should consider the cell as a whole. The cell is divided into zones equally along the direction of shear stress. The upstream region is defined as several zones close to the source of shear stress, while the downstream region is the several zones on

the remote side along the direction of shear stress. The polarity can be detected by whether there is a fluorescence intensity for the FRET ratio difference between upstream and downstream and visualized through a spatial-temporal map. The map comprises the zone data from each frame in the dynamic fluorescence images. Both the time and locations of the polarity occurrence are visible on the map. Based on this method, some mathematical fitting can be applied to the zone data to further descript and evaluate the polarity. It is unnecessary to choose ROI in this method. Thus, it avoids the potential omission of upstream/downstream regions and the misalignment of ROI caused by cell growth, deformation, and migration. However, it is notable that this approach is not suitable for the issues related to actual physical distance because it leads to measurements relative to the cell length scale.

The second approach targets the tension across paxillin suspected to be polarized upon shear stress by identifying the FAs as upstream FA or downstream FA. First, the cell outline is divided into zones with the same width, and the incident angle is calculated based on the orientation of the boundary fragment in each zone. Hence, the outline can be divided into two parts, the edge facing the shear stress and the rear edge opposite the facing edge. It will be considered an upstream flow if a FA is nearer to the facing edge than the rear edge. Otherwise, it will be a downstream FA. This method determines the upstream and downstream mainly by the orientation between cell edge and shear stress direction, instead of only depending on the location relative to the core or centroid. It still performs well when the shape of cells is complex, inhibits the effect of artificial and incidental factors to the definition of upstream/downstream, and provides a manner to connect the tension across paxillin upon shear stress with the mechanical force directly.

Generally, the approaches mentioned in this thesis improve the accuracy of cell body detection when the fluorescence intensity around the cell profile is uneven, lower the difficulty to identify FAs when the grayscale of the image is narrow, and define the upstream/downstream with numerical calculation to adapt to two different types of polarity. It contributes to excavating the biological information hidden in dynamic fluorescence images and further advances the application of live-cell imaging techniques in cell polarity research.

4.1.3 Biological contribution

Based on the above methods, the thesis proposes insights into establishing of shear stress-induced polarity. In this thesis, the occurrence of cell polarity is regarded to be dependent on the direct transmission of intracellular force. The model to describe how cell polarity occurs can be described as follows: the shear stress is applied on the upper surface of the cell, which causes the cytoskeleton to be stretched to convert the extracellular mechanical signals to intracellular force. The intracellular force is transmitted to remote sites (e.g., FAs), resulting in the tension across some specific protein (e.g., paxillin) polarized in spatial. The polar distribution of tension provides spatial information for downstream signals (e.g., RhoGDIα). The downstream signals continue to activate the subsequent

signals to establish cell polarity by proteins such as Rho family GTPases. In this process, the elastic structure and dynamic of the cytoskeleton and the membrane fluidity serve as buffers to attenuate the mechanical impact sensed by cells instead of only sensing or transmitting the force.

4.2 Limitations and future research

Even though the methods proposed in this thesis and the results obtained are encouraging, the work still suffers some limitations.

Firstly, the method in Articles I and II to analyze the polarity, which distributes widely in the whole cell, pays attention to the dimension along the shear stress direction. However, there is still information hidden in the other dimension, which is currently ignored. For instance, the method to classify the upstream and downstream regions ignores the cell shape, mainly focusing on the dimension of flow direction. The polarity sometimes occurs at small branches, but the locations of small branches are sometimes not at the furthest edges on the dimension of shear stress direction. With the method depending on zones, the small branches are probably mistaken as belonging to middle zones. As a result, the zones chosen as upstream and downstream regions may not entirely cover the actual area where polarity occurs. However, selecting multiple zones can minimize the error but not eliminate it. In fact, in particle analysis, the effect of the cell shape on the division of upstream and downstream is more complicated. It involves an issue of whether a local downstream is a downstream even if it is not an absolute downstream on the level of the whole cell. It is probably a question with different answers in different cases, considering the observation target and the analyzing requirements. There are still more complex cases that need to be discussed.

Secondly, two-dimensional fluorescence images are unable to give information on the dimension of cell thickness. Therefore, there is an implicit assumption based on fluorescence images for the analysis. It tacitly approves that the thickness is always the same for the whole cell and has no apparent effect on the fluorescence. The assumption believes that the cell height is small enough, and the changes in height are negligible compared to the scale of cell length and width when the cell adheres to EMC fully and is in a good state. However, in practice, the cell thickness distributes unevenly. It probably interferes with the fluorescence signals.

Similarly, another assumption is that the magnitude of the cell polarity is independent of the cell size when applying the zone method to analyze the data. The zones convert the actual physical distance to relative distance, which considers the polarity as a function between the extracellular shear stress and several biochemical parameters of the cell but not of the characteristic dimensions of the cell. This thesis proposes a view that the extracellular shear stress induces cell polarity through the plasma membrane and cytoskeleton. These two structures can transmit force and buffer external force's impact on the cell,

playing vital roles. However, the dimensional cell characteristics are probably related to the membrane features and the cytoskeleton state. The characteristic dimensions of the cell may affect the mechanical characteristics of the plasma membrane and cytoskeleton, such as the ability to buffer the external shear stress. Hence, the validation of the assumption still needs to be considered in more elaborate mechanical models.

The above problems are waiting for answers and the main research objectives in future research. Generally, I plan to continue my work on fluorescence images, including the design of new biosensors and the establishment of methodology around the analysis of images based on new biosensors, offering more efficient tools to those who major in cell biology but are unfamiliar with the FP-fused biosensors and the analysis methods applying to dynamic fluorescence images.

5 CONCLUSION

This thesis considers the issue of analyzing dynamic fluorescence images for polarity information as independent work for the first time. It develops a set of methods to analyze the dynamic fluorescence images and visualize the hidden polarity information by synthesizing different algorithms. The methods detect the cell body more precisely and identify FAs without prior knowledge in a narrow grayscale, improving the accuracy and reliability of the pretreatment. It also proposes two new manners to identify the upstream and downstream regions for the quantitative polarity analysis. One normalizes the cell length along the shear stress direction to describe the polarity positions with values relative to the rear and leading edge. The other considers the relative orientation between the cell edge and the flow direction by calculating the local incident angle. Combing these methods, the thesis offers an effective and reliable tool for cell polarity based on dynamic fluorescence images. With the tool, the results indicate a pathway for intracellular force transmitting to remote sites, such as FAs, by cytoskeleton with the assistance of membrane fluidity to activate cell polarity.

This work provides an effective tool for analyzing dynamic fluorescence images and visualizing the intracellular polar distribution. From a broader perspective, it promotes the application of techniques related to fluorescent proteins in exploring cellular processes, provides new insights to explain how the cell polarity is established, and further advances the understanding of the mechanotransduction occurring in cells.

YHTEENVETO (SUMMARY IN FINNISH)

Solut ovat kaikkien elävien organismien perusrakenteita, ja organismien toiminta perustuu viimekädessä siihen, miten solut vuorovaikuttavat ympäristönsä kanssa. Solun ja ympäristön välinen vuorovaikutus on harvoin homogeenista solun koko pinnalla vaan ympäristön vaikutus (mekaaninen kuormitus, aineenvaihdunta solun pinnan läpi) on profiloitunut jollakin tapaa. Tällöin on luonnollista kysyä, miten solun sisäinen toiminta riippuu tästä ulkoisen ärsykkeen profiilista, miten solu polarisoituu sisäisesti ulkoisten vaikutusten seurauksena. Viimekädessä sekä normaalit fysiologiset ominaisuudet että erilaiset patologiset ilmiöt, kuten syöpäsolujen leviäminen, perustuvat pohjimmiltaan solujen polaarisuuteen.

Solun sisäisen toiminnan mittaaminen, etenkin kun tavoite on pitää solut elossa mittaussarjan aikana, on varsin vaativaa. Viime vuosina on yleistynyt fluoresenssiin perustuva mittaaminen. Siinä solun sisäisiä kemiallisia yhdisteitä korvataan keinotekoisilla yhdisteillä, jotka fluoresoituvat, kun niihin kohdistetaan valoa. Näin pystytään havainnoimaan yhdisteiden konsentraatioita solun sisällä. Mekaanisen kuormituksen seuraamiseen pelkkä fluoresenssi ei riitä. Tähän soveltuu kuitenkin kahden fluoresoituvan yhdisteen väliseen resonanssiin ja energian siirtoon perustuva FRET (fluorescence resonance energy transfer) teknologia. Se perustuu fluoresoituvien osien välisen etäisyyden ja fluoresenssin voimakkuuden väliseen riippuvuuteen, joka antaa epäsuoran mahdollisuuden mitata räätälöityjen proteiiniketjujen venymää mekaanisen kuormituksen vaikutuksesta.

Fluoresoituviin proteiineihin perustuvat biosensorit pystyvät seuraamaan elävän, mekaanisesti kuormitetun, solun proteiinien dynamiikkaa. Tämä mahdollistaa solun sisäisten prosessien monitoroinnin ja avaa näkymiä tähän asti tuntemattomiin mekanismeihin, joilla solut reagoivat ulkoiseen kuormitukseen, mikäli biosensorien signaaleja osataan tulkita luotettavasti.

Fluoresenssiin perustuvan kuvantamisen signaalit ovat heikkoja ja kohinaisia ja edellyttävät esikäsittelyä ennen analyysiä. Esikäsittely auttaa sekä tunnistamaan solun ja sen alarakenteiden tarkan sijainnin, että erottamaan kiinnostavat fluoresenssisignaalit taustakohinasta. Esikäsittelyn osalta työssä tehostettiin jo aiemmin hyödynnettyä Otsun menetelmää hyödyntämällä reunojen korostamista ylipäästösuotimilla. Näin saatiin aiempaa tarkempia mittauksia solun muodosta. Solun sisäisten rakenteiden, kuten fokaalisten liitosten, tunnistamiseen sovellettiin K-means klusterointimenetelmää, aiemman, tutkijan subjektiiviseen arvioon perustuneen menettelyn sijaan. Tämä paransi rakenteiden tunnistamisen tarkkuutta ja luotettavuutta.

Työn keskeinen tavoite oli tutkia, ensimmäistä kertaa systemaattisesti, solun sisäistä polaarisuutta ja sen eri mekanismeja. Karkealla tasolla mekanismit jakautuvat solutasoiseen polaarisuuteen, jossa polaarisuus ilmenee käytännössä solunesteessä ja solukalvon pinnalla, sekä solun tukirakenteisiin rajautuvaan polaarisuuteen, joka ilmenee jännityksenä sisäisissä tukirakenteissa ja niiden liitok-

sissa. Solutason polaarisuuden havainnoinnissa keskeiset haasteet liittyivät solujen koko- ja muotoeroihin. Kokoerot huomioitiin jakamalla solu kuormituksen suunnassa vakiomäärään vyöhykkeitä ja keskiarvoistamalla solut poikkisuuntaan. Näin alkuperäiset 2+1 -ulotteiset aikasarjat eri muotoisille soluille normalisoitiin 1+1 -ulotteisiksi vakiomuotoisiksi aikasarjoiksi, jotka mahdollistivat systemaattisen tilastollisen analyysin polarisaatioon vaikuttavien tekijöiden suhteen. Sisäisiä tukirakenteita yhdistävien fokaalien liitosten analyysissä puolestaan havaittu fluoresenssi, ja sitä kautta epäsuorasti havaittu proteiiniketjujen venymä suhteutettiin solun seinämän ja ulkoisen kuormituksen väliseen kohtauskulmaan. Näin voitiin tunnistaa paikallisesti kuormituksen suunta ja suhteuttaa se havaintoihin tavalla, joka mahdollisti eri tekijöiden vaikutuksen analysoinnin solun sisäisiin mekaanisiin voimiin.

Yhteenvetona, työssä käsitellään ensimmäistä kertaa solun polaarisuuden analyysiä dynaamisen fluoresenssikuvauksen avulla omana tutkimusongelmanaan. Polaarisuuden havainnointiin kehitettiin menetelmäkokonaisuus, joka soveltuu sekä solutason että solun alarakenteiden polarisoitumismekanismien analyysiin, parantaa tarkkuutta ja luotettavuutta suhteessa aiempiin menetelmiin ja soveltuu niin solun sisäisen kuin solun pintarakenteisiin liittyvän polaarisuuden analysointiin. Työ tukee fluoresoituvien proteiinien hyödyntämistä solutason prosessien tutkimuksessa, lisää ymmärrystä solun polaarisuuden syntymekanismeista ja yleisemminkin mekaanisten voimien vaikutuksesta soluihin.

REFERENCES

Algar, W. R., Hildebrandt, N., Vogel, S. S., & Medintz, I. L. (2019). FRET as a biomolecular research tool - understanding its potential while avoiding pitfalls. *Nat Methods, 16*(9), 815-829. https://doi.org/10.1038/s41592-019-0530-8

Ballabio, A., & Bonifacino, J. S. (2020). Lysosomes as dynamic regulators of cell and organismal homeostasis. *Nat Rev Mol Cell Biol, 21*(2), 101-118. https://doi.org/10.1038/s41580-019-0185-4

Berginski, M. E., Vitriol, E. A., Hahn, K. M., & Gomez, S. M. (2011). High-resolution quantification of focal adhesion spatiotemporal dynamics in living cells. *PLoS One, 6*(7), e22025. https://doi.org/10.1371/journal.pone.0022025

Berney, C., & Danuser, G. (2003). FRET or no FRET: a quantitative comparison. *Biophys J, 84*(6), 3992-4010. https://doi.org/10.1016/s0006-3495(03)75126-1

Biskou, O., Casanova, V., Hooper, K. M., Kemp, S., Wright, G. P., Satsangi, J., Barlow, P. G., & Stevens, C. (2019). The type III intermediate filament vimentin regulates organelle distribution and modulates autophagy. *PLoS One, 14*(1), e0209665. https://doi.org/10.1371/journal.pone.0209665

Butler, P. J., Norwich, G., Weinbaum, S., & Chien, S. (2001). Shear stress induces a time- and position-dependent increase in endothelial cell membrane fluidity. *Am J Physiol Cell Physiol, 280*(4), C962-969. https://doi.org/10.1152/ajpcell.2001.280.4.C962

Chen, S. J., Sinsuebphon, N., & Intes, X. (2015). Assessment of Gate Width Size on Lifetime-Based Forster Resonance Energy Transfer Parameter Estimation. *Photonics, 2*(4), 1027-1042. https://doi.org/10.3390/photonics2041027

Chowdhury, F., Huang, B., & Wang, N. (2021). Cytoskeletal prestress: The cellular hallmark in mechanobiology and mechanomedicine. *Cytoskeleton (Hoboken), 78*(6), 249-276. https://doi.org/10.1002/cm.21658

Chudakov, D. M., Matz, M. V., Lukyanov, S., & Lukyanov, K. A. (2010). Fluorescent proteins and their applications in imaging living cells and tissues. *Physiol Rev, 90*(3), 1103-1163. https://doi.org/10.1152/physrev.00038.2009

Collins, C., & Tzima, E. (2014). Rac[e] to the pole: setting up polarity in endothelial cells. *Small GTPases, 5*, e28650. https://doi.org/10.4161/sgtp.28650

Deal, J., Annamdevula, N., Pleshinger, D. J., Griswold, J. R., Odom, A., Tayara, A., Lall, M., Browning, C., Parker, M., Rich, T. C., & Leavesley, S. J. (2020). Comparison of spectral FRET microscopy approaches for single-cell analysis. *Proc SPIE Int Soc Opt Eng, 11243*. https://doi.org/10.1117/12.2546308

Duff, D., & Long, A. (2017). Roles for RACK1 in cancer cell migration and invasion. *Cell Signal, 35*, 250-255. https://doi.org/10.1016/j.cellsig.2017.03.005

Edelhoch, H., Brand, L., & Wilchek, M. (1967). Fluorescence studies with tryptophyl peptides. *Biochemistry, 6*(2), 547-559. https://doi.org/10.1021/bi00854a024

Eichorst, J. P., Lu, S., Xu, J., & Wang, Y. (2008). Differential RhoA dynamics in migratory and stationary cells measured by FRET and automated image analysis. *PLoS One, 3*(12), e4082. https://doi.org/10.1371/journal.pone.0004082

Emmott, E., Jovanovic, M., & Slavov, N. (2019). Ribosome Stoichiometry: From Form to Function. *Trends Biochem Sci, 44*(2), 95-109. https://doi.org/10.1016/j.tibs.2018.10.009

Esposito, A. (2020). How many photons are needed for FRET imaging? *Biomed Opt Express, 11*(2), 1186-1202. https://doi.org/10.1364/BOE.379305

Fletcher, D. A., & Mullins, R. D. (2010). Cell mechanics and the cytoskeleton. *Nature, 463*(7280), 485-492. https://doi.org/10.1038/nature08908

Garoffolo, G., & Pesce, M. (2021). Vascular dysfunction and pathology: focus on mechanical forces. *Vasc Biol, 3*(1), R69-R75. https://doi.org/10.1530/VB-21-0002

Gould, N. R., Torre, O. M., Leser, J. M., & Stains, J. P. (2021). The cytoskeleton and connected elements in bone cell mechano-transduction. *Bone, 149*, 115971. https://doi.org/10.1016/j.bone.2021.115971

Grashoff, C., Hoffman, B. D., Brenner, M. D., Zhou, R., Parsons, M., Yang, M. T., McLean, M. A., Sligar, S. G., Chen, C. S., Ha, T., & Schwartz, M. A. (2010). Measuring mechanical tension across vinculin reveals regulation of focal adhesion dynamics. *Nature, 466*(7303), 263-266. https://doi.org/10.1038/nature09198

Head, B. P., Patel, H. H., & Insel, P. A. (2014). Interaction of membrane/lipid rafts with the cytoskeleton: impact on signaling and function: membrane/lipid rafts, mediators of cytoskeletal arrangement and cell signaling. *Biochim Biophys Acta, 1838*(2), 532-545. https://doi.org/10.1016/j.bbamem.2013.07.018

Hohmann, T., & Dehghani, F. (2019). The Cytoskeleton-A Complex Interacting Meshwork. *Cells, 8*(4). https://doi.org/10.3390/cells8040362

Hu, Y. L., Lu, S., Szeto, K. W., Sun, J., Wang, Y., Lasheras, J. C., & Chien, S. (2014). FAK and paxillin dynamics at focal adhesions in the protrusions of migrating cells. *Sci Rep, 4*, 6024. https://doi.org/10.1038/srep06024

Janota, C. S., Calero-Cuenca, F. J., & Gomes, E. R. (2020). The role of the cell nucleus in mechanotransduction. *Curr Opin Cell Biol, 63*, 204-211. https://doi.org/10.1016/j.ceb.2020.03.001

Janson, M. E., de Dood, M. E., & Dogterom, M. (2003). Dynamic instability of microtubules is regulated by force. *J Cell Biol, 161*(6), 1029-1034. https://doi.org/10.1083/jcb.200301147

Jares-Erijman, E. A., & Jovin, T. M. (2003). FRET imaging. *Nat Biotechnol, 21*(11), 1387-1395. https://doi.org/10.1038/nbt896

Katoh, M. (2005). WNT/PCP signaling pathway and human cancer (review). *Oncol Rep, 14*(6), 1583-1588.

Kirchhoff, H. (2019). Chloroplast ultrastructure in plants. *New Phytol, 223*(2), 565-574. https://doi.org/10.1111/nph.15730
Kraynov, V. S., Chamberlain, C., Bokoch, G. M., Schwartz, M. A., Slabaugh, S., & Hahn, K. M. (2000). Localized Rac activation dynamics visualized in living cells. *Science, 290*(5490), 333-337. https://doi.org/10.1126/science.290.5490.333
Kreis, S., Schonfeld, H. J., Melchior, C., Steiner, B., & Kieffer, N. (2005). The intermediate filament protein vimentin binds specifically to a recombinant integrin alpha2/beta1 cytoplasmic tail complex and co-localizes with native alpha2/beta1 in endothelial cell focal adhesions. *Exp Cell Res, 305*(1), 110-121. https://doi.org/10.1016/j.yexcr.2004.12.023
Kulkarni-Gosavi, P., Makhoul, C., & Gleeson, P. A. (2019). Form and function of the Golgi apparatus: scaffolds, cytoskeleton and signalling. *FEBS Lett, 593*(17), 2289-2305. https://doi.org/10.1002/1873-3468.13567
LaCroix, A. S., Rothenberg, K. E., Berginski, M. E., Urs, A. N., & Hoffman, B. D. (2015). Construction, imaging, and analysis of FRET-based tension sensors in living cells. *Methods Cell Biol, 125*, 161-186. https://doi.org/10.1016/bs.mcb.2014.10.033
Le Roux, A. L., Quiroga, X., Walani, N., Arroyo, M., & Roca-Cusachs, P. (2019). The plasma membrane as a mechanochemical transducer. *Philos Trans R Soc Lond B Biol Sci, 374*(1779), 20180221. https://doi.org/10.1098/rstb.2018.0221
Legerstee, K., Geverts, B., Slotman, J. A., & Houtsmuller, A. B. (2019). Dynamics and distribution of paxillin, vinculin, zyxin and VASP depend on focal adhesion location and orientation. *Sci Rep, 9*(1), 10460. https://doi.org/10.1038/s41598-019-46905-2
Liu, B., Lu, S., Hu, Y. L., Liao, X., Ouyang, M., & Wang, Y. (2014). RhoA and membrane fluidity mediates the spatially polarized Src/FAK activation in response to shear stress. *Sci Rep, 4*, 7008. https://doi.org/10.1038/srep07008
Lo, W. Y., & Puchalski, S. M. (2008). Digital image processing. *Vet Radiol Ultrasound, 49*(1 Suppl 1), S42-47. https://doi.org/10.1111/j.1740-8261.2007.00333.x
Lu, K., Vu, C. Q., Matsuda, T., & Nagai, T. (2019). Fluorescent Protein-Based Indicators for Functional Super-Resolution Imaging of Biomolecular Activities in Living Cells. *Int J Mol Sci, 20*(22). https://doi.org/10.3390/ijms20225784
Lu, S., Kim, T. J., Chen, C. E., Ouyang, M., Seong, J., Liao, X., & Wang, Y. (2011). Computational analysis of the spatiotemporal coordination of polarized PI3K and Rac1 activities in micro-patterned live cells. *PLoS One, 6*(6), e21293. https://doi.org/10.1371/journal.pone.0021293
Lu, S., Seong, J., Wang, Y., Chang, S. C., Eichorst, J. P., Ouyang, M., Li, J. Y., Chien, S., & Wang, Y. (2014). Decipher the dynamic coordination between enzymatic activity and structural modulation at focal adhesions in living cells. *Sci Rep, 4*, 5756. https://doi.org/10.1038/srep05756

Magalhaes, M. A., Zhu, F., Sarantis, H., Gray-Owen, S. D., Ellen, R. P., & Glogauer, M. (2007). Expression and translocation of fluorescent-tagged p21-activated kinase-binding domain and PH domain of protein kinase B during murine neutrophil chemotaxis. *J Leukoc Biol, 82*(3), 559-566. https://doi.org/10.1189/jlb.0207126

Martinac, B., & Poole, K. (2018). Mechanically activated ion channels. *Int J Biochem Cell Biol, 97*, 104-107. https://doi.org/10.1016/j.biocel.2018.02.011

Matveeva, E. A., Venkova, L. S., Chernoivanenko, I. S., & Minin, A. A. (2015). Vimentin is involved in regulation of mitochondrial motility and membrane potential by Rac1. *Biol Open, 4*(10), 1290-1297. https://doi.org/10.1242/bio.011874

Mishra, M., Tiwari, S., & Gomes, A. V. (2017). Protein purification and analysis: next generation Western blotting techniques. *Expert Rev Proteomics, 14*(11), 1037-1053. https://doi.org/10.1080/14789450.2017.1388167

Na, S., Collin, O., Chowdhury, F., Tay, B., Ouyang, M., Wang, Y., & Wang, N. (2008). Rapid signal transduction in living cells is a unique feature of mechanotransduction. *Proc Natl Acad Sci U S A, 105*(18), 6626-6631. https://doi.org/10.1073/pnas.0711704105

Nekrasova, O. E., Mendez, M. G., Chernoivanenko, I. S., Tyurin-Kuzmin, P. A., Kuczmarski, E. R., Gelfand, V. I., Goldman, R. D., & Minin, A. A. (2011). Vimentin intermediate filaments modulate the motility of mitochondria. *Mol Biol Cell, 22*(13), 2282-2289. https://doi.org/10.1091/mbc.E10-09-0766

Nelson, W. J. (2009). Remodeling epithelial cell organization: transitions between front-rear and apical-basal polarity. *Cold Spring Harb Perspect Biol, 1*(1), a000513. https://doi.org/10.1101/cshperspect.a000513

Nicolson, G. L., & Ferreira de Mattos, G. (2021). A Brief Introduction to Some Aspects of the Fluid-Mosaic Model of Cell Membrane Structure and Its Importance in Membrane Lipid Replacement. *Membranes (Basel), 11*(12). https://doi.org/10.3390/membranes11120947

Ohi, R., & Zanic, M. (2016). Ahead of the Curve: New Insights into Microtubule Dynamics. *F1000Res, 5*. https://doi.org/10.12688/f1000research.7439.1

Orr, A. W., Helmke, B. P., Blackman, B. R., & Schwartz, M. A. (2006). Mechanisms of mechanotransduction. *Dev Cell, 10*(1), 11-20. https://doi.org/10.1016/j.devcel.2005.12.006

Otsu, N. (1979). A Threshold Selection Method from Gray-Level Histograms. *IEEE Transactions on Systems, Man, and Cybernetics, 9*(1), 62-66. https://doi.org/10.1109/TSMC.1979.4310076

Padilla-Parra, S., & Tramier, M. (2012). FRET microscopy in the living cell: different approaches, strengths and weaknesses. *Bioessays, 34*(5), 369-376. https://doi.org/10.1002/bies.201100086

Palmer, A. E., & Tsien, R. Y. (2006). Measuring calcium signaling using genetically targetable fluorescent indicators. *Nat Protoc, 1*(3), 1057-1065. https://doi.org/10.1038/nprot.2006.172

Piroli, M. E., Blanchette, J. O., & Jabbarzadeh, E. (2019). Polarity as a physiological modulator of cell function. *Front Biosci (Landmark Ed), 24*, 451-462. https://doi.org/10.2741/4728
Piston, D. W., & Kremers, G. J. (2007). Fluorescent protein FRET: the good, the bad and the ugly. *Trends Biochem Sci, 32*(9), 407-414. https://doi.org/10.1016/j.tibs.2007.08.003
Poh, Y. C., Na, S., Chowdhury, F., Ouyang, M., Wang, Y., & Wang, N. (2009). Rapid activation of Rac GTPase in living cells by force is independent of Src. *PLoS One, 4*(11), e7886. https://doi.org/10.1371/journal.pone.0007886
Pralle, A. (2020). Modulation and dynamics of cell membrane heterogeneities. *Chem Phys Lipids, 233*, 105006. https://doi.org/10.1016/j.chemphyslip.2020.105006
Qiao, Y., Luo, Y., Long, N., Xing, Y., & Tu, J. (2021). Single-Molecular Forster Resonance Energy Transfer Measurement on Structures and Interactions of Biomolecules. *Micromachines (Basel), 12*(5). https://doi.org/10.3390/mi12050492
Roger, A. J., Munoz-Gomez, S. A., & Kamikawa, R. (2017). The Origin and Diversification of Mitochondria. *Curr Biol, 27*(21), R1177-R1192. https://doi.org/10.1016/j.cub.2017.09.015
Rotty, J. D., & Bear, J. E. (2014). Competition and collaboration between different actin assembly pathways allows for homeostatic control of the actin cytoskeleton. *Bioarchitecture, 5*(1-2), 27-34. https://doi.org/10.1080/19490992.2015.1090670
Ruggiero, C., & Lalli, E. (2021). Targeting the cytoskeleton against metastatic dissemination. *Cancer Metastasis Rev, 40*(1), 89-140. https://doi.org/10.1007/s10555-020-09936-0
Schwarz, D. S., & Blower, M. D. (2016). The endoplasmic reticulum: structure, function and response to cellular signaling. *Cell Mol Life Sci, 73*(1), 79-94. https://doi.org/10.1007/s00018-015-2052-6
Sept, D., Xu, J., Pollard, T. D., & McCammon, J. A. (1999). Annealing accounts for the length of actin filaments formed by spontaneous polymerization. *Biophys J, 77*(6), 2911-2919. https://doi.org/10.1016/s0006-3495(99)77124-9
Shimomura, O., Johnson, F. H., & Saiga, Y. (1962). Extraction, purification and properties of aequorin, a bioluminescent protein from the luminous hydromedusan, Aequorea. *J Cell Comp Physiol, 59*, 223-239. https://doi.org/10.1002/jcp.1030590302
Shrestha, D., Jenei, A., Nagy, P., Vereb, G., & Szollosi, J. (2015). Understanding FRET as a research tool for cellular studies. *Int J Mol Sci, 16*(4), 6718-6756. https://doi.org/10.3390/ijms16046718
Singer, S. J., & Nicolson, G. L. (1972). The fluid mosaic model of the structure of cell membranes. *Science, 175*(4023), 720-731. https://doi.org/10.1126/science.175.4023.720
Srinivasan, S., Wang, F., Glavas, S., Ott, A., Hofmann, F., Aktories, K., Kalman, D., & Bourne, H. R. (2003). Rac and Cdc42 play distinct roles in regulating

PI(3,4,5)P3 and polarity during neutrophil chemotaxis. *J Cell Biol, 160*(3), 375-385. https://doi.org/10.1083/jcb.200208179

Stephens, A. D., Banigan, E. J., & Marko, J. F. (2019). Chromatin's physical properties shape the nucleus and its functions. *Curr Opin Cell Biol, 58*, 76-84. https://doi.org/10.1016/j.ceb.2019.02.006

Steward, A. J., & Kelly, D. J. (2015). Mechanical regulation of mesenchymal stem cell differentiation. *J Anat, 227*(6), 717-731. https://doi.org/10.1111/joa.12243

Suzuki, T., Zhang, J., Miyazawa, S., Liu, Q., Farzan, M. R., & Yao, W. D. (2011). Association of membrane rafts and postsynaptic density: proteomics, biochemical, and ultrastructural analyses. *J Neurochem, 119*(1), 64-77. https://doi.org/10.1111/j.1471-4159.2011.07404.x

Trepat, X., Chen, Z., & Jacobson, K. (2012). Cell migration. *Compr Physiol, 2*(4), 2369-2392. https://doi.org/10.1002/cphy.c110012

Tschumperlin, D. J. (2011). Mechanotransduction. *Compr Physiol, 1*(2), 1057-1073. https://doi.org/10.1002/cphy.c100016

Tsuruta, D., & Jones, J. C. (2003). The vimentin cytoskeleton regulates focal contact size and adhesion of endothelial cells subjected to shear stress. *J Cell Sci, 116*(Pt 24), 4977-4984. https://doi.org/10.1242/jcs.00823

Tzima, E., Kiosses, W. B., del Pozo, M. A., & Schwartz, M. A. (2003). Localized cdc42 activation, detected using a novel assay, mediates microtubule organizing center positioning in endothelial cells in response to fluid shear stress. *J Biol Chem, 278*(33), 31020-31023. https://doi.org/10.1074/jbc.M301179200

Uda, Y., Azab, E., Sun, N., Shi, C., & Pajevic, P. D. (2017). Osteocyte Mechanobiology. *Curr Osteoporos Rep, 15*(4), 318-325. https://doi.org/10.1007/s11914-017-0373-0

Verma, D., Meng, F., Sachs, F., & Hua, S. Z. (2015). Flow-induced focal adhesion remodeling mediated by local cytoskeletal stresses and reorganization. *Cell Adh Migr, 9*(6), 432-440. https://doi.org/10.1080/19336918.2015.1089379

Wang, Y., Shyy, J. Y., & Chien, S. (2008). Fluorescence proteins, live-cell imaging, and mechanobiology: seeing is believing. *Annu Rev Biomed Eng, 10*, 1-38. https://doi.org/10.1146/annurev.bioeng.010308.161731

Wu, Y., Zhang, K., Seong, J., Fan, J., Chien, S., Wang, Y., & Lu, S. (2016). In-situ coupling between kinase activities and protein dynamics within single focal adhesions. *Sci Rep, 6*, 29377. https://doi.org/10.1038/srep29377

Yang, F., Moss, L. G., & Phillips, G. N., Jr. (1996). The molecular structure of green fluorescent protein. *Nat Biotechnol, 14*(10), 1246-1251. https://doi.org/10.1038/nbt1096-1246

Yang, J., Mani, S. A., Donaher, J. L., Ramaswamy, S., Itzykson, R. A., Come, C., Savagner, P., Gitelman, I., Richardson, A., & Weinberg, R. A. (2004). Twist, a master regulator of morphogenesis, plays an essential role in tumor metastasis. *Cell, 117*(7), 927-939. https://doi.org/10.1016/j.cell.2004.06.006

Zaidel-Bar, R., Kam, Z., & Geiger, B. (2005). Polarized downregulation of the paxillin-p130CAS-Rac1 pathway induced by shear flow. *J Cell Sci, 118*(Pt 17), 3997-4007. https://doi.org/10.1242/jcs.02523

Zalba, S., & Ten Hagen, T. L. (2017). Cell membrane modulation as adjuvant in cancer therapy. *Cancer Treat Rev, 52*, 48-57. https://doi.org/10.1016/j.ctrv.2016.10.008

Zamir, E., Katz, B. Z., Aota, S., Yamada, K. M., Geiger, B., & Kam, Z. (1999). Molecular diversity of cell-matrix adhesions. *J Cell Sci, 112 (Pt 11)*, 1655-1669. https://www.ncbi.nlm.nih.gov/pubmed/10318759

Zanotelli, M. R., Zhang, J., & Reinhart-King, C. A. (2021). Mechanoresponsive metabolism in cancer cell migration and metastasis. *Cell Metab, 33*(7), 1307-1321. https://doi.org/10.1016/j.cmet.2021.04.002

APPENDIX: IMPLEMENTATION OF OTSU'S METHOD

To a given image of which the total pixel number is N, it can be divided into L gray levels with the pixel number of ni donates to the level i. In this case, the distribution of gray level can be normalized to a probability model:

$$p_i = n_i/N\,, \qquad p_i \geq 0, \sum_{i=1}^{L} p_i = 1.$$

Supposing that the pixels are dichotomized into two classes C_0 and C_1 at the gray level k, the pixels in class C_0 are marked from 1 to k and the pixels in class C_1 are from k+1 to L. Then the probabilities of the classes occurrence can be obtained as follows:

$$\omega_0 = \Pr(C_0) = \sum_{i=1}^{k} p_i = \omega(k),$$

$$\omega_1 = \Pr(C_1) = \sum_{i=k+1}^{L} p_i = 1 - \omega(k),$$

where

$$\omega(\mathrm{k}) = \sum_{i=1}^{k} p_i\,.$$

The mean level of the classes can be calculated by:

$$\mu_0 = \sum_{i=1}^{k} i\Pr(i|C_0) = \sum_{i=1}^{k} ip_i/\omega_0 = \mu(k)/\omega(k)\,,$$

$$\mu_1 = \sum_{i=k+1}^{L} i\Pr(i|C_1) = \sum_{1=k+1}^{L} ip_i/\omega_1 = \frac{\mu_T - \mu(k)}{1-\omega(k)},$$

where

$$\mu(\mathrm{k}) = \sum_{i=1}^{k} ip_i\,.$$

Then the total mean gray level of the image can be obtained by

$$\mu_T = \mu(L) = \sum_{i=1}^{L} ip_i$$

and

$$\omega_0\mu_0 + \omega_1\mu_1 = \mu_T, \qquad \omega_0 + \omega_1 = 1.$$

Hence, the class variances can be obtained by

$$\sigma_0^2 = \sum_{i=1}^{k} (1-\mu_0)^2 \Pr\,(i|C_0) = \sum_{i=1}^{k} (1-\mu_0)^2\, p_i/\omega_0\,,$$

$$\sigma_1^2 = \sum_{i=k+1}^{L} (1-\mu_1)^2 \Pr\,(i|C_1) = \sum_{i=k+1}^{L} (1-\mu_1)^2\, p_i/\omega_1.$$

To assess k, a criterion η is adopted as:

$$\eta = \sigma_B^2/\sigma_T^2\ ,$$

where σ_B^2 is the between-class variance which can be given as:

$$\sigma_B^2 = \omega_0(\mu_0 - \mu_T)^2 + \omega_1(\mu_1 - \mu_T)^2 = \omega_0\omega_1(\mu_1 - \mu_0)^2$$

and σ_T^2 is the total variance of levels which can be give as:

$$\sigma_T^2 = \sum_{i=1}^{L}(1 - \mu_T)^2 p_i.$$

Then to a value of k, η can be written as:

$$\eta(k) = \frac{\sigma_B^2(k)}{\sigma_T^2},$$

where

$$\sigma_B^2 = \frac{[\mu_T\omega(k) - \mu(k)]^2}{\omega(k)[1 - \omega(k)]}.$$

Now searching the value of k as the best threshold to segment the image is transformed to an optimization problem to maximize σ_B^2.

ORIGINAL PAPERS

I

VISUALIZING THE SPATIOTEMPORAL MAP OF RAC ACTIVATION IN BOVINE AORTIC ENDOTHELIAL CELLS UNDER LAMINAR AND DISTURBED FLOWS

by

Shuai Shao, Cheng Xiang, Kairong Qin, Aziz Ur Rehman Aziz, Xiaoling Liao & Bo Liu 2017

PLoS One, vol 12(11): e0189088

https://doi.org/10.1371/journal.pone.0189088

PLOS ONE

RESEARCH ARTICLE

Visualizing the spatiotemporal map of Rac activation in bovine aortic endothelial cells under laminar and disturbed flows

Shuai Shao[1,2], Cheng Xiang[3], Kairong Qin[1], Aziz ur Rehman Aziz[1], Xiaoling Liao[4], Bo Liu[1]*

1 Department of Biomedical Engineering, Faculty of Electronic Information and Electrical Engineering, Dalian University of Technology, Dalian, China, **2** Mathematical Information Technology, Faculty of Information Technology, Department of Math, University of Jyvaskyla. Jyvaskyla, Finland, **3** Department of Electrical and Computer Engineering, National University of Singapore, Singapore, Singapore, **4** Biomaterials and Live Cell Imaging Institute, Chongqing University of Science and Technology, Chongqing, China

* lbo@dlut.edu.cn

Citation: Shao S, Xiang C, Qin K, ur Rehman Aziz A, Liao X, Liu B (2017) Visualizing the spatiotemporal map of Rac activation in bovine aortic endothelial cells under laminar and disturbed flows. PLoS ONE 12(11): e0189088. https://doi.org/10.1371/journal.pone.0189088

Editor: Juan Carlos del Alamo, University of California San Diego, UNITED STATES

Received: March 12, 2017

Accepted: November 17, 2017

Published: November 30, 2017

Data Availability Statement: All relevant data are within the paper and its Supporting Information files.

Funding: This work was supported in part by grants from National Natural Science Foundation of China (NSFC No. 31670867, No. 31670961, No.11532004), and Natural Science Key Foundation Project of CQ in China (CSTC2015JCYJBX0003).

Competing interests: The authors have declared that no competing interests exist.

Abstract

Disturbed flow can eliminate the alignment of endothelial cells in the direction of laminar flow, and significantly impacts on atherosclerosis in collateral arteries near the bifurcation and high curvature regions. While shear stress induced Rac polarity has been shown to play crucial roles in cell polarity and migration, little is known about the spatiotemporal map of Rac under disturbed flow, and the mechanism of flow-induced cell polarity still needs to be elucidated. In this paper, disturbed flow or laminar flow with 15 dyn/cm^2 of average shear stress was applied on bovine aortic endothelial cells (BAECs) for 30 minutes. A genetically-encoded PAK-PBD-GFP reporter was transfected into BAECs to visualize the real-time activation of Rac in living cell under fluorescence microscope. The imaging of the fluorescence intensity was analyzed by Matlab and the normalized data was converted into 3D spatiotemporal map. Then the changes of data upon chemical interference were fitted with logistic curve to explore the rule and mechanism of Rac polarity under laminar or disturbed flow. A polarized Rac activation was observed at the downstream edge along the laminar flow, which was enhanced by benzol alcohol-enhanced membrane fluidity but inhibited by nocodazole-disrupted microtubules or cholesterol-inhibited membrane fluidity, while no obvious polarized Rac activation could be found upon disturbed flow application. It is concluded that disturbed flow inhibits the flow-induced Rac polarized activation, which is related to the interaction of cell membrane and cytoskeleton, especially the microtubules.

Introduction

Usually, atherosclerosis occurs at the branch points and curved regions of the arterial tree, where the blood flow remains unsteady and the shear stress shows marked spatial and temporal variations [1]. This should be due to the variations of flow patterns-induced functional differences of endothelial cells (ECs), such as migration and proliferation, in vascular system [2].

ECs orient prominently parallel to the direction of blood flow in the straight part of the arterial tree, while little orientation of ECs is found at the branch points and curved regions where flow patterns are more disturbed with no clear forward direction [3]. In vitro experiments have also proved the relationship between the flow patterns and ECs orientation. Laminar fluid shear would cause cell deformation along the flow direction [4], while Bovine aortic endothelial cells (BAECs) subjected to disturbed flow have a morphology and random orientations similar to those under static condition [5].

Rac is a group of plasma membrane bound proteins and plays important roles in controlling membrane ruffling and the formation of lamellipodia [6]. It is activated significantly in BAECs upon shear stress application, and then participates in the cell elongation and directionality of cell movement [7]. Other researchers have deeply explored that Rac was primarily activated at the leading edges of cells along the flow direction, or inhibited at the edges facing to the flow [8–10]. This polarity of Rac activation will promote the lamellipodium extension and the formation of new adhesions in migrating cells, and finally results in cell orientation [11]. Therefore, Rac should be one of the key signal proteins in the shear stress-mediated ECs orientation, and its local activation under different flow patterns may determine the direction of cell polarity. However, no experimental report could be found on the spatiotemporal model of Rac activation upon disturbed flow application, and the mechanism of Rac activation upon flow application also needed to be elucidated.

In this study, the spatiotemporal model of Rac was examined in BAECs under disturbed or laminar flows, analyzed the image with a developed and implemented software package in MATLAB (Mathworks; Natick, MA), and further explored the mechanism of shear stress-induced Rac local activation. It may present new molecular-level insights into the pathogenic mechanism of atherosclerosis.

Methods

Cell culture and transient transfection

Before transfection, the high glucose of Dulbecco's modified Eagle medium (DMEM, GIBCO, Invitrogen, USA) containing 10% fetal bovine serum, 2 mmol/l L-glutamine, 100 unit/ml penicillin and 100 mg/ml sodium pyruvate (GIBCO BRL) were used to culture BAECs isolated from bovine aorta(provided by local slaughterhouse) in a humidified CO_2 incubator. According to the product specification, Lipofectamine 2000(Invitrogen) was used to transfect different DNA plasmids into cells[12]. Cells were starved in cell culture medium with 0.5% FBS for 36 hr for expressing various exogenous proteins. After that, cells were passed onto fibronectin-coated cover slips for 12 hr.

The fluorescent probe used in our experiment was a genetically-encoded PAK-PBD-GFP reporter containing a PAK domain to bind to active Rac and transfected into BAECs to obverse the real-time translocation of active Rac in living cell[13–15].

Flow systems

As shown in Fig 1, a parallel-plate flow chamber was used to provide a laminar flow and a classic vertical-step, close to the entrance, was devised to impose the disturbed flow [16]. Silicone gasket with rectangular space was sandwiched between a glass slide, seeded with separated BAECs, and a cover glass. The laminar or disturbed flow in the flow channel was provided by one or two silicone gaskets respectively. The channel was 10 mm wide and the entrance was 0.25 mm high. The heights of the main channel for providing disturbed flow and the whole channel for laminar flow were both 0.5 mm. The total length of the flow chamber was 45 mm and the length of the entrance was 15 mm. In this flow system, flow patterns were confirmed by medium

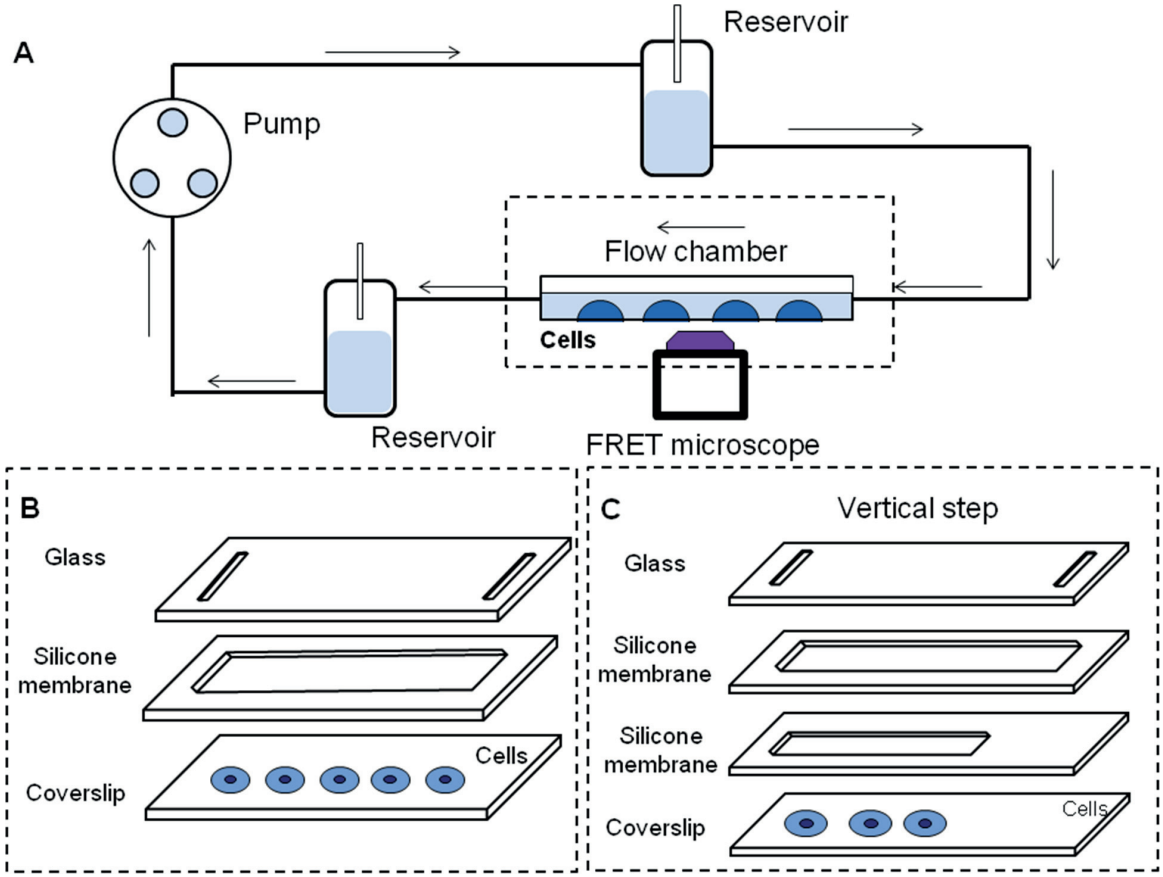

Fig 1. The system providing laminar flow or disturbed flow. (A) The whole system for providing different flows. (B) The structure in flow chamber to provide laminar flow contained a slip of glass, a silicone membrane with rectangular space and a coverslip. (C) The structure of vertical step to provide disturbed flow is consist of a slip of glass, two silicone membranes with different sizes of rectangular space and a coverslip.

https://doi.org/10.1371/journal.pone.0189088.g001

containing polystyrene particles which perfused the whole system and the region of disturbed flow in the chamber was marked out. The height difference between two reservoirs led to a hydrostatic pressure which induced the flow to which the cells were exposed. Laminar shear stress was set to 15 dyn/cm^2 and the same mean flow was set in disturbed flow [17]. The conditions of the flow experiments were 37˚C with 5% CO_2 to maintain the pH at 7.4.

Microscope image acquisition

All images were obtained only on isolated single cell under an inverted microscope (Nikon Eclipse Ti Se-ries, Ti-Fl Epi-fl/1) equipped with a cold CCD (Evolve512, Photometrics). Time lapse fluorescence images were acquired by MetaFluor 7.0 software (Universal Imaging) once after every 30 or 60 sec and arranged in chronological order beginning from 001.

Image analysis

To analyze the fluorescence data rapidly, a software package in Matlab (Mathworks; Natick, MA) was developed. It contained two sections to allow the pre-treatment and fluorescence analysis

respectively and allowed users to input the time of shear stress applied to cells. In both sections, the fluorescence intensity images were dyed by pseudo colors closer to red representing higher intensities and the pseudo colors closer to blue representing low intensities, respectively.

All the fluorescence images were regulated rightly according to the flow direction to ensure that the downstream region was to the left of the cell. Because the single cell was in migration upon laminar flow, the edge position needed to be identified in each image. The background was the average fluorescence intensity of the four corners of images and was subtracted before image quantification and analysis. The boundary, outlining the mask of the cell body, was enhanced by filtering speckle and close operation. The second module divided the cells both along the flow direction and the vertical direction into 50×50 parts averagely. The temporal changes of the fluorescence percentage in each part were calculated and saved as numbered mat file. The first image after shear stress application was named as I_1, the second was I_2 and the last one was I_{30}. Subtraction was used to eliminate the fluorescent interference of the cellular nuclear or biosensor itself. The specific solution is as below:

$$I = (I_2 - I_1) + (I_3 - I_2) + \ldots\ldots + (I_{30} - I_{29}) \quad (1)$$

Moreover, fluorescence matrix data of one sample at a certain time was compressed into a line along the direction of flow through projection. The specific method was calculating the percentage of fluorescence intensity in each column (columns are arranged along the direction of flow) from the whole cell. Percentages were arranged in chronological sequence to describe the spatiotemporal map of Rac activation by matrix. All fluorescence percentage data were normalized to a same basal level to avoid individual differences. Average matrix of samples in a same group were calculated and drawn into three-dimensional images by the Matlab function of 'imagesc'. The fifty parts of the cell were numbered from 1 to 50 corresponding to the last part of the downstream and the first part of upstream, respectively. The diagrammatic sketch of image analysis is shown in Fig 2.

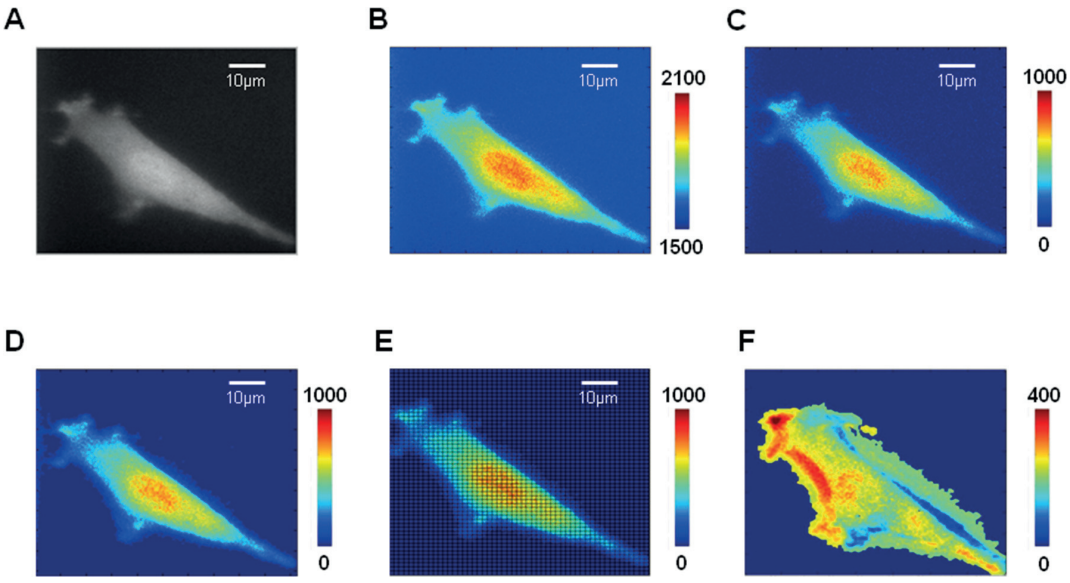

Fig 2. The diagrammatic sketch of image analysis. The original fluorescence image of BAECs (A) were added Pseudo color (B), then subtracted the background(C) and enhanced the edge of cell (D). After that, the image was divided into 50×50 parts (E) to calculate and eliminate the interference of nucleus (F).

https://doi.org/10.1371/journal.pone.0189088.g002

Mathematical model analysis

All the fluorescence percentage data was normalized by their basal levels before stimulation in the same cell. In order to describe the level of the polarity more precisely, the normalized fluorescence percentage along the flow was fitted with logistic curve as follows,

$$y = \frac{A_1 - A_2}{1 + e^{(x - X_0)/D}} + A_2 \quad (2)$$

where x is a spatial variable indexed by the serial number of each part divided along the flow direction, y is the fitting value of the normalized actual fluorescence percentage, and A_1, A_2, X_0 and D denote the maximum, the minimum, the inflection point and the parameter related to the slope, respectively. Among all the logistic parameters obtained by curve fitting, the absolute value of difference between A_1 and A_2, $|A_1\text{-}A_2|$, was related to the intensity of polarity. The slope of each point was calculated from the first derivative of the logistic curve. The point X' could be considered as the position where Rac polarity appears when the slope of X' or (X'+1) was very close to zero (<0.005) but (X'-1) was not. The slope of the inflection point X_0 was related to the parameter D as shown in Eq (3).

$$y'(X_0) = \frac{A_2 - A_1}{4D} \quad (3)$$

Statistical analysis for fitting parameters was performed by using a Student's T-test function in the Excel software (Microsoft) to evaluate the statistical difference between groups. A significant difference was determined by the p-value (< 0.05).

Results

Disturbed flow inhibits the polarity of Rac

The PAK-PBD-GFP translocation at the downstream edge of the cell was observed gradually upon 15 dyn/cm^2 of laminar flow application for 30 min. However, after 30 min of disturbed flow stimulation, with the same average shear stress 15 dyn/cm^2, the fluorescence was found distributed uniformly in the whole cell (Fig 3A and 3B). After further quantification by our software, as shown in Fig 3C and 3D, no obvious fluorescence accumulation could be found at downstream edge of the spatiotemporal map, suggesting that there was not much activated Rac at downstream part.

Through fitting the data with logistic curve, the resulting parameters were applied in T-test to measure the differences between the two groups (Table 1). The result of T-test showed that X', which was related to the starting position of Rac polarity, was much different from control. In addition, the range of the logistic curve, $|A_1\text{-}A_2|$, which described the intensity of the polarity, decreased. Together with the reduced slope, the two parameters indicated that the polarity peak almost disappeared due to the disturbed flow. Therefore, Rac could not be activated in a polarized way upon disturbed flow, and the polarity of Rac should be related to the exact flow direction on the cell surface under flow.

Cytoskeleton relates to Rac polarity

Since cytoskeleton plays a critical role in providing mechanical support for the plasma membrane [18], its role in flow-induced Rac polarity has also been explored. BAECs were pretreated with 5 μmol/l of myosin light chain kinase (MLCK) inhibitor ML-7[12, 19], which could only eliminate the force transmission through microfilaments while the structure could remain intact, for 1 hr before laminar shear stress application. The results in Fig 4 showed that the Rac

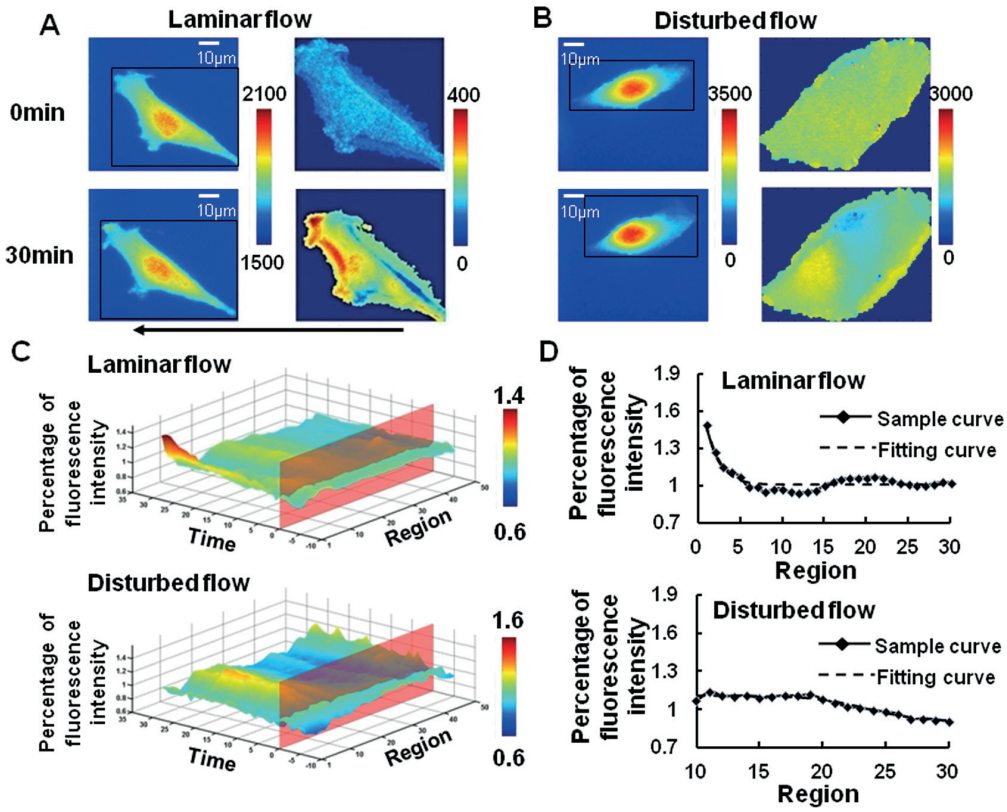

Fig 3. Polarized Rac activation in BAECs was caused by laminar flow but not disturbed flow. The image of BAECs transfected with PAK-PBD-GFP biosensor to represent the Rac activation (Left panel) upon laminar flow (A, n = 12) or disturbed flow (B, n = 5) application were dealt by our imaging analysis software (Right panel). The 3D spatiotemporal map (C) of averaged single cell images showed an obvious Rac activation at the downstream of BAECs from laminar flow group (Above), but not disturbed flow group (Below). After that, the data of the thirtieth minute from laminar flow (Above) and disturbed flow (Below) were fitted by logistic curve (D). The arrow indicated the main flow direction.

https://doi.org/10.1371/journal.pone.0189088.g003

activation still appeared in a polarized manner, and the logistic parameters indicated that ML-7 only had gentle effect on the intensity or slope of Rac polarity($p>0.05$).

After that, 2 μmol/l of Cytochalasin D (CytoD), incubation for 1 hr, was used to destroy the structure of microfilament in BAECs. After 30 min of laminar shear stress application, the course of Rac activation at downstream along the flow direction was not much affected by

Table 1. The parameters from fitting curve in different groups.

	$\|A_1-A_2\|$	X'	Slope
Control	1.1476±0.4368	12.3000±5.7108	-0.2946±0.2286
Disturbed Flow	0.4075±0.1738*	24.2500±12.3879*	-0.0702±0.0230*
ML-7	1.2948±0.8423	17.0000±4.4136	-0.2241±0.1414
CytoD	1.3153±0.8565	31.5000±15.9123*	-0.1330±0.0860
NOCO	0.3086±0.1357*	30.0000±12.4685*	-0.0523±0.0462*
CHO	0.2640±0.1574*	22.7500±11.5660*	-0.0070±0.0734*
BA	2.3877±1.5229*	15.16831±5.27111	-0.1869±0.1007

(*$p<0.05$ compare to control)

https://doi.org/10.1371/journal.pone.0189088.t001

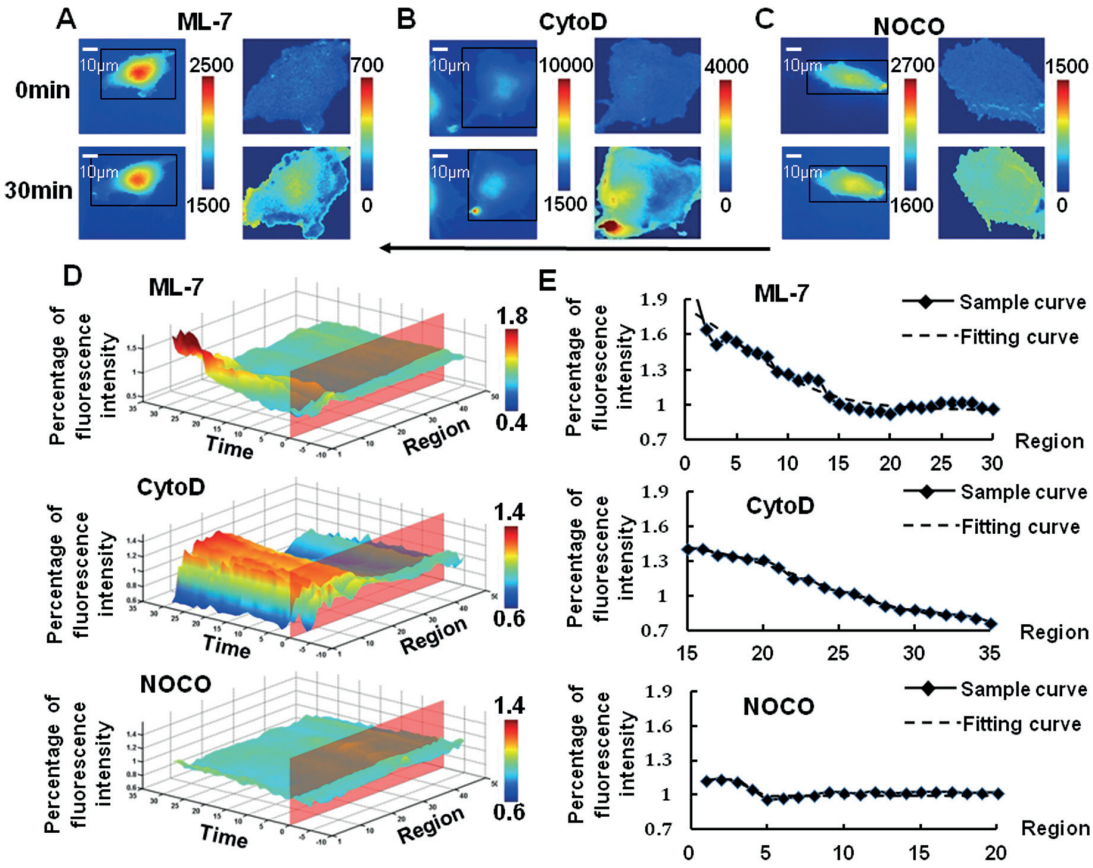

Fig 4. Shear stress caused a polarized Rac activation in BAECs after pre-treatment of ML-7 and CytoD but eliminated by NOCO. The images of BAECs transfected with biosensor (left panel) pretreated with ML-7(A, n = 7), CytoD(B, n = 6) or NOCO(C, n = 8) upon laminar flow application were dealt by the imaging analysis(right panel). The 3D spatiotemporal map (D) of averaged single cell images showed an obvious shear stress-induced Rac activation at the downstream of BAECs from ML-7 (Above) and CytoD group (Middle), but not NOCO (Below). After that, the data of the thirtieth minute from three groups were fitted by logistic curve. Above was the ML-7 group, middle was CytoD and below was the NOCO group (E). The arrow indicated the main flow direction.

https://doi.org/10.1371/journal.pone.0189088.g004

CytoD, while the parameter X' increased obviously($p<0.05$), indicating that the Rac polarity moved away from the downstream (Fig 4, Table 1).

However, a visible suppression of Rac polarity could be observed at the downstream of the cell upon being dealt with 1 μmol/l of nocodazole (NOCO), a depolymerizing agent of microtubules, for 1 hr of incubation before laminar shear stress application (Fig 4). The fitting result showed that the $|A_1-A_2|$ slumped obviously($p<0.05$), indicating that the amount of activated Rac at downstream was reduced by NOCO upon laminar flow. The parameter $X^{'}$ migrating and slope reducing obviously($p<0.05$), indicating that activated Rac distributed evenly across the whole cell. It was clear that Rac activation disappeared when microtubules were destroyed.

Changing cell membrane fluidity alters shear stress induced-Rac polarity

In our further experiment, 0.1 mmol/L of Cholesterol (CHO) for 3 hr or 45 mmol/L benzol alcohol (BA) for 45 min of pre-incubation were applied before laminar shear stress to reduce or enhance the fluidity of cell membrane, respectively[19, 20]. The result of CHO treatment

showed no obvious deformation of the cells under shear stress compared with control group. However, the level and slope of shear stress-induced Rac activation both were affected by CHO. Upon laminar flow, after CHO pre-treatment, little Rac could be found activated at the opposite side facing the flow, and the Rac polarity activation was suppressed more when the stiffness of cell membrane was increased. It was obvious that CHO had an inhibitory effect on the overall level of Rac activation and the shear stress-induced Rac polarity (Fig 5). Conversely, the result of BA pre-treatment enhancing the fluidity of cell membrane showed an aggravated deformation of cells. The fitting analysis showed an earlier and more obvious polarity peak of Rac upon shear stress application (Fig 5, Table 1). These results demonstrated that cell membrane fluidity had an evident effect on the Rac polarity definitely.

Discussion

The Rac is activated in a polarized manner by shear stress and inhibited by disturbed flow

In this paper, the different flow pattern-induced local activation of Rac has been investigated in BAECs using a genetically-encoded PAK-PBD-GFP reporter, as well as the effects of various

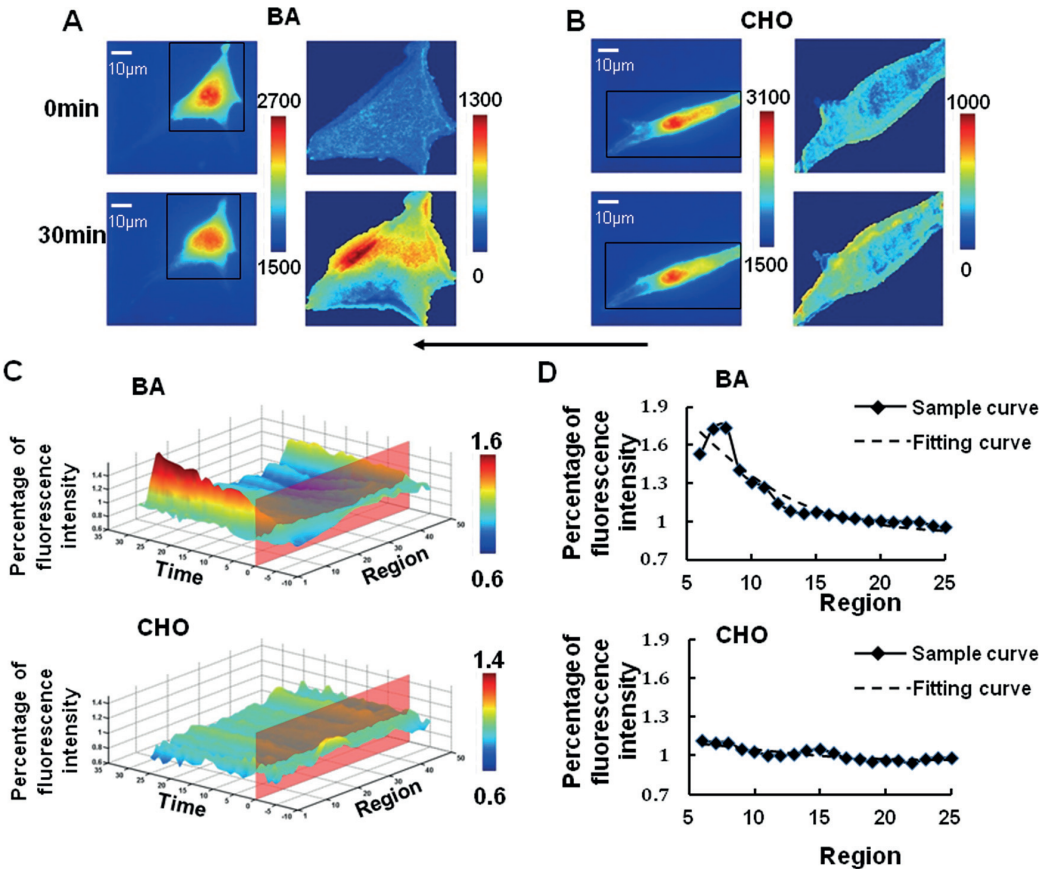

Fig 5. Shear stress caused a polarized Rac activation after pre-treatment of BA but eliminated by CHO. The images of transfected BAECs (left panel) pretreated with BA (A, n = 5) or CHO (B, n = 5) upon laminar flow application were dealt by the imaging analysis (right panel). The 3D spatiotemporal map (C) of averaged single cell images showed an obvious shear stress-induced Rac activation at the downstream of BAECs from BA (Above) group, but not CHO group (Below). After that, the data of the thirtieth minute from BA group (Above) and CHO group(Below) is extracted and fitted by logistic curve(D). The arrow indicated the main flow direction.

https://doi.org/10.1371/journal.pone.0189088.g005

inhibitors in flow-induced Rac polarity. It has been proved that PBD can bind the activated GTP-bound forms of both Rac and Cdc42 in vitro, while its GFP-tagged counterpart (PAK-PBD-GFP) mainly detects activated Rac rather than activated Cdc42 in living cells[13–15]. Depending on this feature, the biosensor can only show the localization of activated Rac. In addition to the experiments, we have established a calculation method to analyze and visualize the subcellular distribution of molecular activity based on imaging analysis and Logistic curve fitting. Three-dimensional images containing the spatial and temporal course were used for the whole visual representation. After 30 min of shear stress application, the 3D images showed that the Rac polarity became steady. Hence the image of the thirtieth minute was chosen as fitting data which should be a good description of shear stress induced-Rac polarity.

Although the appearance or disappearance of Rac polarity could be observed directly in 3D figures, the mathematical model (1) made it more accurate and objective to measure the level of Rac polarity. The parameters of the Logistic curve represented different meanings as discussed earlier in the paper. $|A_1\text{-}A_2|$ decreasing or even disappearing implied that the intensity of Rac activation declines. The subcellular position of activated Rac could be measured by X' and D was a parameter related to the slope of the fitting curve. When the activated speed of Rac changed, the slope calculated from D would be changed. With this method of imaging analysis and the four parameters of Logistic curve fitting, we can easily evaluate the shear stress induced Rac polarity comprehensively.

Although Rac would concentrate in the downstream region of ECs upon shear stress treatment [9], which is a course containing a transient increase, a peak and a decline down to basal level [21], there is no clear evidence on, how does the disturbed flow affect subcellular Rac translocation? Consistently, our results also showed an obvious local activation of Rac at the downstream edge of BAECs along the flow direction after a relative steady phase. However, flow with irregular directions could not trigger the polar distribution of activated Rac. The quantitative results confirmed the experimental phenomena, since all the parameters obviously were differences between the group of laminar and disturbed flow, which would be the reason why disturbed flow could affect the cell migration and arrangement.

The laminar flow-induced Rac polarity is based on cell membrane fluidity

It has been reported that nuclear bulge, caused by laminar flow, increases the tension in upstream region, thus the cell membrane fluidity will be increased in a polar manner [21]. Moreover, the apical cell membrane enduring a direct perturbation reflected in membrane fluidity would help cell to distinguish different temporal shear gradients [20]. Hence, we postulate that the directional shear stress-induced asymmetric change of cell membrane fluidity will impact on the Rac polarized activation. Indeed, laminar fluid shear leads to temporally varying and spatially heterogeneous stresses on the cell membrane [20], which has also been proved by our previous report [19], and then causes cell deformation along the flow direction, resulting in an increase in lamellipodia protrusion along the flow [22]. The formation of lamellipodia in the direction of flow is fast and structurally identifiable, which is an essential process in formatting focal adhesion to support friction force for cell migration [7]. Based on our further results of logistic curve fitting, when the membrane fluidity was inhibited, the decline degree of activated Rac was reflected by the distinct reduction of $|A_1\text{-}A_2|$, and the slope was much smaller than the control group, indicating that there was no outstanding polarity peak. On the contrary, the intensity of Rac polarity increased, after softening the membrane and enhancing the fluidity. This may be due to the reason that softer cell membrane becomes much easier to deform, and the directional shift of lipid rafts will be stronger under the shear stress, which may leads to stretch of cytoskeleton alone the direction of stress and then the higher activation

of Rac at the downstream; the harder membrane is more resistant in deformation when shear stress is applied to BAECs, which leads to the decline of flow-induced polar activation of Rac. While under disturbed flow without apparent direction, the local difference of cell membrane fluidity and the shift of lipid rafts will be eliminated, which cannot result in the polar Rac activity.

The laminar flow-induced Rac polarity is mediated by microtubules

Since cell membrane and the bound cytoskeleton on some sites constitute a complex network [23], stress waves on the membrane could be transmitted via cytoskeleton [24]. It's reported that when ECs are exposed to sustained shear stress with a clear direction, the cytoskeletal fibers undergo remodeling by staining of cytoskeleton proteins such as actin, tubulin and vimentin, and become oriented along the direction of shear flow with a consequent alignment of the cell [25]. But under disturbed flow, the cytoskeletal fibers and the cell orient randomly similar to that in static condition. It seems that the whole cell polarity, including the Rac, should be the result of cytoskeletal fibers remodeling upon flow pattern stimulation. Indeed, shear stress induced-Rac activation depends on cytoskeletal integrity [26], which is also verified by our results. Furthermore, our finding showed that shear stress induced Rac activation promptly, which is consistent with the previous report [26]. This force transmission is too rapid for rearrangement of cytoskeleton and should happen before the rearrangement. Therefore, according to our results, cytoskeleton is associated with the planar polarity of shear stress force transmittion along cytoskeleton, but a great possibility also exists that cytoskeletal arrangements, caused by local force transmittion, and could contribute to Rac polarity in turn.

However, which component of the cytoskeletal fiber plays more significant roles in shear stress-induced Rac polarity is still elusive. Some experiments suggested more important role of filament system, while the microtubules maybe just changed passively to play gentle roles in the process of stress-induced cell polarity [27, 28],while microfilaments provide driving force in migrating cells by actin polymerization [29], and actin alignment is also an essential biological processes in Rac activation upon shear stress [30]. However, there was also a different mechanism considering that microtubule should be the major structure which transduced the stress to activate the local Rac of the far end of the cell upon local stress application [24]. Since microtubules were reported growing into the downstream edge contributes to Rac1 activation and formation of short branched F-actin in migrating cells [31, 32], and disruption of microtubules affected the polarity of actin cytoskeleton [33, 34]. It is easy to understand that our experiments support a more decisive role of microtubules than microfilaments in shear stress-induced Rac polarity [24]. We also find that filament system participates in the process, and without the integrity of filament system, the intracellular stress from the flow could not transmit to the far end of the cell through microtubules only. Since destroying microfilaments will also change its anchoring function to the lipid rafts in kinetic features[35], and Rac associates with membranes in lipid rafts primarily[36], filaments will also affects the manner of Rac polarization probably. However, the exact reason which causes this difference still needs to be deeply elucidated in the future.

The model of shear stress-induced Rac polarity

Force applied to the cell membrane led to the deformation of upstream region directly, but Rac was activated at the downstream periphery. How was the effect of shear stress transmitted from the upstream region to the other side, and transduced into biochemical activities in a process remained vague. Rac activation was eliminated during microtubules depolymerization or the decrease of cell membrane fluidity, while the activated manner and duration of Rac

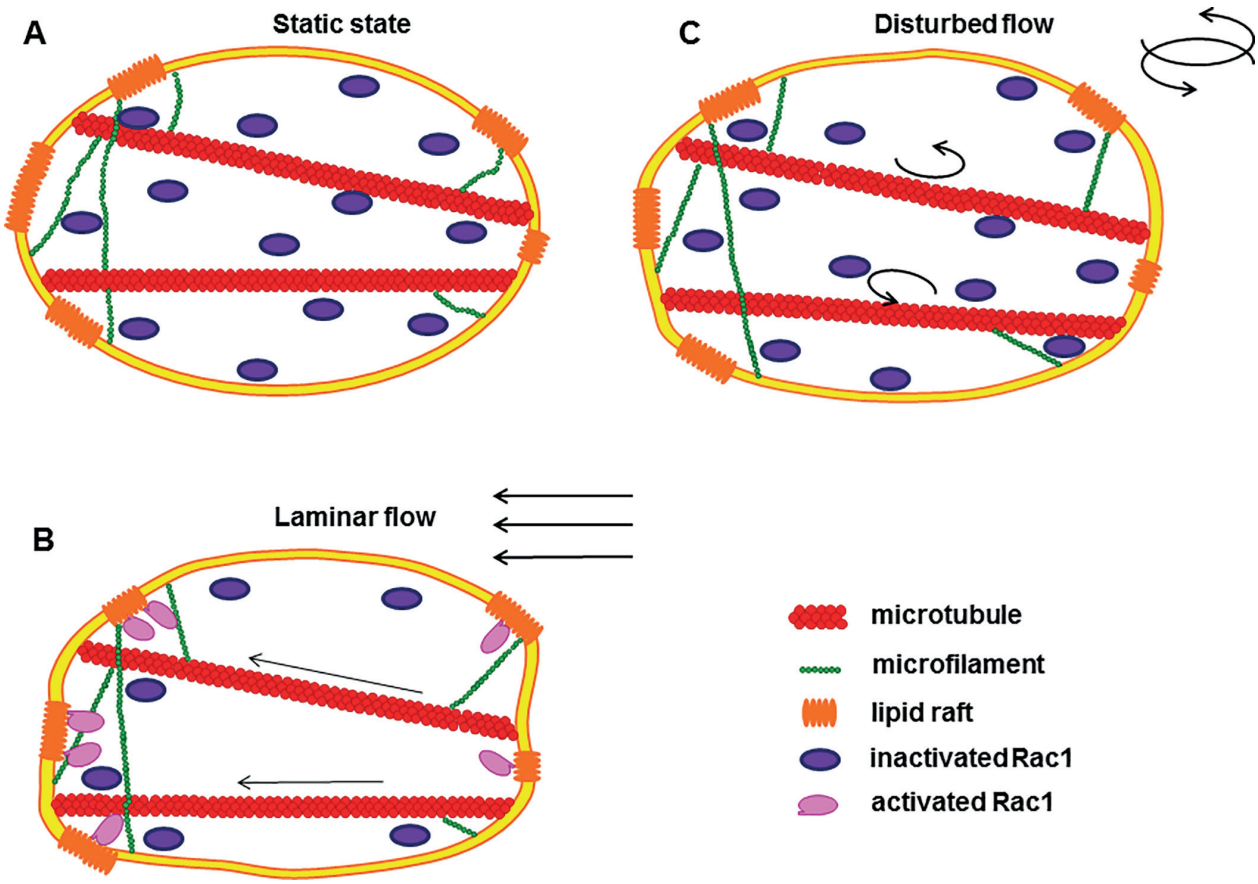

Fig 6. The model of Rac activation under laminar flow and disturbed flow. (A) The static condition before shear stress application. (B)Under laminar flow, cell membrane deformed along the flow and transmitted force to the downstream edges of cells with the help of cytoskeleton, especially microtubule, and then active Rac.(C)While under disturbed flow, the cell membrane and cytoskeletal fibers changed randomly without any obvious spatial direction.

https://doi.org/10.1371/journal.pone.0189088.g006

were changed by microfilament depolymerization. These evidences suggested that shear stress induced-Rac activation was depending on the interaction between membrane and cytoskeleton. A local force applied on the cell membrane could be transmitted along the cytoskeletal network to induce Rac activation on the sites cytoskeleton forming strong connections to the plasma membrane [26]. This interaction probably involved the cytoskeleton deformation caused by local deformation of cell membrane and the cytoskeleton in turn regulating cell membrane fluidity. The two components, membrane and cytoskeleton, are required.

In summary, although the disturbed flow inhibits the shear stress induced Rac activation, the mechanism still could be discovered by changing experimental conditions under laminar flow. Therefore, the model of shear stress-induced Rac polarity can be illuminated (Fig 6). When mechanical forces with clear direction loading, ECs perceive the spatial pattern of force and deform along the flow because of the change of plasma membrane fluidity. Force is being transmitted to the downstream edge of cells rapidly and cytoskeleton network participate in this process, which is mainly microtubule binding to the membrane. Then the alternation of local strain at the downstream edge of cell promotes the polar Rac activation. But under the disorder of the direction and the magnitude of disturbed flow, the cell membrane should be

changed randomly without any obvious spatial direction. The cytoskeleton fibers are not polarized in a clear direction and the cell orient is random. Therefore, force would not be transmitted to downstream to induce polar activation of Rac.

Supporting information

S1 Code. The code of analyzing Rac1 polarity.
(M)

S2 Code. The function code to make details of cell outline clear.
(M)

S1 ZIP File. Initial data of cells dealt with BA.
(ZIP)

S2 ZIP File. Initial data of cells dealt with CHO.
(ZIP)

S3 ZIP File. Initial data of cells in control group, part 1.
(ZIP)

S4 ZIP File. Initial data of cells in control group, part 2.
(ZIP)

S5 ZIP File. Initial data of cells dealt with CytoD.
(ZIP)

S6 ZIP File. Initial data of cells upon disturbed flow.
(ZIP)

S7 ZIP File. Initial data of cells dealt with ML-7.
(ZIP)

S8 ZIP File. Initial data of cells dealt with NOCO.
(ZIP)

Acknowledgments

This work was supported in part by grants from National Natural Science Foundation of China (NSFC No. 31670867, No. 31670961, No.11532004), and Natural Science Key Foundation Project of CQ in China (CSTC2015JCYJBX0003). We appreciate Yingxiao Wang's lab in University of California, San Diego for the kindly gifted plasmids.

Author Contributions

Data curation: Shuai Shao, Xiaoling Liao, Bo Liu.

Funding acquisition: Xiaoling Liao, Bo Liu.

Methodology: Cheng Xiang, Bo Liu.

Writing – original draft: Shuai Shao, Cheng Xiang, Kairong Qin, Aziz ur Rehman Aziz, Bo Liu.

Writing – review & editing: Shuai Shao, Bo Liu.

References

1. Barakat A, Lieu D. Differential responsiveness of vascular endothelial cells to different types of fluid mechanical shear stress. Cell biochemistry and biophysics. 2003; 38(3):323–43. PMID: 12794271.
2. Wang C, Lu H, Schwartz MA. A novel in vitro flow system for changing flow direction on endothelial cells. Journal of biomechanics. 2012; 45(7):1212–8. https://doi.org/10.1016/j.jbiomech.2012.01.045 PMID: 22386042; PubMed Central PMCID: PMC3327813.
3. Hahn C, Schwartz MA. The role of cellular adaptation to mechanical forces in atherosclerosis. Arteriosclerosis, thrombosis, and vascular biology. 2008; 28(12):2101–7. https://doi.org/10.1161/ATVBAHA.108.165951 PMID: 18787190; PubMed Central PMCID: PMC2737679.
4. Li YS, Haga JH, Chien S. Molecular basis of the effects of shear stress on vascular endothelial cells. Journal of biomechanics. 2005; 38(10):1949–71. https://doi.org/10.1016/j.jbiomech.2004.09.030 PMID: 16084198.
5. Chien S. Effects of disturbed flow on endothelial cells. Annals of biomedical engineering. 2008; 36 (4):554–62. https://doi.org/10.1007/s10439-007-9426-3 PMID: 18172767; PubMed Central PMCID: PMC3718045.
6. Kato T, Kawai K, Egami Y, Kakehi Y, Araki N. Rac1-dependent lamellipodial motility in prostate cancer PC-3 cells revealed by optogenetic control of Rac1 activity. PloS one. 2014; 9(5):e97749. https://doi.org/10.1371/journal.pone.0097749 PMID: 24848679; PubMed Central PMCID: PMC4029798.
7. Tzima E. Role of small GTPases in endothelial cytoskeletal dynamics and the shear stress response. Circulation research. 2006; 98(2):176–85. https://doi.org/10.1161/01.RES.0000200162.94463.d7 PMID: 16456110.
8. Tzima E, Del Pozo MA, Kiosses WB, Mohamed SA, Li S, Chien S, et al. Activation of Rac1 by shear stress in endothelial cells mediates both cytoskeletal reorganization and effects on gene expression. The EMBO journal. 2002; 21(24):6791–800. https://doi.org/10.1093/emboj/cdf688 PMID: 12486000; PubMed Central PMCID: PMC139108.
9. Wojciak-Stothard B, Ridley AJ. Shear stress-induced endothelial cell polarization is mediated by Rho and Rac but not Cdc42 or PI 3-kinases. The Journal of cell biology. 2003; 161(2):429–39. https://doi.org/10.1083/jcb.200210135 PMID: 12719476; PubMed Central PMCID: PMC2172912.
10. Kraynov VS, Chamberlain C, Bokoch GM, Schwartz MA, Slabaugh S, Hahn KM. Localized Rac activation dynamics visualized in living cells. Science. 2000; 290(5490):333–7. PMID: 11030651.
11. Hu YL, Li S, Miao H, Tsou TC, del Pozo MA, Chien S. Roles of microtubule dynamics and small GTPase Rac in endothelial cell migration and lamellipodium formation under flow. Journal of vascular research. 2002; 39(6):465–76. doi: 67202. https://doi.org/10.1159/000067202 PMID: 12566972.
12. Liu B, Lu S, Zheng S, Jiang Z, Wang Y. Two distinct phases of calcium signalling under flow. Cardiovascular research. 2011; 91(1):124–33. https://doi.org/10.1093/cvr/cvr033 PMID: 21285296; PubMed Central PMCID: PMC3112016.
13. Srinivasan S, Wang F, Glavas S, Ott A, Hofmann F, Aktories K, et al. Rac and Cdc42 play distinct roles in regulating PI(3,4,5)P3 and polarity during neutrophil chemotaxis. The Journal of cell biology. 2003; 160(3):375–85. https://doi.org/10.1083/jcb.200208179 PMID: 12551955; PubMed Central PMCID: PMC2172671.
14. Magalhaes MA, Zhu F, Sarantis H, Gray-Owen SD, Ellen RP, Glogauer M. Expression and translocation of fluorescent-tagged p21-activated kinase-binding domain and PH domain of protein kinase B during murine neutrophil chemotaxis. Journal of leukocyte biology. 2007; 82(3):559–66. https://doi.org/10.1189/jlb.0207126 PMID: 17535984.
15. Magalhaes MA, Sun CX, Glogauer M, Ellen RP. The major outer sheath protein of Treponema denticola selectively inhibits Rac1 activation in murine neutrophils. Cellular microbiology. 2008; 10(2):344–54. https://doi.org/10.1111/j.1462-5822.2007.01045.x PMID: 17868382.
16. Chen CN, Chang SF, Lee PL, Chang K, Chen LJ, Usami S, et al. Neutrophils, lymphocytes, and monocytes exhibit diverse behaviors in transendothelial and subendothelial migrations under coculture with smooth muscle cells in disturbed flow. Blood. 2006; 107(5):1933–42. https://doi.org/10.1182/blood-2005-08-3137 PMID: 16293605; PubMed Central PMCID: PMC1895706.
17. Choi HW, Barakat AI. Modulation of ATP/ADP concentration at the endothelial surface by shear stress: effect of flow disturbance. Conf Proc IEEE Eng Med Biol Soc. 2004; 7:5065–8. https://doi.org/10.1109/IEMBS.2004.1404400 PMID: 17271456.
18. Janmey PA. The cytoskeleton and cell signaling: component localization and mechanical coupling. Physiological reviews. 1998; 78(3):763–81. PMID: 9674694.
19. Liu B, Lu S, Hu YL, Liao X, Ouyang M, Wang Y. RhoA and Membrane Fluidity Mediates the Spatially Polarized Src/FAK Activation in Response to Shear Stress. Scientific reports. 2014; 4:7008. https://doi.org/10.1038/srep07008 PMID: 25387906; PubMed Central PMCID: PMC4228346.

20. Butler PJ, Tsou TC, Li JY, Usami S, Chien S. Rate sensitivity of shear-induced changes in the lateral diffusion of endothelial cell membrane lipids: a role for membrane perturbation in shear-induced MAPK activation. FASEB journal: official publication of the Federation of American Societies for Experimental Biology. 2002; 16(2):216–8. https://doi.org/10.1096/fj.01-0434fje PMID: 11744620.

21. Butler PJ, Norwich G, Weinbaum S, Chien S. Shear stress induces a time- and position-dependent increase in endothelial cell membrane fluidity. American journal of physiology Cell physiology. 2001; 280(4):C962–9. PMID: 11245613.

22. Hsu S, Thakar R, Liepmann D, Li S. Effects of shear stress on endothelial cell haptotaxis on micropatterned surfaces. Biochemical and biophysical research communications. 2005; 337(1):401–9. https://doi.org/10.1016/j.bbrc.2005.08.272 PMID: 16188239.

23. Head BP, Patel HH, Insel PA. Interaction of membrane/lipid rafts with the cytoskeleton: impact on signaling and function: membrane/lipid rafts, mediators of cytoskeletal arrangement and cell signaling. Biochimica et biophysica acta. 2014; 1838(2):532–45. https://doi.org/10.1016/j.bbamem.2013.07.018 PMID: 23899502; PubMed Central PMCID: PMC3867519.

24. Na S, Collin O, Chowdhury F, Tay B, Ouyang M, Wang Y, et al. Rapid signal transduction in living cells is a unique feature of mechanotransduction. Proceedings of the National Academy of Sciences of the United States of America. 2008; 105(18):6626–31. https://doi.org/10.1073/pnas.0711704105 PMID: 18456839; PubMed Central PMCID: PMC2373315.

25. Huveneers S, Danen EH. Adhesion signaling—crosstalk between integrins, Src and Rho. Journal of cell science. 2009; 122(Pt 8):1059–69. https://doi.org/10.1242/jcs.039446 PMID: 19339545.

26. Poh YC, Na S, Chowdhury F, Ouyang M, Wang Y, Wang N. Rapid activation of Rac GTPase in living cells by force is independent of Src. PloS one. 2009; 4(11):e7886. https://doi.org/10.1371/journal.pone.0007886 PMID: 19924282; PubMed Central PMCID: PMC2773925.

27. Euteneuer U, Schliwa M. Persistent, directional motility of cells and cytoplasmic fragments in the absence of microtubules. Nature. 1984; 310(5972):58–61. PMID: 6377086.

28. Keller HU, Naef A, Zimmermann A. Effects of colchicine, vinblastine and nocodazole on polarity, motility, chemotaxis and cAMP levels of human polymorphonuclear leukocytes. Experimental cell research. 1984; 153(1):173–85. PMID: 6329793.

29. Wang X, Carlsson AE. Feedback mechanisms in a mechanical model of cell polarization. Physical biology. 2014; 11(6):066002. https://doi.org/10.1088/1478-3975/11/6/066002 PMID: 25313164.

30. Collins C, Tzima E. Rac[e] to the pole: setting up polarity in endothelial cells. Small GTPases. 2014; 5: e28650. https://doi.org/10.4161/sgtp.28650 PMID: 25202973; PubMed Central PMCID: PMC4160343.

31. Kaverina I, Straube A. Regulation of cell migration by dynamic microtubules. Seminars in cell & developmental biology. 2011; 22(9):968–74. https://doi.org/10.1016/j.semcdb.2011.09.017 PMID: 22001384; PubMed Central PMCID: PMC3256984.

32. Akhshi TK, Wernike D, Piekny A. Microtubules and actin crosstalk in cell migration and division. Cytoskeleton. 2014; 71(1):1–23. https://doi.org/10.1002/cm.21150 PMID: 24127246.

33. Etienne-Manneville S. Actin and microtubules in cell motility: which one is in control? Traffic. 2004; 5 (7):470–7. https://doi.org/10.1111/j.1600-0854.2004.00196.x PMID: 15180824.

34. Omelchenko T, Vasiliev JM, Gelfand IM, Feder HH, Bonder EM. Mechanisms of polarization of the shape of fibroblasts and epitheliocytes: Separation of the roles of microtubules and Rho-dependent actin-myosin contractility. Proceedings of the National Academy of Sciences of the United States of America. 2002; 99(16):10452–7. https://doi.org/10.1073/pnas.152339899 PMID: 12149446; PubMed Central PMCID: PMC124937.

35. Ritchie K, Iino R, Fujiwara T, Murase K, Kusumi A. The fence and picket structure of the plasma membrane of live cells as revealed by single molecule techniques (Review). Molecular membrane biology. 2003; 20(1):13–8. PMID: 12745919.

36. Moissoglu K, Kiessling V, Wan C, Hoffman BD, Norambuena A, Tamm LK, et al. Regulation of Rac1 translocation and activation by membrane domains and their boundaries. Journal of cell science. 2014; 127(Pt 11):2565–76. https://doi.org/10.1242/jcs.149088 PMID: 24695858; PubMed Central PMCID: PMC4038948.

II

FRET BIOSENSOR ALLOWS SPATIO-TEMPORAL OBSERVATION OF SHEAR STRESS-INDUCED POLAR RHOGDIα ACTIVATION

by

Shuai Shao, Xiaoling Liao, Fei Xie, Sha Deng, Xue Liu, Tapani Ristaniemi & Bo Liu
2018

Communications Biology vol 1, 224

https://doi.org/10.1038/s42003-018-0232-2

COMMUNICATIONS BIOLOGY

ARTICLE

https://doi.org/10.1038/s42003-018-0232-2 OPEN

FRET biosensor allows spatio-temporal observation of shear stress-induced polar RhoGDIα activation

Shuai Shao[1,2], Xiaoling Liao[3], Fei Xie[1], Sha Deng[1], Xue Liu[3], Tapani Ristaniemi[2] & Bo Liu[1]

Rho GDP-dissociation inhibitor α (RhoGDIα) is a known negative regulator of the Rho family that shuts off GDP/GTP cycling and cytoplasm/membrane translocation to regulate cell migration. However, to our knowledge, no reports are available that focus on how the RhoGDIα-Rho GTPases complex is activated by laminar flow through exploring the activation of RhoGDIα itself. Here, we constructed a new biosensor using fluorescence resonance energy transfer (FRET) technology to measure the spatio-temporal activation of RhoGDIα in its binding with Rho GTPases in living HeLa cells. Using this biosensor, we find that the dissociation of the RhoGDIα-Rho GTPases complex is increased by shear stress, and its dissociation rate varies with subcellular location. Moreover, this process is mediated by membrane fluidity, cytoskeleton and Src activity, which indicates that the regulation of RhoGDIα activation under shear stress application represents a relatively separate pathway from the shear stress-induced Rho pathway.

[1] School of Biomedical Engineering, Dalian University of Technology, Liaoning IC Technology Key Lab, 116024 Dalian, China. [2] Faculty of Information Technology, University of Jyväskylä, 40014 Jyväskylä, Finland. [3] Biomaterials and Live Cell Imaging Institute, Chongqing University of Science and Technology, 401331 Chongqing, China. These authors contributed equally: Shuai Shao, Xiaoling Liao. Correspondence and requests for materials should be addressed to B.L. (email: lbo@dlut.edu.cn)

Cell migration is a complicated process regulated by physical and chemical factors, playing a significant role in diverse physiological and pathological events, especially in tumor metastasis[1]. Before cell migration can occur, the concentrations of relevant factors are distributed in a spatially asymmetric manner, referred to as cell polarity[2]. This distribution pattern indicates the direction for migration and tumor metastasis[3]. A crucial factor contributing to the establishment of cell polarity is the Rho-family GTPases, which regulate the formation of lamellipodia and rearrangement of the cytoskeleton[4]. Rho GDP-dissociation inhibitor α (RhoGDIα), also known as RhoGDI1, is the main member of the RhoGDI family, is expressed ubiquitously[5] and participates in the Rho cycle between the GTP-bound (active state, on membrane) form and GDP-bound (inactive state, in cytoplasm) form[6]. The steady state of GDP-binding Rho GTPases in cytosol is associated with RhoGDIα forming a RhoGDIα-Rho GTPases complex. The complex translocates to the plasma membrane when activated by Rho guanine nucleotide exchange factors (Rho GEFs) and then the complex dissociates. After completing their functions, inactive Rho GTPases will be extracted from the membrane by RhoGDIα[7].

To date, most work has considered RhoGDIα as a negative regulator to Rho GTPases merely, ignoring its own mechanism of activation[8,9]. In fact, inhibiting RhoGDIα expression could promote invasion and metastasis of breast cancer cells and trophoblast stem cells[10,11], but overexpression in hepatoma cells has a similar effect[12,13]. Moreover, some reports have proved that RhoGDIα can be mediated by other molecules. For example, the ezrin-radixin-moesin protein family (ERM) can bind RhoGDIα directly to release Rho GTPases[14], and plexin-B3, a cell surface receptor of Semaphorin 5A, can interact with RhoGDIα transiently to promote the extraction of Rac-GTP from RhoGDIα to the cytoplasm[15]. Some kinases can even phosphorylate several amino acid sites of RhoGDIα directly to affect the formation process of RhoGDIα-Rho GTPases complex[16,17]. These findings indicate that there should exist a regulating pathway to RhoGDIα directly, ignored but important and independent of Rho GTPases.

However, because Rho GTPases can exert their regulation on RhoGDIα[9], and RhoGDIα can play its role only when it is combined with the Rho GTPases, which can be considered as RhoGDIα activation for its function of inhibiting Rho GTPases activation, the absence of an efficient tool makes it challenging to observe RhoGDIα activation in its binding with Rho GTPases in living cells. In this study, we designed a biosensor using fluorescence resonance energy transfer (FRET) and tested its ability to detect RhoGDIα and Rho GTPase binding levels in living cells while avoiding the effect of Rho GTPases. We constructed a spatiotemporal model of the binding degree distribution of the RhoGDIα-Rho GTPases complex in living HeLa cells, and analyzed the effects of different magnitudes of shear stress. We also describe the pathways of RhoGDIα binding with Rho GTPases in cell migration. The results show that RhoGDIα activation has a regulating method relatively independent of Rho GTPases, which is activated under shear stress and is influenced by cell membrane fluidity, microfilaments, and Src.

Results

The sl-RhoGDIα FRET biosensor reflects RhoGDIα activity. To monitor real-time change in RhoGDIα-Rho GTPases binding caused by the regulation of RhoGDIα, rather than by the Rho GTPases, a FRET-based biosensor, sl-RhoGDIα, was designed according to the fact that RhoGDIα molecular can bind with a switch II domain (Fig. 1a). A variant biosensor R66E-sl-RhoGDIα was constructed, in which the 66 Arg of switch II was mutated to Glu to prevent its binding with RhoGDIα, as a negative control to inhibit the combination of RhoGDIα and switch II (Fig. 1b). S-RhoGDIα (without linker) and nsl-RhoGDIα (without Switch II and linker) were also constructed as controls to demonstrate the necessity of switch II and the linker sequence in the biosensor (Fig. 1b). Proteins of biosensors were purified from BL21-competent cells in vitro, and RhoGDIα antibody was utilized (1:1000, ARHGDIA polyclonal antibody, ABclonal) to detect RhoGDIα (23 kDa) and sl-RhoGDIα biosensor (79 kDa) by western blot. As shown in Fig. 1c (Supplementary Figure 1), clear bands could be observed near the weight of 23 kDa in the disruption product of cells transfected with the biosensor or control group without transfection, while at a weight ~79 kDa clear bands were also detected in purified sl-RhoGDIα biosensor protein, R66E-sl-RhoGDIα biosensor protein and the disruption product of cells transfected with sl-RhoGDIα biosensor, but not in control group. The results showed its stable expression in both eukaryotic cells and colibacillus.

To verify the function of the biosensor, the fluorescence emission spectra between 450–530 nm of purified sl-RhoGDIα protein was measured upon excitation at 420 nm (SpectraMax M2, Molecular Devices). A lower energy transmission efficiency was observed after adding a specific RhoGDIα antibody (dilution 1:25) to inhibit the binding between RhoGDIα and switch II (Fig. 1d). Moreover, the FRET efficiency (emission ratio of 475 nm/515 nm) of purified proteins of sl-RhoGDIα and its negative control biosensor R66E-sl-RhoGDIα was also measured upon excitation at 420 nm for 20 min. An increase was observed upon RhoGDIα antibody application in sl-RhoGDIα, but not in R66E-sl-RhoGDIα (Fig. 1e). These results indicated the validity of the biosensor design for the binding between RhoGDIα and switch II, and also showed the specificity of sl-RhoGDIα biosensor for the detection of RhoGDIα activation.

To further verify the validity, specificity, and reversibility of the biosensor in vivo, 20 dyn cm^{-2} of shear stress was applied on biosensor-transfected cells as the stimulation. An obvious decrease of the FRET efficiency, indicating the separation of switch II from RhoGDIα under stimulation, was found in sl-RhoGDIα but not in R66E-sl-RhoGDIα (Fig. 1f, Supplementary Figure 2a and 2b). It was interesting that the decrease stopped when the shear stress was removed after application lasting for 5 min, and then the FRET efficiency increased slowly with time after the shear stress was removed (Supplementary Figure 2b and 2c). Obvious differences between control group and reverse test began to occur when shear stress had been removed for 26 min and remained ($p_{26min} = 0.034$, $p_{27min} = 0.037$, $p_{28min} = 0.042$, $p_{29min} = 0.044$, and $p_{30min} = 0.041$, Supplementary Figure 2c). However, the decrease of FRET efficiency disappeared when the cell with sl-RhoGDIα was co-transfected with V-Rac or N-Rac plasmid, both of which provided exogenous switch II domain although they can enhance or inhibit Rac activity, respectively (Fig. 1f). These findings reconfirmed that the sl-RhoGDIα biosensor could effectively and specifically test the RhoGDIα activation. In addition, 2 mmol per L NaOH was used to destroy the hydrogen bonds between RhoGDIα and switch II within the biosensor, which caused a remarkable decrease of the FRET efficiency in sl-RhoGDIα biosensor, but not so obvious in s-RhoGDIα, nsl-RhoGDIα or R66E-sl RhoGDIα (Supplementary Figure 2d). The results implied that the main cause of energy transfer was the combination of RhoGDIα with switch II by hydrogen bonds, and the linker between them was necessary to enhance the energy transfer efficiency. Cells with biosensors were also treated with GTP since GTP participates in RhoGDIα-Rho GTPases binding. Ten μmol per L of GTP causes the reduction of FRET efficiency in sl-RhoGDIα and a gentle decrease in R66E-sl-RhoGDIα, while no effect was found in s-RhoGDIα or nsl-

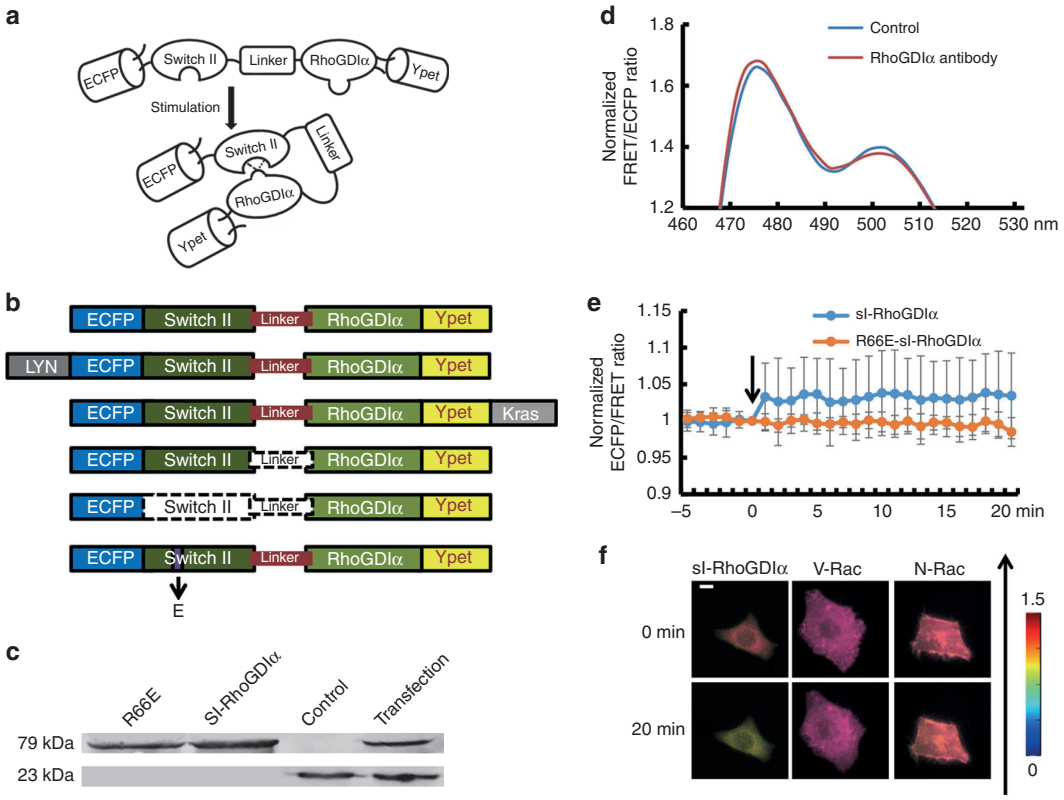

Fig. 1 The verification experiments of sl-RhoGDIα biosensor. **a** The diagram of sl-RhoGDIα biosensor. **b** The structure of sl-RhoGDIα and derived biosensors. Dotted line means these parts do not exist in biosensor structure. **c** Western blot results at 23 and 79 kDa. From left to right is shown the purified R66E-sl-RhoGDIα protein, sl-RhoGDIα protein, and the disruption product of cells from the control group without transfection and transfected with sl-RhoGDIα biosensor. **d** The emission spectrum of sl-RhoGDIα biosensor before and after RhoGDIα antibody stimulation. **e** The FRET efficiency time series of sl-RhoGDIα and R66E-sl-RhoGDIα biosensor with stimulation of RhoGDIα antibody. **f** The living cell images of sl-RhoGDIα ($n = 11$), V-Rac and sl-RhoGDIα ($n = 8$), N-Rac and sl-RhoGDIα ($n = 7$) upon shear stress. The direction of shear stress is from bottom to up as shown by the arrow. The scale bar is 10 μm

RhoGDIα (Supplementary Figure 2e). It also proved that switch II was required for energy transfer and the linker improves its efficiency.

These results implied that the sl-RhoGDIα biosensor could effectively detect the change of FRET efficiency caused by RhoGDIα's combination with switch II through hydrogen bonds in both in vitro and living cells. Moreover, the transfer efficiency was specially affected by the alternation of RhoGDIα activity, but not Rho GTPases.

Sublocation and magnitude of flow affect RhoGDIα activity. Since Rho GTPases existed in two different states, activated on the membrane and non-activated in the cytoplasm[18], sl-RhoGDIα was designed to show the affinity of the RhoGDIα-Rho GTPases in the cytoplasm, while Kras- and Lyn-sl-RhoGDIα indicated the presence of the complex on the cell membrane, at the non-lipid raft regions or on lipid rafts. Images of cells transfected with sl-RhoGDIα, Kras-sl-RhoGDIα, and Lyn-sl-RhoGDIα biosensor, respectively, showed obvious local differences in living cells, proving that sl-RhoGDIα biosensor existed in the cytoplasm, and Kras/Lyn sequence linked the biosensor to the cell membrane as expected. Shear stress was applied for 30 min to ensure biosensors had long enough time to become steady. A shear stress of 5 dyn cm^{-2} led to a FRET ratio decrease of ~25% in sl-RhoGDIα (Supplementary Movie 1, Supplementary Figure 3a, Supplementary Table 1) and Kras-sl-RhoGDIα (Supplementary Movie 2, Supplementary Figure 3a, Supplementary Table 2). Thus, RhoGDIα activity in cytoplasm and non-lipid raft regions on membrane decreased similarly with shear stress application (Supplementary Table 3, $p_{\text{Kras-Cyto}} = 0.618$).

H owever, in Lyn-sl-RhoGDIα (Supplementary Movie 3), RhoGDIα activity remained relatively unchanged after flow application and differed from sl-RhoGDIα and Kras-sl-RhoGDIα (Fig. 2b, $p_{\text{Lyn-Cyto}} = 0.012$, $p_{\text{Lyn-Kras}} = 0.007$). Moreover, the differences between these biosensors disappeared when the magnitude of shear stress rose to 20 dyn cm^{-2}, which indicated similar responses of RhoGDIα activity, decreasing about 20% at different positions (Fig. 3b, Supplementary Movie 4–6, Supplementary Figure 3b, Supplementary Table 3, $p_{\text{Lyn-Cyto}} = 0.820$, $p_{\text{Lyn-Kras}} = 0.880$, $p_{\text{Kras-Cyto}} = 0.745$). For a shear stress of 40dyn cm^{-2}, the dissociation of RhoGDIα and Rho GTPases in the cytoplasm and lipid rafts was less than the other two flow patterns, but it remained remarkable in non-lipid raft regions (Fig. 4b, Supplementary Movie 7–9, Supplementary Figure 3d).

All three biosensors showed that the RhoGDIα-Rho GTPases complex dissociated under shear stress, and the distribution of complex dissociation varied with magnitude of the shear stress. With the Kras-sl-RhoGDIα biosensor, 5 dyn cm^{-2} of shear stress caused an obvious difference ($p = 0.015$) between upstream (the edge facing the flow) and downstream measures (the edge opposite to the upstream along the direction of flow), with higher activity of RhoGDIα downstream in non-lipid raft regions on the cell membrane. However, the corresponding activity in the

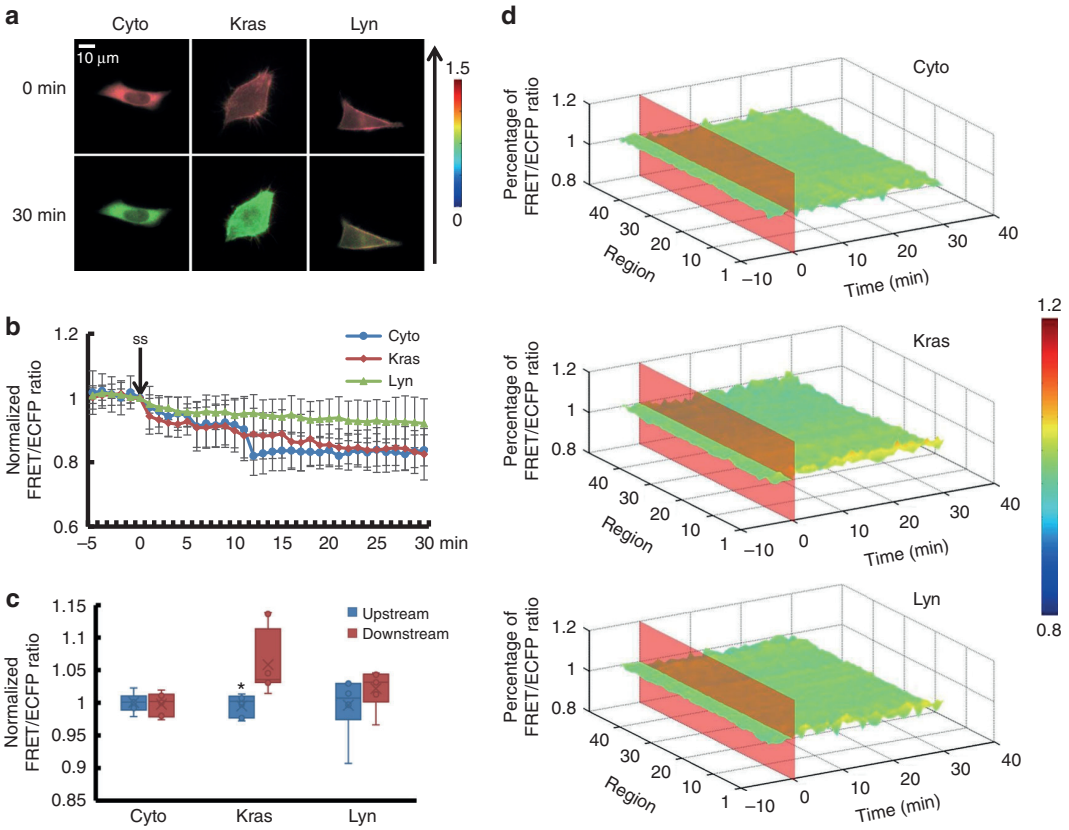

Fig. 2 The affinity of RhoGDIα and Rho GTPases at different subcellular locations under 5 dyn cm^{-2} of shear stress. **a** Living cell images of three biosensors under 5 dyn cm^{-2} of shear stress. Cyto represents the biosensor sl-RhoGDIα ($n = 6$), which exists in the cytoplasm. Kras represents Kras-sl-RhoGDIα ($n = 8$) and Lyn represents Lyn-sl-RhoGDIα ($n = 6$). The arrow shows the direction of shear stress. The scale bar is 10 μm. **b** Effect of shear stress on the binding degree of RhoGDIα and Rho. **c** The FRET/ECFP ratio comparison of upstream to downstream, after normalization. The asterisk denotes that there is an obvious difference between upstream and downstream. **d** The binding degree distribution of RhoGDIα and Rho. The FRET ratio percentage of each region overall is normalized before shear stress application. The dissociation of the RhoGDIα-Rho complex is inhibited downstream along the flow direction

cytoplasm of the overall region measured with the sl-RhoGDIα biosensor and in lipid rafts measured by the Lyn-sl-RhoGDIα biosensor did not change (Fig. 2c, d). In addition, RhoGDIα activity showed polarization ($p_{Cyto} = 0.004$, $p_{Kras} = 0.026$, $p_{Lyn} = 0.034$) for all three biosensors under 20 dyn cm^{-2} of shear stress (Fig. 3c, d). Under 40 dyn cm^{-2} of shear stress, the difference disappeared for sl-RhoGDIα and Lyn-sl-RhoGDIα ($p = 0.001$), but remained for Kras-sl-RhoGDIα (Fig. 4c, d). These results indicated that RhoGDIα-Rho GTPases had complex dissociation patterns under shear stress that were affected by the magnitudes of flow, and that the polarization of RhoGDIα activity was more obvious on the cell membrane, especially on non-lipid raft regions.

Membrane fluidity affects RhoGDIα activity with laminar flow. As shown above, shear stress-induced RhoGDIα activity change on the cell membrane had a more obvious polarity, so the Lyn-sl-RhoGDIα biosensor was applied in the following experiments for testing the effect of membrane fluidity. Since membrane fluidity was the most notable feature of cell membrane and inseparable from lipid rafts, benzol alcohol (BA) pre-incubation at 45 mmol per L for 15 min was used to enhance membrane fluidity[19]. The effect of membrane fluidity on RhoGDIα activity under 20 dyn cm^{-2} of shear stress was then assessed. Affinity polarity became stronger compared to the control group (p=0.015, Fig. 5b–d), while overall activity still decreased similarly to the control group (Supplementary Movie 10, Supplementary Figure 4a, Supplementary Table 4, $p_{BA\text{-}Control} = 0.722$). When cells were treated with cholesterol (CHO) at 0.1 mmol per L for 3 h to reduce membrane fluidity, RhoGDIα activity decreased about 30% upon laminar flow application, which was more significant than the control (Supplementary Figure 4a and Supplementary Movie 11). Although polarity still existed after CHO pretreatment, no obvious difference could be found on comparing this treatment to the control group (Fig. 5b–d, Supplementary Table 4, $p_{CHO\text{-}Control} = 0.007$). Thus, enhancing membrane fluidity aggravated the polarization of shear stress-induced RhoGDIα activity, while inhibiting membrane fluidity only affected the activity.

Cytoskeleton participates in RhoGDIα polarity upon shear stress. Since the cytoskeleton was closely related to the cell membrane, it seemed that the cytoskeleton would affect the RhoGDIα-Rho GTPases complex. To test this, cells were pretreated with different drugs to depolymerize different components of the cytoskeleton before 20 dyn cm^{-2} of shear stress was applied. ML-7 was an inhibitor of myosin light chain kinase (MLCK) that could eliminate force transmissions only through microfilaments while the structure remains intact[19,20]. When microfilaments were treated with 5 μmol per L of ML-7 for 1 h before laminar shear stress application, more obvious RhoGDIα activity reduction, nearly 38%, under shear stress was observed (Supplementary Movie 12, Supplementary Figure 4b,

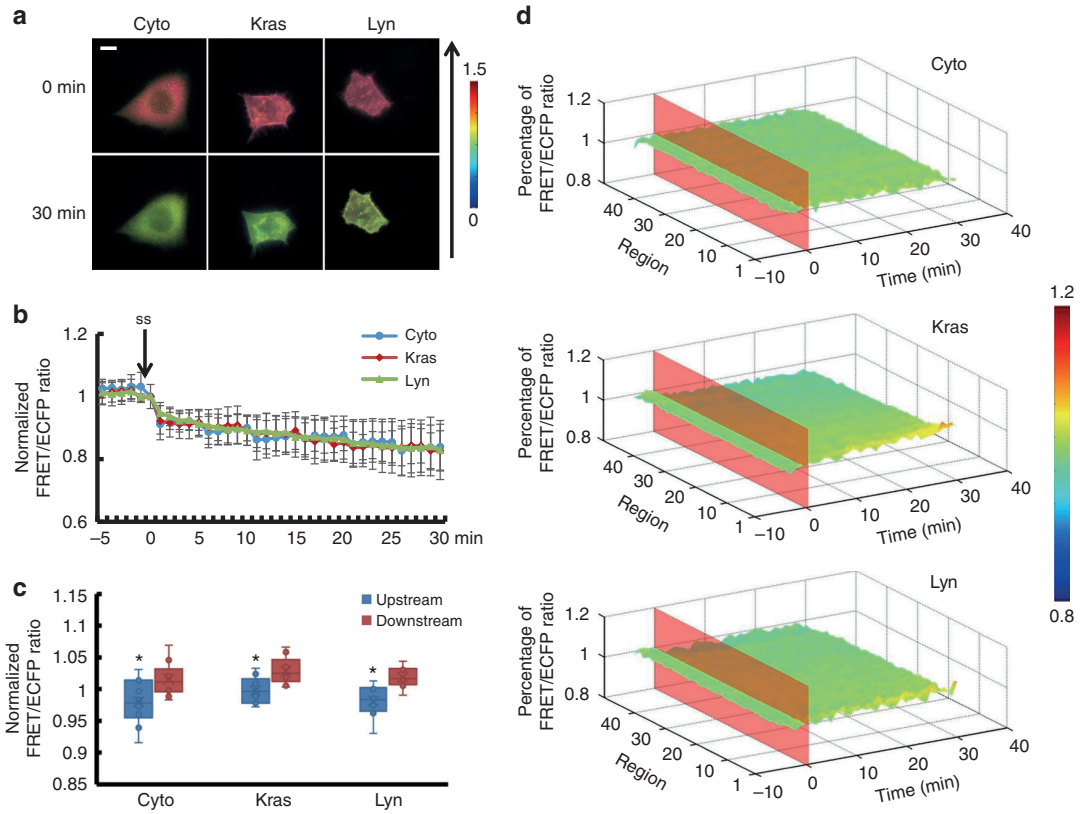

Fig. 3 The affinity of RhoGDIα and Rho GTPases at different subcellular locations under 20 dyn cm^{-2} of shear stress. **a** Living cell images of three biosensors under 20 dyn cm^{-2} of shear stress. Biosensors are indicated as in Fig. 2, Cyto ($n = 10$), Kras ($n = 9$) and Lyn ($n = 8$). The arrow shows the direction of shear stress. The scale bar is 10 μm. **b** Binding degree of RhoGDIα and Rho as a function of shear stress. **c** The FRET/ECFP ratio comparison of upstream to downstream, after normalization. The asterisk denotes that there is an obvious difference between upstream and downstream. **d** The binding degree distribution of RhoGDIα and Rho. The FRET ratio percentage of each region overall is normalized before shear stress application. The dissociation of RhoGDIα-Rho GTPases complex is inhibited downstream along the flow direction

Supplementary Table 4, $p_{\text{ML7-Control}} = 0.005$). The local activity distribution was more polarized ($p = 0.007$) compared to the control group (Fig. 6). Cytochalasin D (CytoD) pre-incubation at 2 μmol per L for 1 h to destroy the microfilament caused a similar effect on the RhoGDIα-Rho GTPases complex after 30 min of laminar shear stress application. The dissociation of the complex decreased to 35% and the polarity increased compared to the control group ($p = 0.032$; Fig. 6 and Supplementary Figure 4b and Supplementary Movie 13). This indicated that microfilaments participated in shear stress-induced RhoGDIα activation. However, compared to the control group, no significant change of RhoGDIα activity could be observed after application of 1 μmol per L of nocodazole (NOCO), a depolymerizing agent of microtubules, for 1 h before laminar shear stress was applied. However, RhoGDIα activity had a polarized distribution that was more noticeable than that of the control group when microtubules were destroyed ($p = 0.025$; Fig. 6d and Supplementary Movie 14). Thus, the cytoskeleton participated in the dissociation of the RhoGDIα-Rho GTPases complex under shear stress, and microfilaments played a more important role than microtubules.

Shear stress-induced RhoGDIα polarity is related to Src. Since Src can phosphorylate RhoGDIα to inhibit RhoGDIα and Rho GTPases from forming complexes[21], the effect of Src was tested by pre-treating cells with 50 mmol per L of Src inhibitor PP1 for 30 min[19]. The result clearly revealed that the RhoGDIα activity declined dramatically downstream when shear stress was applied (Fig. 7d, Supplementary Table 4, $p_{\text{pp1-Control}} = 0.006$), and the overall activity rose after laminar flow application, compared to the control group (Supplementary Movie 15, Supplementary Figure 4c).

RhoGDIα activation is different on non-lipid raft regions. As the results revealed, the activity and polarity of RhoGDIα upon shear stress were related to membrane fluidity, cytoskeleton and Src, while the Kras-based biosensor performaned differently. Inhibiting Src activity can keep the complex of RhoGDIα and Rho GTPases dissociating at non-lipid raft regions upon shear stress (Supplementary Movie 21, Supplementary Figures 5a and 5d, $n_{\text{pp1}} = 5$), which accorded with the result of Lyn-based biosensor. However, with the same pretreatment to membrane fluidity and cytoskeleton, the overall activity of RhoGDIα showed no obvious difference compared to the control group (Supplementary Figures 5a, 5b and 5c, Supplementary Movie 17–20).

As to the affinity distribution of RhoGDIα and Rho GTPases at non-lipid raft regions, inhibiting Src activity caused a polarity exchange between upstream and downstream (Supplementary Figure 6), and increasing membrane fluidity promoted the polarity after shear stress application ($p = 0.007$, Supplementary Figure 7), which were consistent with the polar distribution on lipid rafts. However, the changes in microfilaments status caused by ML-7 and CytoD did not affect RhoGDIα polarity, while destroying microtubules by NOCO improved the polarity (Supplementary Figure 8).

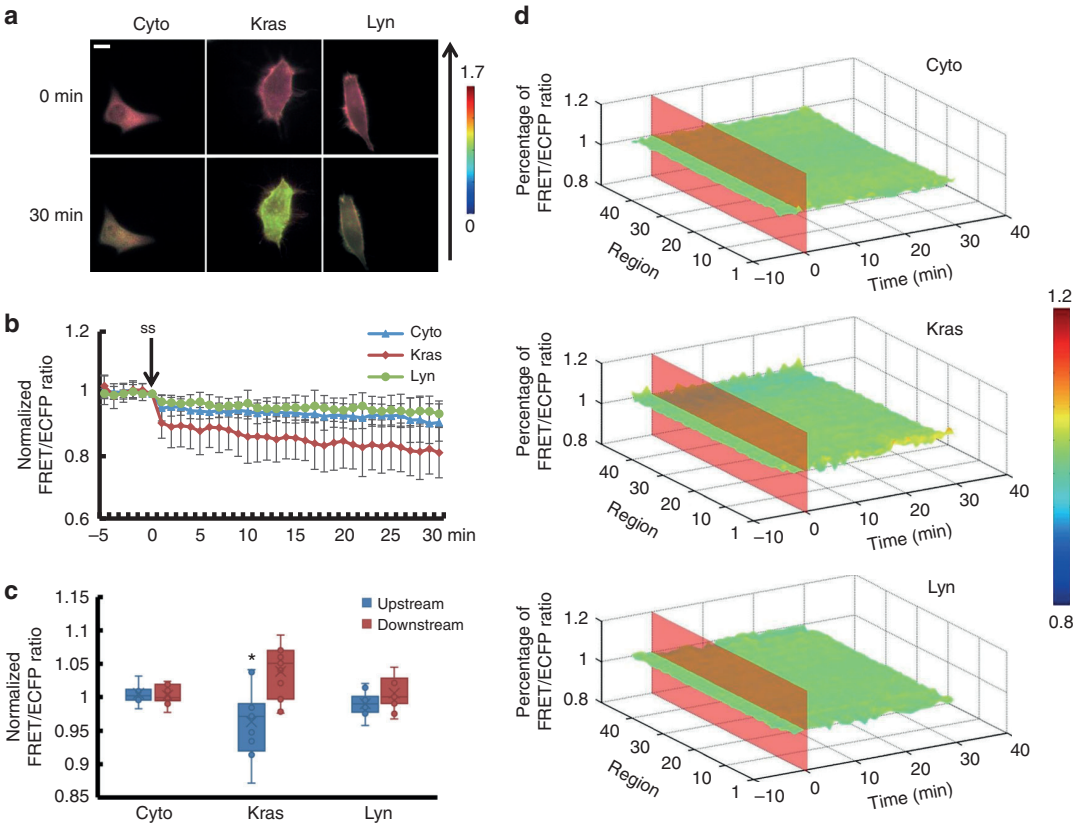

Fig. 4 The affinity of RhoGDIα and Rho GTPases at different subcellular locations under 40 dyn cm^{-2} of shear stress. **a** Living cell images of three biosensors under 40 dyn cm^{-2} of shear stress. Biosensors labeled as in Fig. 2, Cyto ($n = 11$), Kras ($n = 11$) and Lyn ($n = 11$). The arrow shows the direction of shear stress. The scale bar is 10 μm. **b** Binding degree of RhoGDIα and Rho as a function of shear stress. **c** The FRET/ECFP ratio comparison of upstream to downstream, after normalization. The asterisk denotes that there is an obvious difference between upstream and downstream. **d** The binding degree distribution of RhoGDIα and Rho. The FRET ratio percentage of each region overall is normalized before shear stress application. The dissociation of RhoGDIα-Rho GTPases complex is inhibited at downstream along the flow direction

Discussion

Previous studies on RhoGDIα mainly focused on its regulation of Rho GTPases. Less attention has been given to how RhoGDIα is activated in the physiologic processes. The likely reason for this gap in the field was the lack of an adequate tool to detect uncoupled RhoGDIα in living cells without the interference of Rho GTPases. Wu et al. have reported a RhoGDIα-YFP biosensor that was co-transfected with CFP-ROP2 and CFP-ROP6 to form energy transfers in living cells, which could catch the interaction between RhoGDIα and ROPs[22]. Konstadinos provided another assay to visualize the control of Rac1 membrane targeting. Two different GFP-tagged Rac, co-expressed with RhoGDIα and without RhoGDIα, were transfected with MCherry into cells. When GFP-tagged Rac was transmitted to cell membrane, the FRET ratio between MCherry and GFP changed. By comparing the ratio difference between GFP-tagged RhoGDIα-Rac and GFP-tagged Rac, this assay can show the ability of RhoGDIα to inhibit the membrane-targeted translocation of Rac[23]. Hodgson attached a fluorescence protein pair to the N-terminus of Cdc42 with a binding antenna. The FRET ratio between two fluorescence proteins responded strongly only to the interaction with RhoGDIα, which can exhibit the spatio-temporal dynamics of the RhoGDIα-Cdc42 interaction[24]. However, these biosensors could only show the interaction of RhoGDIα with a single Rho family membrane, which is affected by the activation of Rho GTPases. Therefore, the change of RhoGDIα itself without the effect of Rho GTPases could not be tested, because of the conformational changes of Rho GTPases caused by its activation.

Based on FRET technology, a new biosensor is designed in this project to observe the binding of RhoGDIα and Rho GTPases, indicating the activity of RhoGDIα. The efficiency of energy transfer is related to the distance between fluorescence protein pairs, which is adjusted by RhoGDIα combining with switch II through hydrogen bonds. Destroying hydrogen bonds by alkaline or mutating switch II declines the efficiency, which confirms the conformational changes caused by combination within the biosensor and also proves that the principle of sl-RhoGDIα biosensor is effective.

The central structure of sl-RhoGDIα biosensor is switch II, a sequence shared by Rho GTPases that can combine with RhoGDIα through hydrogen bonds. The switch II domain within the biosensor prevents the potential effects of RhoGDIα overexpression on endogenous Rho GTPases. In living cells, the FRET efficiency of sl-RhoGDIα biosensor decreases after shear stress application and recovers slightly when the shear stress is removed. This trend of slow increasing after the shear stress removal implies that the FRET efficiency responding to stimulus is reversible. Besides, the energy transfer efficiency changed by spatial reconstruction should be accomplished only through RhoGDIα activation, but not switch II due to its stable characteristics[11]. This is proved by the co-transfection of sl-RhoGDIα with N-Rac or V-Rac. Although specific sites are mutated in

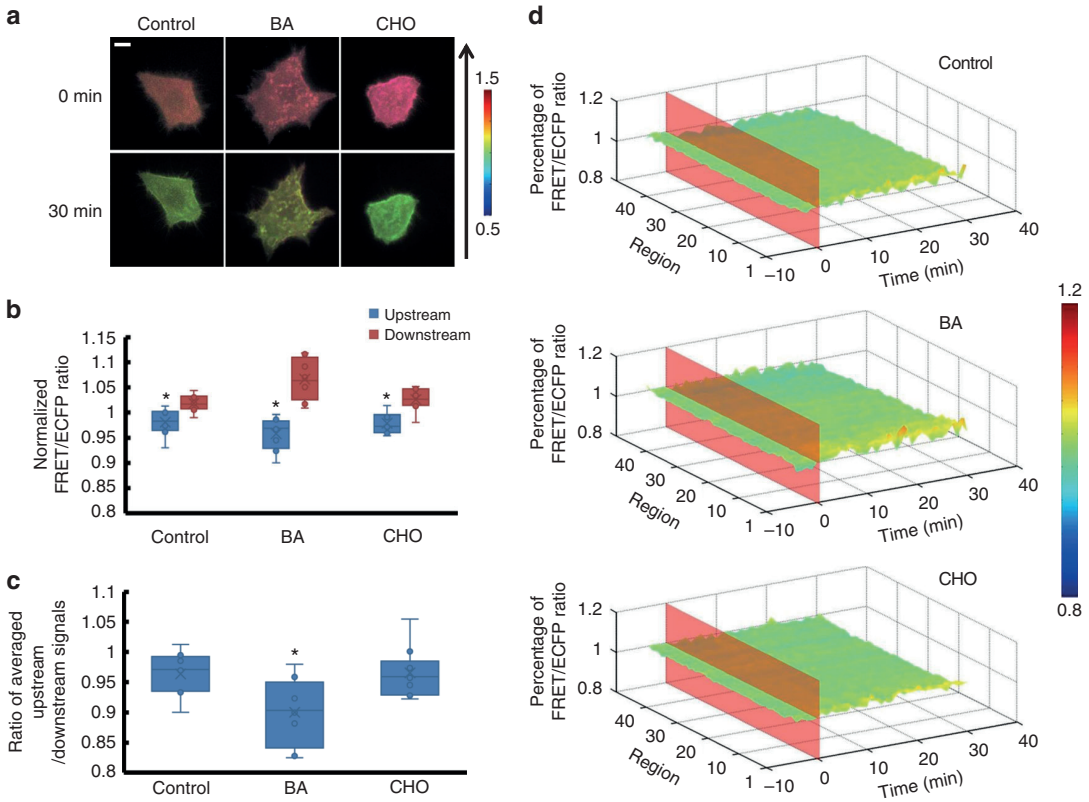

Fig. 5 The affinity of RhoGDIα and Rho GTPases under shear stress is affected by membrane fluidity. **a** Living cell images of Lyn-sl-RhoGDIα biosensor under 20 dyn cm^{-2} of shear stress with 45 mmol per L benzol alcohol (BA, $n = 8$) or 0.1 mmol per L of cholesterol (CHO, $n = 10$). The scale bar is 10 μm. **b** The FRET/ECFP ratio comparison of upstream to downstream, after normalization. **c** The ratio of averaged upstream/downstream for the control group and the BA/CHO group. The asterisk denotes that there is an obvious difference between upstream and downstream. **d** The binding degree distribution of RhoGDIα and Rho GTPases when membrane fluidity is changed. The FRET ratio percentage of each region overall is normalized before shear stress application. The dissociation of the RhoGDIα-Rho GTPases complex is inhibited more downstream along the flow direction when membrane fluidity is enhanced by BA. The asterisk denotes that there is an obvious difference compared to control group

N-Rac or V-Rac to inhibit or enhance Rac activity respectively[25,26], a same inhibition of shear stress-induced FRET efficiency is observed in the biosensor, since both N-Rac or V-Rac can bind to the RhoGDIα within the sl-RhoGDIα biosensor in living cells. The RhoGDIα antibody experiment in vitro shows a similar testification in specificity. The antibody can bind to RhoGDIα specifically in the biosensor and block its switch II binding sites. In addition, the biosensor shows its reversibility in living cells and prefect stability in both vitro and living cells, thus providing a visual tool for exploring the mechanism of RhoGDIα regulation in its association with Rho GTPases. However, it should be noted that the sl-RhoGDIα biosensor indicates the alternation of spatio-temporal RhoGDIα activity responding to stimulus, not the real binding degree between RhoGDIα and Rho GTPases in living cells.

The current study shows that RhoGDIα separates from switch II when laminar flow is applied to the cell, which means that the RhoGDIα-Rho GTPases complex dissociates and the inhibition of RhoGDIα to Rho GTPases decreases under shear stress. This phenomenon accords with the fact that Rho GTPases are activated by shear stress[27]. In addition, this dissociation is not uniform along the direction of laminar flow. This finding is similar to the feature of shear stress-induced Rho GTPases activation, which typically shows a strong spatial pattern. It was verified that the family member RhoA activity peaks at the leading edge followed by Cdc42 and Rac[28]. Upon shear stress application, Rac1 is activated at the leading edge of cells along the flow direction[29–31], and activated Cdc42 also polarizes at downstream regions[32]. Interestingly, RhoGDIα activation decreases more slowly at similar positions in the current work, indicating that negative regulation occurs in the process of RhoGDIα regulating Rho GTPases upon shear stress. Activated Rho GTPases assemble at downstream regions along the direction of shear stress, while the RhoGDIα-Rho GTPase complex binding at the same region is higher than in other regions. Paradoxically, a similar phenomenon has been observed in another work. RhoGDIα activated by the phosphorylation of Src exhibits lower affinity with Rho-GDP and translocates to the leading edge of cells where the GTP binding-Rho assemble[33], which seems to show that RhoGDIα attempts to regulate Rho activation to a normal level. However, the mechanism detail is still unclear.

The RhoGDIα activity is strongly related to subcellular location and force magnitudes. The expression of activated Rac1 increases under low shear stress (5 dyn cm^{-2}) compared to normal shear stress (20 dyn cm^{-2})[34]. As a negative regulator, the complex dissociation in cytoplasm experiences more under low-shear stress than normal or high-shear stress. The results conform to previous reports suggesting that low-shear stress would abate the dissociation of the RhoGDIα-Rho GTPases complex and release more Rho GTPases transformed to bind GTP[34]. However, RhoGDIα activity on the membrane appears to undergo eccentric changes. The activity of RhoGDIα in non-lipid raft regions is insensitive to force magnitudes. This is probably because after the dissociation of Rac1 or related Rho GTPases from RhoGDIα, they

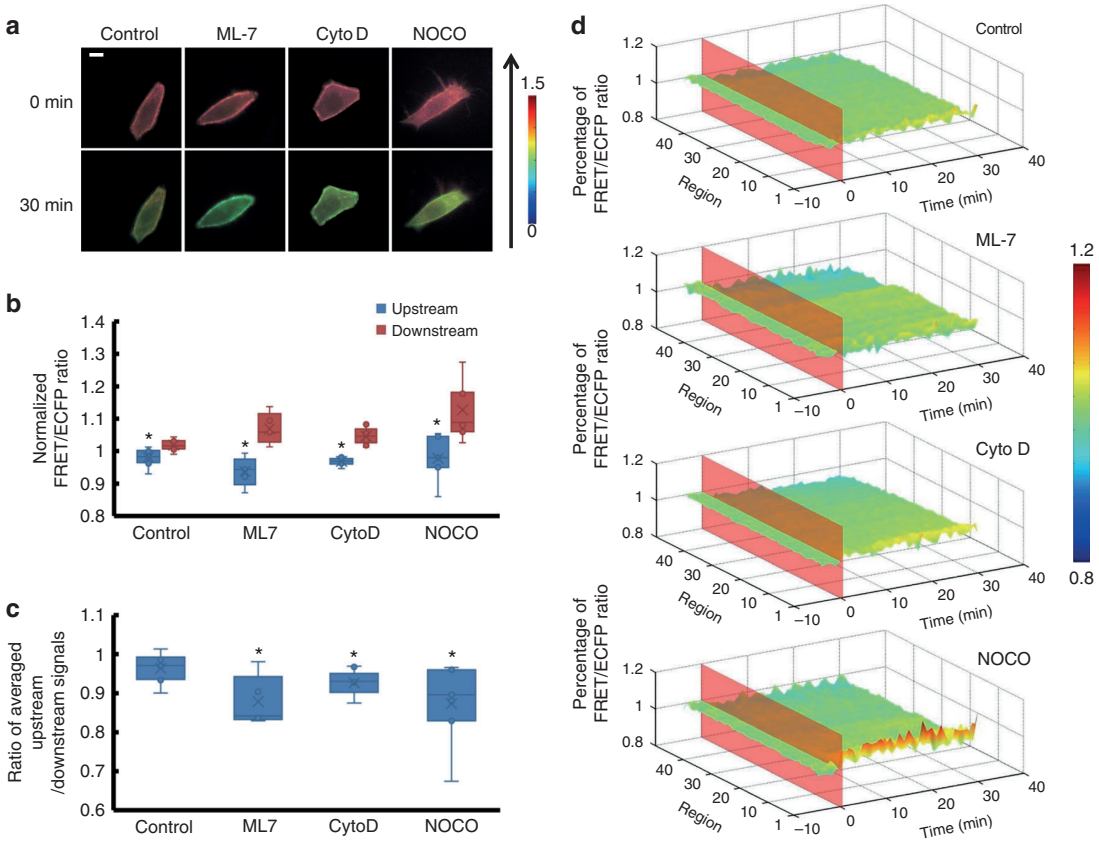

Fig. 6 The affinity of RhoGDIα and Rho GTPases under shear stress is affected by cytoskeleton. **a** The living cell images of Lyn-sl-RhoGDIα biosensor under 20 dyn cm^{-2} of shear stress treated with 5 μmol/l of ML-7($n = 5$), 2 μmol per L of Cytochalasin D (CytoD, $n = 9$), or 1 μmol per L of nocodazole (NOCO, $n = 7$). The scale bar is 10 μm. **b** The FRET/ECFP ratio comparison of upstream to downstream after normalization. **c** The averaged upstream/downstream ratio in the control group and in BA/CHO groups. The asterisk denotes that there is an obvious difference between upstream and downstream. **d** The binding degree distribution of RhoGDIα and Rho GTPases is enhanced downstream along the flow direction when cytoskeleton is disturbed. The FRET ratio percentage of each region overall is normalized before shear stress application. The asterisk denotes that there is an obvious difference compared to the control group

will be affected by some GTPase-activating proteins (GAPs) and then turn into non-activated status if they transfer to non-lipid raft regions[23]. It means that the key to keeping Rho GTPases non-activated at non-lipid raft regions should be GAPs, not RhoGDIα, and therefore the activity shown by the biosensor remains steady upon different levels of shear stress. However, the activity of RhoGDIα on lipid rafts decreases to a greater extent under normal than high- or low-shear stress. The difference may be attributable to the structure of lipid rafts and cytoskeleton. Lipid rafts are membrane domains that are enriched with cholesterol and certain saturated acyl lipids[35,36]. Those domains are dynamic and anchored by actin filaments. This anchoring of lipid rafts with actin filaments allows lipid rafts to move in a limited range[37], and differences observed among force magnitudes might reflect the kinetic features of lipid rafts or actin filaments. Actin filaments are the basic intracellular traction force. Actin stress fibers gradually disappear in response to intermediate shear stress but increase with low- or high-shear stress[38,39]. There is a close relationship between actin stress fibers and Src, the important regulator to RhoGDIα activity, which helps actin stress fibers to mediate RhoGDIα. In our results, RhoGDIα activity on lipid rafts is promoted when actin filaments are increased by low- or high-shear stress (Supplementary Figure 4f), while destroying microfilaments with drugs aggravates dissociation of the RhoGDIα-Rho GTPases complex (Supplementary Figure 4b). It is possible that the dissociation of the RhoGDIα-Rho GTPases complex is regulated by shear stress depending on its magnitude, which causes actin filament reorganization and then affects Src polarity. The phenomenon is most prominent in lipid raft regions, probably because actin filaments link to lipid rafts directly.

The cell membrane isolates the cell from the external environment and transmits force in a polarized manner upon mechanical loading[40]. The cytoskeleton may sense and transmit mechanical force to specific sites of the cell, since many sites on the membrane can be coupled with actin microfilaments[41]. Shear stress can be sensed by the membrane initially and then transferred to the actin cytoskeleton directly by membrane deformation, and then transmitted through the actin cytoskeleton to activate subsequent signaling pathways[42,43]. Indeed, our results show that membrane fluidity and cytoskeleton affect shear stress-induced RhoGDIα-Rho GTPase complex formation and dissociation. This mediation is more obvious on lipid rafts, while to the complex at non-lipid raft regions, only the polarity of combination is impacted by the status of membrane fluidity or cytoskeleton. The overall activity of RhoGDIα at non-lipid raft regions has no distinct response when the membrane fluidity or cytoskeleton is interfered. Together with the results that the RhoGDIα activity at non-lipid raft region has no clear relationship with the shear stress magnitudes mentioned above, it seems that the RhoGDIα mediated by shear stress is on lipid rafts

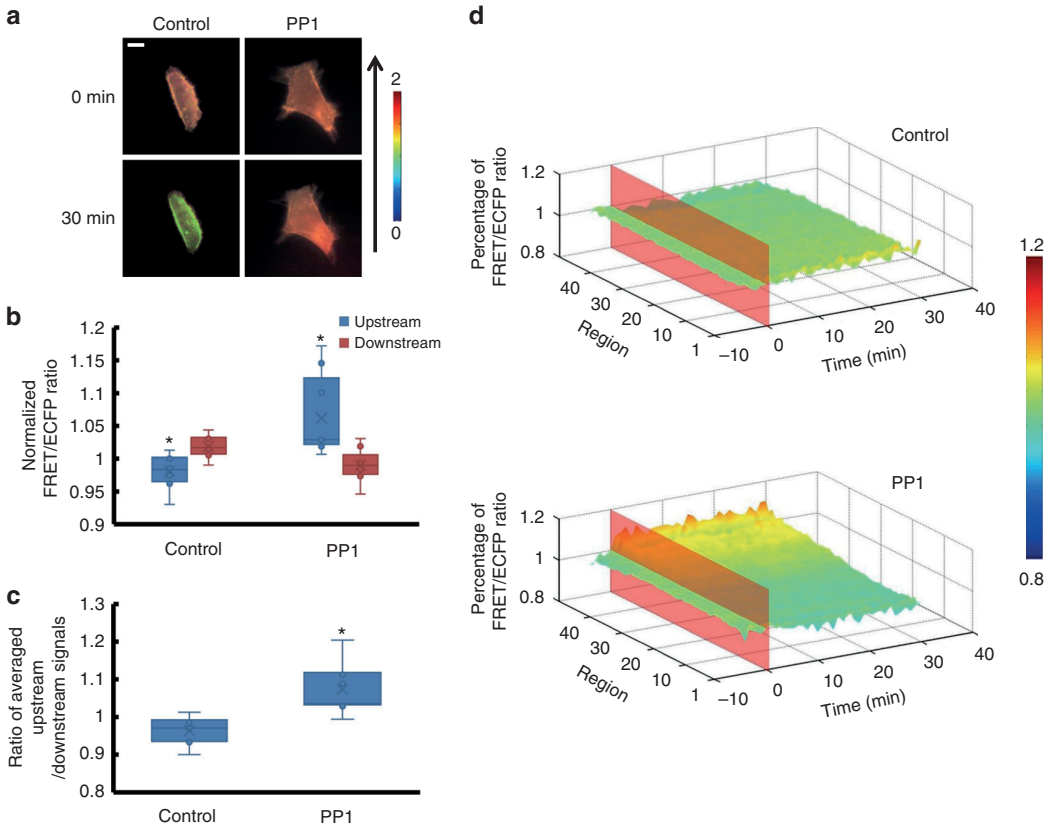

Fig. 7 The affinity of RhoGDIα and Rho GTPases under shear stress is affected by Src. **a** Living cell images of Lyn-sl-RhoGDIα biosensor under 20 dyn cm^{-2} of shear stress with 50 mmol per L of the Src inhibitor PP1($n = 7$). The scale bar is 10 μm. **b** The FRET/ECFP ratio comparison of upstream to downstream, after normalization. **c** Averaged upstream/downstream ratio for the control group and the PP1 group. The asterisk denotes that there is an obvious difference between upstream and downstream. **d** Binding degree distribution of RhoGDIα and Rho GTPases is enhanced at upstream regions along the flow direction when Src is inhibited. The FRET ratio percentage of each region overall is normalized before shear stress application. The asterisk denotes that there is an obvious difference compared to the control group

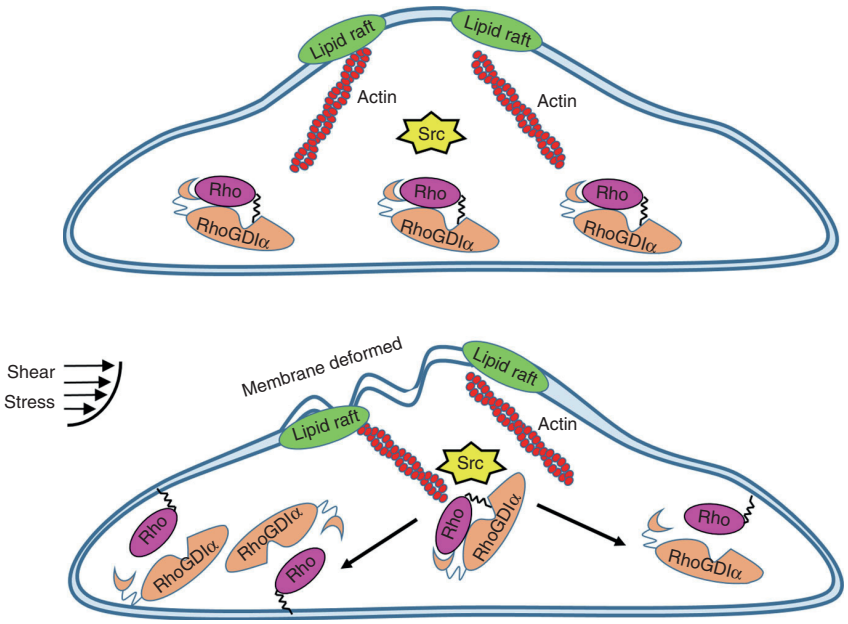

Fig. 8 The proposed mechanism of shear stress induced-RhoGDIα activation

mainly, not at non-lipid raft regions. Interestingly, promoting membrane fluidity alone can change the affinity distribution of the RhoGDIα-Rho GTPases complex on both of non-lipid raft regions and lipid rafts, while inhibiting membrane fluidity has no effects. This may be because inhibiting membrane fluidity causes the positions of lipid rafts to become more fixed and thus it is more difficult for the polarity to be formed. However, it seems that RhoGDIα activity is not changed by membrane fluidity or cytoskeleton directly upon shear stress in our results.

Src localizes on the endosomal membranes as a type of non-receptor kinase. Shear stress can cause a polarized Src activation in endothelial cell at the edge facing the flow[19]. ß$_3$ integrins are anchored to actin stress fibers and function as mechanosensors[44]. Its cytoplasmic tail recruits Src and Shp-1/2 to form a signaling complex, and then PKG II transforms to the ß$_3$-Shp-Src complex to dephosphorylate Shp-1; Shp-1 activation courses Src phosphorylation to active Src in a non-uniform manner;[19,45] Src-mediated RhoGDIα phosphorylation prevents the interaction and rebinding of membrane-associated Rho GTPases with RhoGDIα[21]. The polarizing activity of Src provides the spatial guide and regulates the dissociation of RhoGDIα and Rho GTPases through phosphorylating the former or maintains the complex in its original state. In the HeLa cells used for this study, when Src is specifically inhibited by PP1[19,46], the distribution of RhoGDIα-Rho GTPases still generates a polarization transfer. This is probably because Src polarity is eliminated or weakened by PP1 at the upstream region, and then Src-mediated phosphorylation of RhoGDIα decreases accordingly at those regions. Furthermore, the ability of RhoGDIα to form a complex with Rho GTPases is enhanced dramatically at the location. Further evidence is that polarized Src activation is affected by actin filaments and membrane fluidity under laminar flow. Disruption of actin filaments may enhance Src polarized activation, causing more Rho GTPases dissociation from RhoGDIα. Benzyl alcohol-mediated enhancement of membrane fluidity could inhibit shear stress-induced Src polarity[19]. A similar conclusion is suggested from the result that the RhoGDIα-Rho GTPases complex separates more obviously when membrane fluidity is inhibited. Therefore, shear stress-induced dissociation of RhoGDIα and Rho could be attributed to Src activation changes that occur under shear stress.

As a regulatory factor of Rho GTPases, most researches have reported that the combination of RhoGDIα and Rho is based on Rho GTPases activation. However, some upstream molecules target RhoGDIα directly to alter its conformation, modify it, and change its location to affect downstream signaling pathways[47]. Those microfilaments play different roles in the binding of RhoGDIα and Rho GTPases mediated by shear stress on lipid rafts and non-lipid rafts, which was an unexpected result. Upon stimulation of growth factors, Src transports to lipid rafts from perinuclear regions and is activated in an actin-dependent manner, but activated without transmission at non-lipid raft regions with the help of microtubules[48], indicating that Src activation is dependent on subcellular location. It may be the reason why microfilaments can affect RhoGDIα polarity on lipid rafts, but microtubules affect the polarity at non-lipid rafts. In a previous study, Rac1 was activated by shear stress directly by the force transmitting downstream with the help of the cell membrane and microtubules, but this has no relationship with Src[49]. In addition, Src activation is slower than Rac1[49] upon shear stress application, which means that Src-mediated RhoGDIα activation would be much slower than Rac1. Based on these results, shear stress-induced Rac1 activation should have no direct connection with RhoGDIα activation. In addition, it was also found that the cell membrane sensed the pattern of flow and deformed to transmit force to active Rho GTPases on lipid rafts under shear stress through microtubules[27,50], while active RhoGDIα was recruited through actin with the help of Src. Different cytoskeleton components mediate Rho GTPases and RhoGDIα activation when shear stress is applied. Therefore, it can be hypothesized that shear stress-induced RhoGDIα activation occurs in a different manner from Rho GTPases, although RhoGDIα is a negative regulator of Rho GTPases.

In this paper, a FRET biosensor that can measure the degree of binding for RhoGDIα and Rho in living cells is proposed, providing a useful visual tool to observe the activation of RhoGDIα in real-time without the interference of Rho GTPases. With results from the biosensor, a model of the regulation of the RhoGDIα-Rho GTPases complex and how RhoGDIα exerts its function under shear stress is built. The model can be simplified as follows (Fig. 8): the plasma membrane deforms when extracellular shear stress is applied to increase the cell membrane fluidity inhomogeneously, and then transfers the stress into intracellular forces, which are transmitted along actin filaments to the stress concentration point at the distal end through their contractions. Some mechanosensors such as ß$_3$ integrins anchored to the actin stress fibers[44] swing their tails and phosphorylate Src locally through ß$_3$-Shp-Src complex;[19,45] the polarizing activity of Src provides the spatial guide and regulates the dissociation of RhoGDIα and Rho GTPases through phosphorylating the former, or maintains the complex in its original state. This pathway is relatively independent, having no direct relationship with shear stress-induced Rho GTPase activation.

Methods

Design and establishment of sl-RhoGDIα-FRET biosensor. The biosensor, named sl-RhoGDIα, consists of a complete RhoGDIα sequence, a switch II sequence, a linker sequence, and ECFP/Ypet fluorescent protein pairs for FRET[51] (Fig. 1b). Switch II is a common domain shared by Rho GTPases and can form contacts with RhoGDIα, which do not appear to create dramatic changes in its own conformation[11]. In the biosensor construction, the distance changes between switch II and RhoGDIα represent the affinity changes of RhoGDIα and Rho GTPases, which should be only caused by variation in RhoGDIα activity[11]. A linker sequence (GGSGGT) was designed between the RhoGDIα and switch II domain to provide a site for bending to improve the FRET efficiency. To demonstrate the necessity of switch II and the linker sequence, contrast biosensors with the switch II sequence only and without the switch II sequence or linker were also designed as s-RhoGDIα and nsl-RhoGDIα, respectively (Fig. 1b). Since the combination of switch II and RhoGDIα depends on hydrogen bonds between 185 Asp, 30 Ala, and 31 Pro in RhoGDIα and 66 Arg in switch II, the 66 Arg in switch II domain of sl-RhoGDIα was mutated to Glu in order to destroy hydrogen bonds between RhoGDIα and switch II[11] to create a negative control biosensor, R66E-sl-RhoGDIα.

Utilizing the basic structure of sl-RhoGDIα, a Kras sequence was inserted after Ypet to link the whole biosensor to the non-lipid rafts regions on the plasma membrane[52], to create Kras-sl-RhoGDIα (Fig. 1b). A Lyn sequence was added behind the ECFP to link the biosensor to lipid rafts[52], giving Lyn-sl-RhoGDIα (Fig. 1b). These two membrane biosensors reflect the binding degree of RhoGDIα and Rho GTPases, respectively, on different positions of the membrane.

All biosensors mentioned above were constructed into pcDNA3.1(+) plasmids for expression in HeLa cells, and biosensor sequences of sl-RhoGDIα and R66E-sl-RhoGDIα were also inserted into a BL21 plasmid to produce and purify proteins for spectrum analysis and western blot in vitro.

Cell culture and transient transfection. Before transfection, HeLa cells were cultured with the high glucose version of Dulbecco's modified Eagle medium containing 10% fetal bovine serum, 2 mmol per L L-glutamine, 100 units/ml penicillin and 100 mg/ml sodium pyruvate (GIBCO BRL). Lipofectamin 3000 was chosen as the transfection reagent to transfect different DNA plasmids into cells. Cells were passed onto fibronectin-coated cover slips after transfection for 24 h and cultured with 0.5% FBS for 12 h before laminar flow application.

Flow systems. Laminar flows were provided by a classic parallel-plate flow chamber, modified to fit for dynamic observations under a FRET microscope[19]. Separated HeLa cells were seeded on a glass slide, which was covered by a silicone gasket, and a cover glass. Laminar shear stress was set to 5, 20, and 40 dyn cm^{-2}, respectively, by adjusting fluid flow in the chamber[53]. The flow experiments were done at 37 °C with 5% CO_2 to maintain the pH at 7.4.

Microscope image acquisition. The microscope image acquisition set-up contained an inverted microscope (Nikon Eclipse Ti Se-ries, Ti-Fl Epi-fl/1) and a cold CCD (Evolve^{TM}512, Photometrics). All fluorescence images were acquired on an isolated single cell by MetaFluor software (Universal Imaging) once in every 60s and arranged in chronological order beginning from 001. Images of different channels were created by MetaMorph software (Universal Imaging) for FRET ratio images. The excitation and emission wavelengths of ECFP are 420 and 475 nm, respectively, and the emission wavelength of Ypet is 535 nm.

Image analysis. A software package using Matlab (Mathworks; Natick, MA) was developed to rapidly analyze the spatio-temporal fluorescence data, which contains three different sections to allow pre-treatment and polarity analysis. First, all fluorescence images are read from two channels of one sample, including parameters indicating the direction of shear stress and the time points when laminar flow was applied. Fluorescence intensity from the four corners of the images was averaged to set the background, which must be subtracted before image quantification and analysis. After filtering speckle and edge recognition, ratio images showing FRET efficiency are achieved by calculating the specific value of FRET/ECFP. The average ratio of whole cell changing with time is shown by a linechart to analyze how shear stress affects the affinity of RhoGDIα and switch II. Second, polarity analysis is processed using ratio images. Single cells in the ratio images are divided into 50 parts, on average, of equal width along the direction of laminar flow. The first part was numbered as 1 to represent the downstream, and the last as 50 to represent the upstream. The percentage of fluorescence intensity in each part from the whole cell is calculated to represent the binding level of local RhoGDIα-Rho GTPases (Supplementary Figure 9). Third, data are combined with continuous time points, and the spatial and temporal changes of RhoGDIα are normalized and drawn into a three-dimensional graph.

Statistical analysis. All the ratio data were normalized by their basal levels before stimulation in the same cell. Statistical analysis was performed by using a two-tailed t-test function contained in the Excel software (Microsoft) to evaluate the statistical difference between groups. A significant difference was determined by the *p*-value (<0.05). To decrease the discreteness caused by choosing a single region, the first five regions were chosen and averaged at each time point to represent downstream of the cell and the last five regions represented the upstream. When a statistically significant difference existed (compared by two-tailed *t*-test) between the upstream and downstream values at 30 min by using a two-tailed *t*-test, it indicated polarity is present. All means involved in the manuscript are modified by standard deviation.

Code availability. MATLAB source code for image processing is provided as Supplementary Software 1.

Data availability

The data supporting the study that are not provided in the manuscript and Supplementary Data 1–3 are available from the corresponding author on reasonable request.

Received: 5 January 2018 Accepted: 14 November 2018
Published online: 10 December 2018

References

1. Lintz, M., Munoz, A. & Reinhart-King, C. A. The mechanics of single cell and collective migration of tumor cells. *J. Biomech. Eng.* **139**, 0210051–0210059 (2016).
2. Mazel, T. Crosstalk of cell polarity signaling pathways. *Protoplasma.* **254**, 1241–1258 (2017).
3. Narayanan, A. S., Reyes, S. B., Um, K., McCarty, J. H. & Tolias, K. F. The Rac-GAP Bcr is a novel regulator of the Par complex that controls cell polarity. *Mol. Biol. Cell* **24**, 3857–3868 (2013).
4. Moissoglu, K. & Schwartz, M. A. Spatial and temporal control of Rho GTPase functions. *Cell. Logist.* **4**, e943618 (2014).
5. Ueyama, T. et al. Negative charges in the flexible N-terminal domain of Rho GDP-dissociation inhibitors (RhoGDIs) regulate the targeting of the RhoGDI-Rac1 complex to membranes. *J. Immunol.* **191**, 2560–2569 (2013).
6. Tzima, E. Role of small GTPases in endothelial cytoskeletal dynamics and the shear stress response. *Circ. Res.* **98**, 176–185 (2006).
7. Boulter, E. & Garcia-Mata, R. RhoGDI: a rheostat for the Rho switch. *Small GTPases* **1**, 65–68 (2010).
8. Desiderio, V. et al. Increased fucosylation has a pivotal role in invasive and metastatic properties of head and neck cancer stem cells. *Oncotarget* **6**, 71–84 (2015).
9. Giang, Ho. T. T. et al. RhoGDIalpha-dependent balance between RhoA and RhoC is a key regulator of cancer cell tumorigenesis. *Mol. Biol. Cell* **22**, 3263–3275 (2011).
10. Zhang, J., Li, T., Ji, W., Yu, Y. & Tan, T. Rho GDIalpha modulates rabbit trophoblast stem cell survival and migration. *Biol. Reprod.* **93**, 144 (2015).
11. Hoffman, G. R., Nassar, N. & Cerione, R. A. Structure of the Rho family GTP-binding protein Cdc42 in complex with the multifunctional regulator RhoGDI. *Cell* **100**, 345–356 (2000).
12. Xiao, Y. et al. 14-3-3tau promotes breast cancer invasion and metastasis by inhibiting RhoGDIalpha. *Mol. Cell. Biol.* **34**, 2635–2649 (2014).
13. Wang, H. et al. Overexpression of RhoGDI, a novel predictor of distant metastasis, promotes cell proliferation and migration in hepatocellular carcinoma. *FEBS Lett.* **588**, 503–508 (2014).
14. Chiappetta, C. et al. Correlation of the Rac1/RhoA pathway with ezrin expression in osteosarcoma. *Appl. Immunohistochem. Mol. Morphol.* **22**, 162–170 (2014).
15. Li, X. & Lee, A. Y. Semaphorin 5A and plexin-B3 inhibit human glioma cell motility through RhoGDIalpha-mediated inactivation of Rac1 GTPase. *J. Biol. Chem.* **285**, 32436–32445 (2010).
16. Abramovici, H. et al. Diacylglycerol kinase zeta regulates actin cytoskeleton reorganization through dissociation of Rac1 from RhoGDI. *Mol. Biol. Cell* **20**, 2049–2059 (2009).
17. Tkachenko, E. et al. Protein kinase A governs a RhoA-RhoGDI protrusion-retraction pacemaker in migrating cells. *Nat. Cell Biol.* **13**, 660–667 (2011).
18. Garcia-Mata, R., Boulter, E. & Burridge, K. The 'invisible hand': regulation of RHO GTPases by RHOGDIs. *Nat. Rev. Mol. Cell Biol.* **12**, 493–504 (2011).
19. Liu, B. et al. RhoA and membrane fluidity mediates the spatially polarized Src/FAK activation in response to shear stress. *Sci. Rep.* **4**, 7008 (2014).
20. Liu, B., Lu, S., Zheng, S., Jiang, Z. & Wang, Y. Two distinct phases of calcium signalling under flow. *Cardiovasc. Res.* **91**, 124–133 (2011).
21. DerMardirossian, C., Rocklin, G., Seo, J. Y. & Bokoch, G. M. Phosphorylation of RhoGDI by Src regulates Rho GTPase binding and cytosol-membrane cycling. *Mol. Biol. Cell* **17**, 4760–4768 (2006).
22. Wu, Y. et al. CPK3-phosphorylated RhoGDI1 is essential in the development of *Arabidopsis* seedlings and leaf epidermal cells. *J. Exp. Bot.* **64**, 3327–3338 (2013).
23. Moissoglu, K. et al. Regulation of Rac1 translocation and activation by membrane domains and their boundaries. *J. Cell Sci.* **127**, 2565–2576 (2014).
24. Hodgson, L. et al. FRET binding antenna reports spatiotemporal dynamics of GDI-Cdc42 GTPase interactions. *Nat. Chem. Biol.* **12**, 802–809 (2016).
25. Salgado, A. P. et al. Study of vaccinia and cowpox viruses' replication in Rac1-N17 dominant-negative cells. *Mem. do Inst. Oswaldo Cruz* **108**, 554–562 (2013).
26. Jefferies, C. A. & O'Neill, L. A. Rac1 regulates interleukin 1-induced nuclear factor kappaB activation in an inhibitory protein kappaBalpha-independent manner by enhancing the ability of the p65 subunit to transactivate gene expression. *J. Biol. Chem.* **275**, 3114–3120 (2000).
27. Collins, C. & Tzima, E. Rac[e] to the pole: setting up polarity in endothelial cells. *Small GTPases* **5**, e28650 (2014).
28. Newell-Litwa, K. A. & Horwitz, A. R. Cell migration: PKA and RhoA set the pace. *Curr. Biol.* **21**, R596–R598 (2011).
29. Tzima, E. et al. Activation of Rac1 by shear stress in endothelial cells mediates both cytoskeletal reorganization and effects on gene expression. *EMBO J.* **21**, 6791–6800 (2002).
30. Wojciak-Stothard, B. & Ridley, A. J. Shear stress-induced endothelial cell polarization is mediated by Rho and Rac but not Cdc42 or PI 3-kinases. *J. Cell Biol.* **161**, 429–439 (2003).
31. Kraynov, V. S. et al. Localized Rac activation dynamics visualized in living cells. *Science* **290**, 333–337 (2000).
32. Tzima, E., Kiosses, W. B., del Pozo, M. A. & Schwartz, M. A. Localized cdc42 activation, detected using a novel assay, mediates microtubule organizing center positioning in endothelial cells in response to fluid shear stress. *J. Biol. Chem.* **278**, 31020–31023 (2003).
33. Lee, H. S. et al. Protein tyrosine phosphatase-PEST and beta8 integrin regulate spatiotemporal patterns of RhoGDI1 activation in migrating cells. *Mol. Cell. Biol.* **35**, 1401-1413 (2015).
34. Qi, Y. X. et al. Rho-GDP dissociation inhibitor alpha downregulated by low shear stress promotes vascular smooth muscle cell migration and apoptosis: a proteomic analysis. *Cardiovasc. Res.* **80**, 114–122 (2008).
35. Head, B. P., Patel, H. H. & Insel, P. A. Interaction of membrane/lipid rafts with the cytoskeleton: impact on signaling and function: membrane/lipid rafts, mediators of cytoskeletal arrangement and cell signaling. *Biochim. Biophys. Acta* **1838**, 532–545 (2014).
36. Gonnord, P., Blouin, C. M. & Lamaze, C. Membrane trafficking and signaling: two sides of the same coin. *Semin. Cell Dev. Biol.* **23**, 154–164 (2012).
37. Ritchie, K., Iino, R., Fujiwara, T., Murase, K. & Kusumi, A. The fence and picket structure of the plasma membrane of live cells as revealed by single molecule techniques (Review). *Mol. Membr. Biol.* **20**, 13–18 (2003).

38. Wan, Q., Kim, S. J., Yokota, H. & Na, S. Differential activation and inhibition of RhoA by fluid flow induced shear stress in chondrocytes. *Cell Biol. Int.* **37**, 568–576 (2013).
39. Lijuan, W. et al. Integrins mediate the migration of HepG2 cells induced by low shear stress. *J. Biomed. Eng.* **31**, 336–340 (2014).
40. Butler, P. J., Norwich, G., Weinbaum, S. & Chien, S. Shear stress induces a time- and position-dependent increase in endothelial cell membrane fluidity. *Am. J. Physiol. Cell Physiol.* **280**, C962–C969 (2001).
41. Hsu, S., Thakar, R., Liepmann, D. & Li, S. Effects of shear stress on endothelial cell haptotaxis on micropatterned surfaces. *Biochem. Biophys. Res. Commun.* **337**, 401–409 (2005).
42. Tabouillot, T., Muddana, H. S. & Butler, P. J. Endothelial cell membrane sensitivity to shear stress is lipid domain dependent. *Cell. Mol. Bioeng.* **4**, 169–181 (2011).
43. Provenzano, P. P. & Keely, P. J. Mechanical signaling through the cytoskeleton regulates cell proliferation by coordinated focal adhesion and Rho GTPase signaling. *J. Cell Sci.* **124**, 1195–1205 (2011).
44. Wang, Y. et al. A model for the role of integrins in flow induced mechanotransduction in osteyocytes. In *Bioengineering Conference, 2007 NEBC '07 IEEE 33rd Annual Northeast* (IEEE, New York, 2007).
45. Hema, R. Cyclic GMP and protein kinase G control a Src-containing mechanosome in osteoblasts. *Sci. Signal.* **153**, ra91 (2010).
46. Xu, W. et al. Regulation of BMP2-induced intracellular calcium increases in osteoblasts. *J. Orthop. Res.* **34**, 1725–1733 (2016).
47. Xie, F. et al. Role of Rho-specific guanine nucleotide dissociation inhibitor alpha regulation in cell migration. *Acta Histochem.* **119**, 183–189 (2017).
48. Seong, J. et al. Visualization of Src activity at different compartments of the plasma membrane by FRET imaging. *Chem. Biol.* **16**, 48–57 (2009).
49. Poh, Y. C. et al. Rapid activation of Rac GTPase in living cells by force is independent of Src. *PloS ONE* **4**, e7886 (2009).
50. Shao, S. et al. Visualizing the spatiotemporal map of Rac activation in bovine aortic endothelial cells under laminar and disturbed flows. *PLoS ONE* **12**, e0189088 (2017).
51. Xiang, X. et al. A FRET-based biosensor for imaging SYK activities in living cells. *Cell. Mol. Bioeng.* **4**, 670–677 (2011).
52. Jura, N. & Bar-Sagi, D. Mapping cellular routes of Ras: a ubiquitin trail. *Cell Cycle* **5**, 2744–2747 (2006).
53. Chachisvilis, M., Zhang, Y. L. & Frangos, J. A. G protein-coupled receptors sense fluid shear stress in endothelial cells. *Proc. Natl Acad. Sci. USA* **103**, 15463–15468 (2006).

Acknowledgements

The study was supported in part by grants from the National Natural Foundation of China (No. 31670867, 31670961, 11532004) and Natural Science Key Foundation Project of CQ in China (CSTC2015JCYJBX0003).

Author contributions

S. S. and B.L. designed the research of this paper; S. S., F.X. and S. D. performed research and analyzed data; S. S., X.L., X.L.L., T.R. and B.L. wrote the paper.

Additional information

Supplementary Information accompanies this paper at https://doi.org/10.1038/s42003-018-0232-2.

Competing interests: The authors declare no competing interests.

Reprints and permission information is available online at http://npg.nature.com/reprintsandpermissions/

Publisher's note: Springer Nature remains neutral with regard to jurisdictional claims in published maps and institutional affiliations.

III

A DNA-ENCODED FRET BIOSENSOR FOR VISUALIZING THE TENSION ACROSS PAXILLIN IN LIVING CELLS UPON SHEAR STRESS

by

Shuai Shao, Sha Deng, Qingyun Jiang, Hangyu Zhang, Zhengyao Zhang, Na Li, Fengyu Cong, Timo Tiihonen & Bo Liu 2021

Analysis&Sensing vol 1: e202100061

https://doi.org/10.1002/anse.202100033

Analysis & Sensing

Chemistry Europe
European Chemical Societies Publishing

Accepted Article

Title: A DNA-Encoded FRET Biosensor for Visualizing the Tension across Paxillin in Living Cells upon Shear Stress

Authors: Shuai Shao, Sha Deng, Qingyun Jiang, Hangyu Zhang, Zhengyao Zhang, Na Li, Fengyu Cong, Timo Tiihonen, and Bo Liu

To be cited as: *Anal. Sens.* 10.1002/anse.202100033

Link to VoR: https://doi.org/10.1002/anse.202100033

WILEY-VCH

A DNA-Encoded FRET Biosensor for Visualizing the Tension across Paxillin in Living Cells upon Shear Stress

Shuai Shao[a][b], Sha Deng[a], Qingyun Jiang[a], Hangyu Zhang[a], Zhengyao Zhang[c], Na Li[a], Fengyu Cong[a], Timo Tiihonen[b], Bo Liu* [a]

[a] S. Shao, S. Deng, Q. Jiang, Prof. H. Zhang, Prof. N. Li, Prof F. Cong, Prof. B.Liu
School of Biomedical Engineering, Liaoning Key Lab of Integrated Circuit and Biomedical Electronic System
Dalian University of Technology
Dalian 116024 (China)
E-mail: lbo@dlut.edu.cn
[b] Dr. S. Shao, Prof. T. Tiihonen
Faculty of Information Technology
University of Jyväskylä
Jyväskylä 40014 (Finland)
[c] Prof. Z. Zhang
School of Life and Pharmaceutical Sciences
Dalian University of Technology
Panjin 124221 (China)

Abstract: Paxillin is a potential participant in the direct intracellular force transmission which is considered as the foundation of cells sensing and responding to extracellular environment. However, the detection of tension across paxillin has not been achieved due to lacking microsized tools. Herein, a paxillin tension sensor (PaxTs) based on Fluorescence Resonance Energy Transfer (FRET) technique was constructed. PaxTs can be expressed and assembled to FA sites spontaneously to visualize the tension across paxillin with FRET efficiency of ~62.4% in living cells. The tension across paxillin was found to decrease upon shear stress, in which the membrane fluidity and contractility of actin acted as cushions. It is observed that paxillin participates in the pathway of cell membrane-cytoskeleton-FAs for force transmission upon mechanical force in real time visualization, which provides a promising new method to investigate the direct intracellular force transmission in biology and technology.

Introduction

The migration of cells is a complicated and coordinated process related to numerous signaling pathways. It plays a significant role in various physiological and pathological process including cancer invasion and metastasis[1]. Migrating cells experience various forces and the relevant signal proteins are activated asymmetrically in space to establish cell polarity as a reaction to the surrounding mechanical environment in the early stage of migration [2]. The establishment of polarity is very rapid and recognized to be in connection with the direct participation of stress transmission through cytoskeleton[3]. As the initial sites of mechanotransduction occurring on cells, focal adhesions are micron-sized multi-component protein complexes that assemble at the front edge and disassemble at the rear edge dynamically in the process of cell migration[4] . Cells are anchored to extracellular matrix (ECM) with integrins in FAs, a family of transmembrane proteins that can sense the mechanical properties of surroundings [5]. In addition, FAs are also linked to cytoskeleton, which establishes a connection to ECM[6]. This structure, with numbers of structure proteins contained in FAs, provides the foundation for the transduction of extracellular mechanical signals into intracellular responses[7].

Paxillin, a main component of FAs, is anchored to FA sites on the plasma membrane by its four LIM domains on the C-terminal region and connected to cytoskeleton by its five LD motifs on the N-terminal region[8]. During cell movement and migration, paxillin is recruited at nascent FAs at the front of cells to assemble the adhesion complex and also necessary to disassemble FAs at the rear end of cells[9]. Instead of exhibiting enzyme activity, paxillin acts as a scaffolding protein to provide docking sites for multiple FA-associated proteins to facilitate the formation of the complex. Many of the binding partners to paxillin have been proved to have close relationships with the rapid establishment of cell polarity or force transmission[10]. Thus, paxillin contacting those proteins extensively enables itself to participate in force transmission and the subsequent cell polarity establishment, implying a potential direct pathway for force transfer through the structure consisting of ECM, FAs and cytoskeletons. However, how force is transferred across paxillin is not clear because of lacking effective tools to visualize the paxillin tension on a micro scale.

Previously, a tension sensor module (TSMod) in which an elastic domain was inserted between a pair of fluorophores was developed to measure the force through the nano-spring by fluorescence resonance energy transfer (FRET) technique. The application of tension stretched the nano-spring which was compact without tension and decreased FRET. Using tension sensors constructed with TSMod, paxillin and talin in FAs were proved to under mechanical tension[11]. In this study, a paxillin tension sensor (PaxTS) was designed with a modified tension sensor module and verified on its ability to visualize the force transmission across paxillin in living cells. With PaxTS biosensor, the stress condition of paxillin during shear stress application was analyzed and the results demonstrated the stress transmission pathway of cell membrane-cytoskeleton-FAs in cells. The stress transmission across paxillin within cellular FAs was directly related to the fluidity of cell membrane and the integrity of cytoskeleton, especially the microfilament system.

Results and Discussion

The two major sets of motifs in paxillin, the LIM domains in the carboxyl terminal and the LD domains close to the amino terminus, are essential parts for its localization to FAs and cytoskeleton. The fluorescence protein pairs ECFP/Ypet was connected with an improved nano-spring[12], which formed a unique structure converting tension changes to FRET efficiency. The structure was inserted between LD12 domain and LIM1234 domain to construct a FRET biosensor named PaxTS, which was used to detect the tension across paxillin upon shear stress (Fig 1A). A LD12-less contrast biosensor (PaxDL, Fig1B) was

constructed to confirm whether PaxTS was assembled correctly to FA sites. PaxTS expressed steadily in U-2 OS, CHO and SH-SY5Y cells with prominent plaques respectively with some presented in the cytosol and nucleus, while no obvious plaques could be observed with the expression of PaxDL (Fig 1C, 1D). The results demonstrated that PaxTS was recruited to FAs spontaneously instead of endogenous paxillin with superior specificity and adaptability.

To evaluate the relationship between the tension across paxillin and FRET ratio, hypotonic treatment with H_2O was applied to cells, which stretched the cytoskeleton by water swelling and increased the tension across paxillin. Cells expressing PaxTS showed low FRET ratio after hypotonic treatment (Fig 2A-2D). Furthermore, when adding more volume of H_2O (1/2/3 times) into culture medium respectively, PaxTS displayed lower FRET ratio (Fig 2E, Supplementary Movie 1-3). It suggested that the FRET ratio was corresponding to the force sensed by paxillin and PaxTS achieved its desired function. On this basis, hypertonic treatment with sucrose solution of 0.025 g/ml was applied after the hypotonic treatment with 1-time volume of H_2O for 10 min, and the FRET ratio increased after decline (Fig 2F-2H, Supplementary Movie 4). In addition, removing shear stress after application for 10 min, the FRET ratio recovered nearly to the ground state (Fig S1). Both the results proved the reversibility of PaxTS. Generally, these results indicated that PaxTS can be used as a tool to detect the force transmission in living cells.

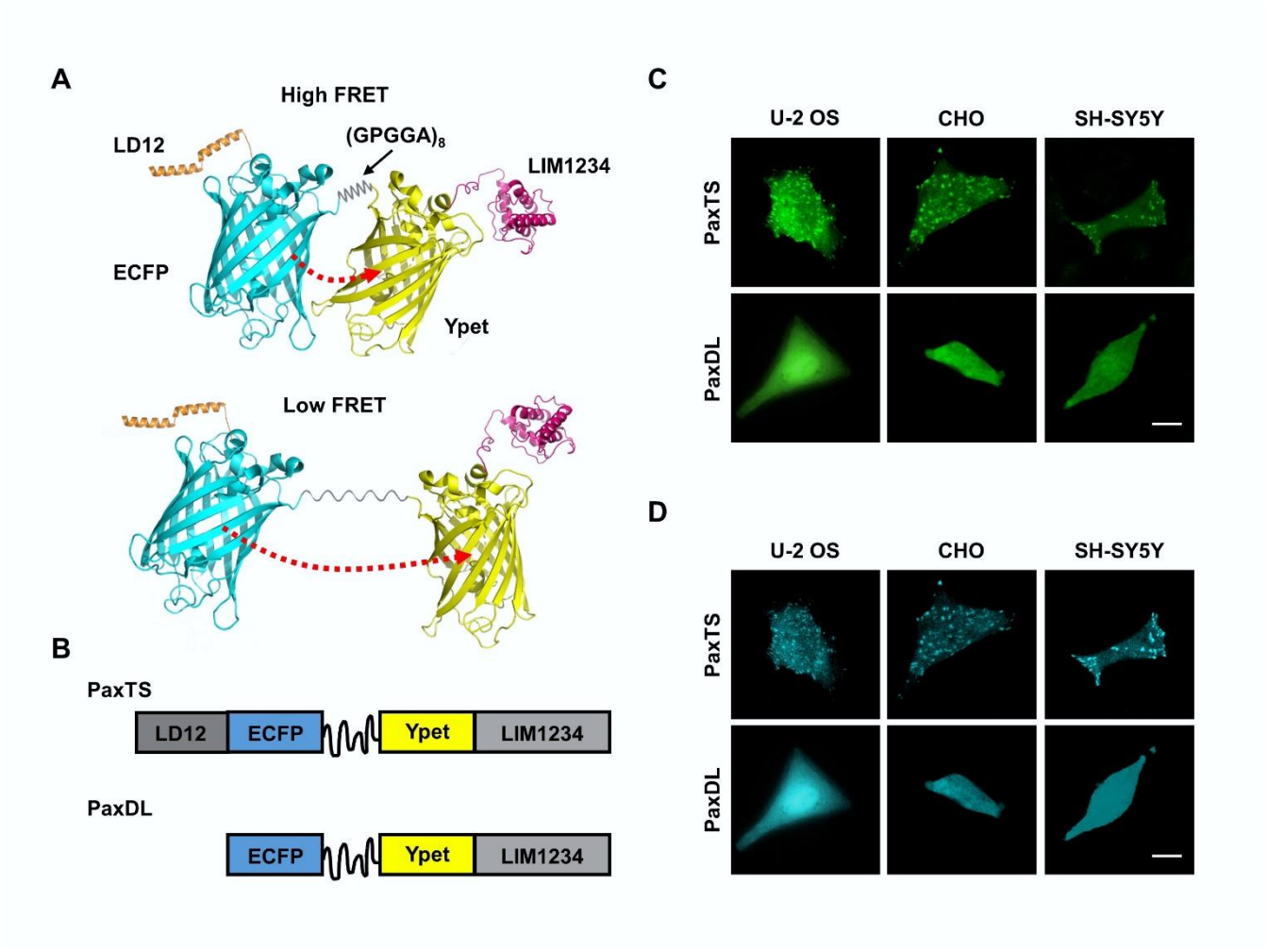

Figure 1. The PaxTS and its expression in multiple living cells. A) The mechanism of PaxTS. B) The structure of PaxTS and the derived biosensor PaxDL. C) The images of PaxTS expressing in U-2 OS cells, CHO cells and SH-SY5Y cells (Ypet channel). Scale bar: 20 μm. D) The images of PaxTS expressing in U-2 OS cells, CHO cells and SH-SY5Y cells (ECFP channel). Scale bar: 20 μm.

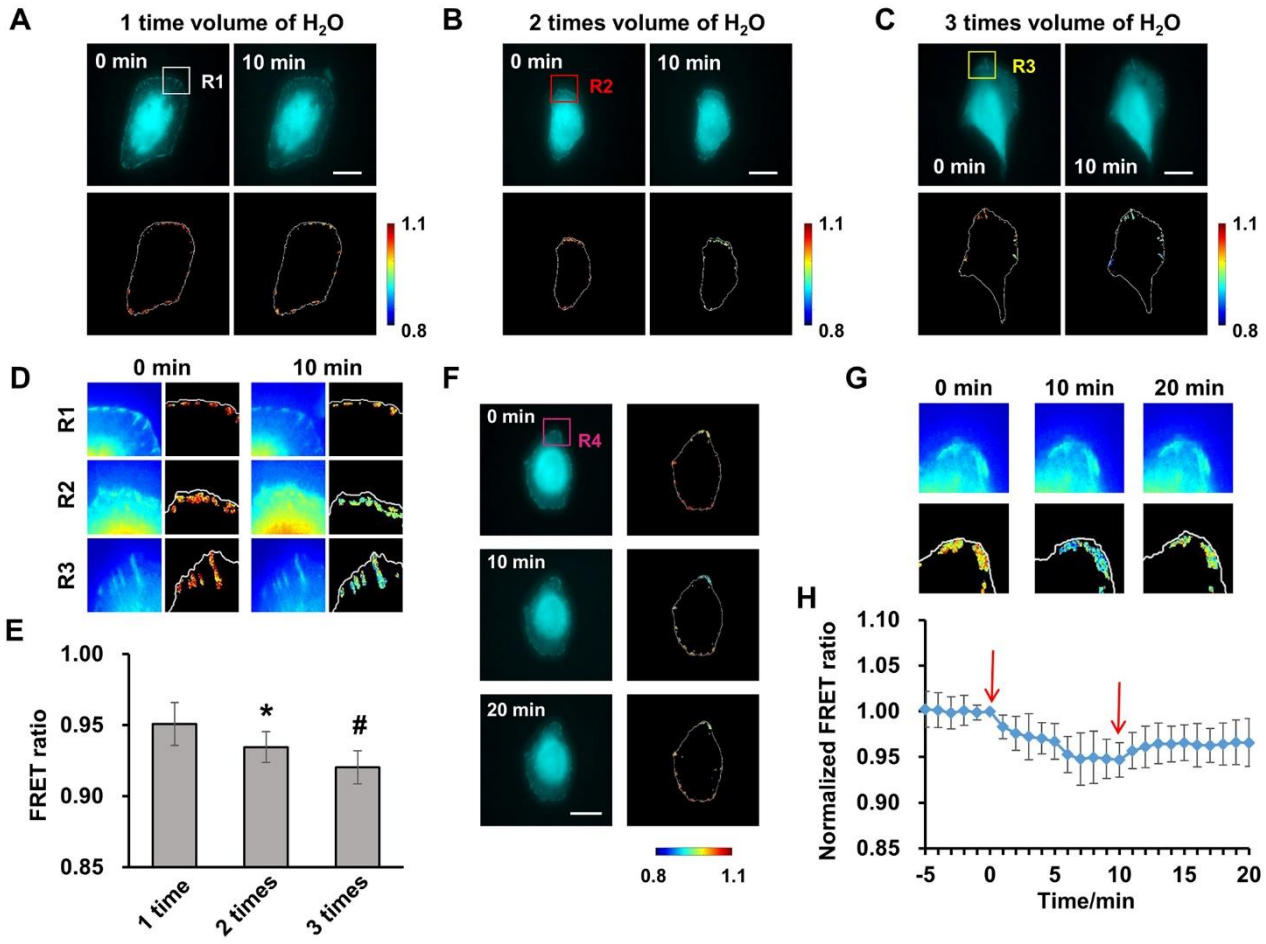

Figure 2. The verification experiments of PaxTS. A-C) FRET ratio decreased differently after hypotonic treatment with different volumes of H_2O. The volume of H_2O was 1/2/3-times volume respectively from Fig A to Fig C. The top line showed the live-cell images of PaxTS (ECFP channel), and the bottom line exhibited the segmentation results of FAs, corresponding to the top line. Scale bar: 20 μm. D) The partial enlargement of Region 1 (R1), Region 2 (R2) and Region 3 (R3) from A-C. E) The FRET ratio at 10 min after three kinds of hypotonic treatment (n=5, 6, 5, respectively). * represented there was an obvious difference between 1-time group and 2-times group. # represented there was an obvious difference between 2-times group and 3-times group. F) FRET decreased after hypotonic treatment but increased with hypertonic treatment. The left column showed the live-cell images of PaxTS after hypotonic treatment and hypertonic treatment (ECFP channel). 1-time volume of H_2O was applied at 0 min and sucrose solution of 0.025 g/ml was applied at 10 min. The right column exhibited the segmentation results FAs, corresponding to the left column. Scale bar: 20 μm. G) The partial enlargement of Region 4 (R4) from F. H) The time series of FRET ratio after hypotonic and hypertonic treatment (n=8) with normalized. Red arrows represented the application time of hypotonic and hypertonic treatment.

The structure of paxillin implied that the maintaining of its internal tension under static state probably depended on the membrane and cytoskeleton. Without shear stress application, the FRET efficiency indicated by PaxTS was ~62.4%. Destroying microfilaments with Cytochalasin D (CytoD) pre-incubation at 2 μmol/l for 1 h and depolymerizing microtubules by 1 μmol/l of nocodazole (NOCO) for 1 h increased the FRET ratio of PaxTS significantly ($p<0.05$), promoted the FRET efficiency to ~66.9% and ~65.8% respectively (Fig S2A). However, inhibiting the microfilaments contractility by the inhibitor of myosin light chain kinase (MLCK), ML-7, at 5 μmol/l for 1 h leaded the FRET ratio to be higher than control group but lower than treatment of CytoD or NOCO ($p<0.05$, Fig 3A, 3B), as well as increase the FRET efficiency to ~63.9% (Fig S2A). These results exhibited that paxillin endured tension in static cells and the tension was maintained by both microfilaments and microtubules.

Paxillin has a close relationship with other FA-associated proteins and interacts with cytoskeleton, which probably is the key point in the pathway of mechanical signals transduced into chemistry signals. To evaluate the force transferred across paxillin, cells transfected with PaxTS were exposed to 20 dyn/cm^2 of shear stress for 10 min. FA sites at the periphery were segmented as described in Method. The FRET ratio on those sites increased sharply by ~11% within 1 min and finally increased by ~14% (Fig 3C, 3D). It indicated that the tension across paxillin was decreased due to shear stress application.

10.1002/anse.202100033

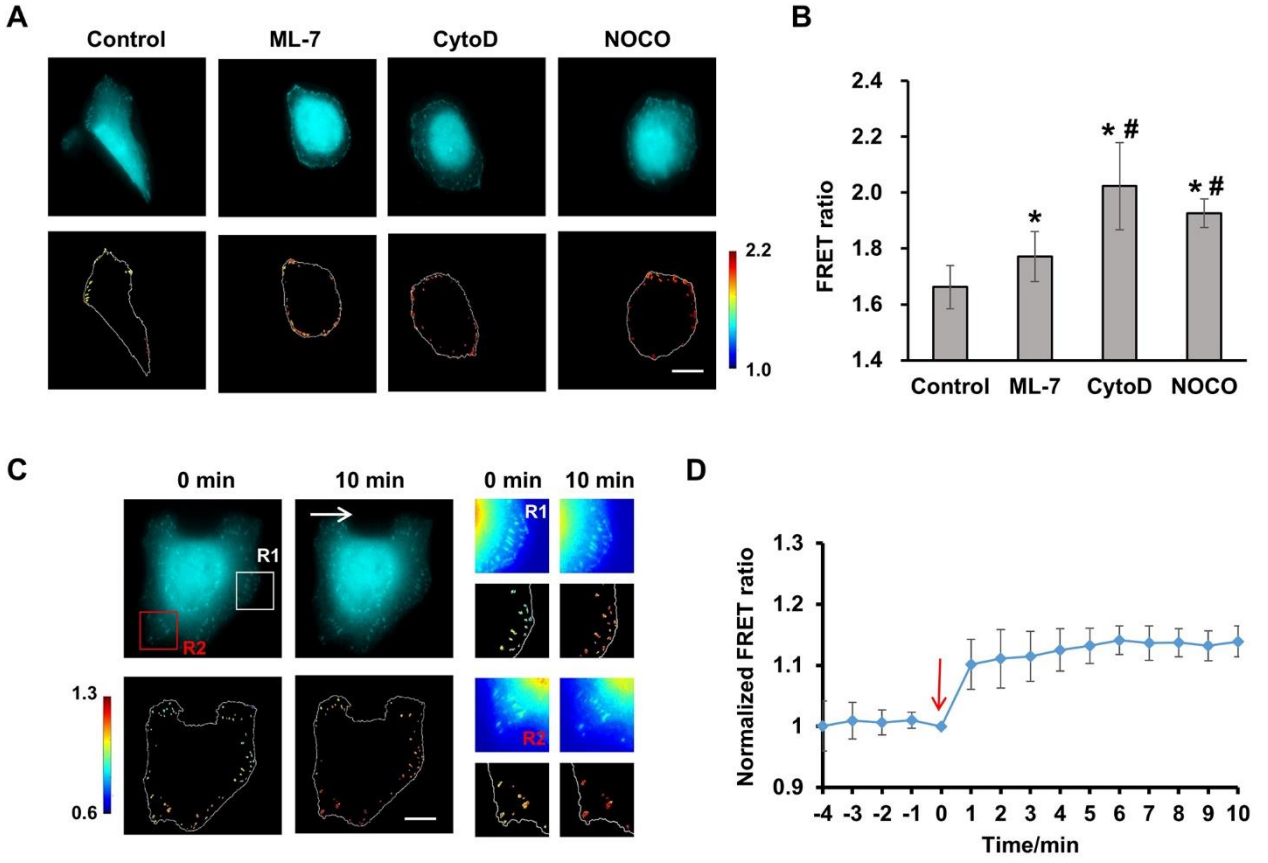

Figure 3. The expression of PaxTS in living cells under different conditions. A) Cells with PaxTS treated with different drugs. The top line showed the live-cell images of PaxTS in static state with treatment of 5 μmol/l of ML-7, 2 μmol/l of Cytochalasin D (Cyto D) and 1 μmol/l of nocodazole (NOCO) respectively. The bottom line exhibited the segmentation results of FAs, corresponding to the top line. Scale bar: 20 μm. B) The histogram of FRET ratio in control group (n=7), ML-7 group (n=8), CytoD group (n=5), and NOCO group (n=7). * represented there was an obvious difference compared to control group. # represented there was an obvious difference compared to ML-7 group. C) FRET ratio increased upon shear stress. The top line showed the live-cell images of PaxTS upon shear stress including the partial enlargement of Region 1 (R1) and Region 2 (R2). The bottom line exhibited the segmentation results of FAs, corresponding to the top line. The white arrows showed the direction of shear stress application. Red arrow represented shear stress applied at zero time. Scale bar: 20 μm. D) The time series of FRET ratio upon shear stress.

The plasma membrane is probably related to mechanotransduction closely, since paxillin-linked FAs sites on the membrane are the initial locations of force sensing[4b]. Considering membrane fluidity is the most notable physical feature of cell membrane, the pre-incubation of benzol alcohol (BA) at 45 mmol/l for 15 min was used to enhance membrane fluidity[13], and then the shear stress of 20 dyn/cm^2 was applied. Compared to control group, the result revealed that when membrane fluidity was enhanced, the increase of the FRET ratio induced by shear stress was significantly dampened after 10 minutes of flow application ($p<0.05$, Fig 4A,4B,4D-4F Supplementary Movie 5, Supplementary Movie 6). However, treatment of cholesterol (CHO) at 0.1 mmol/l for 3 h to reduce membrane fluidity has no obvious effect on FRET ratio (Fig 4C-4F, Supplementary Movie 7). Thus, higher membrane fluidity restrained the shear stress-induced tension decline across paxillin, while inhibiting fluidity has no obvious effect.

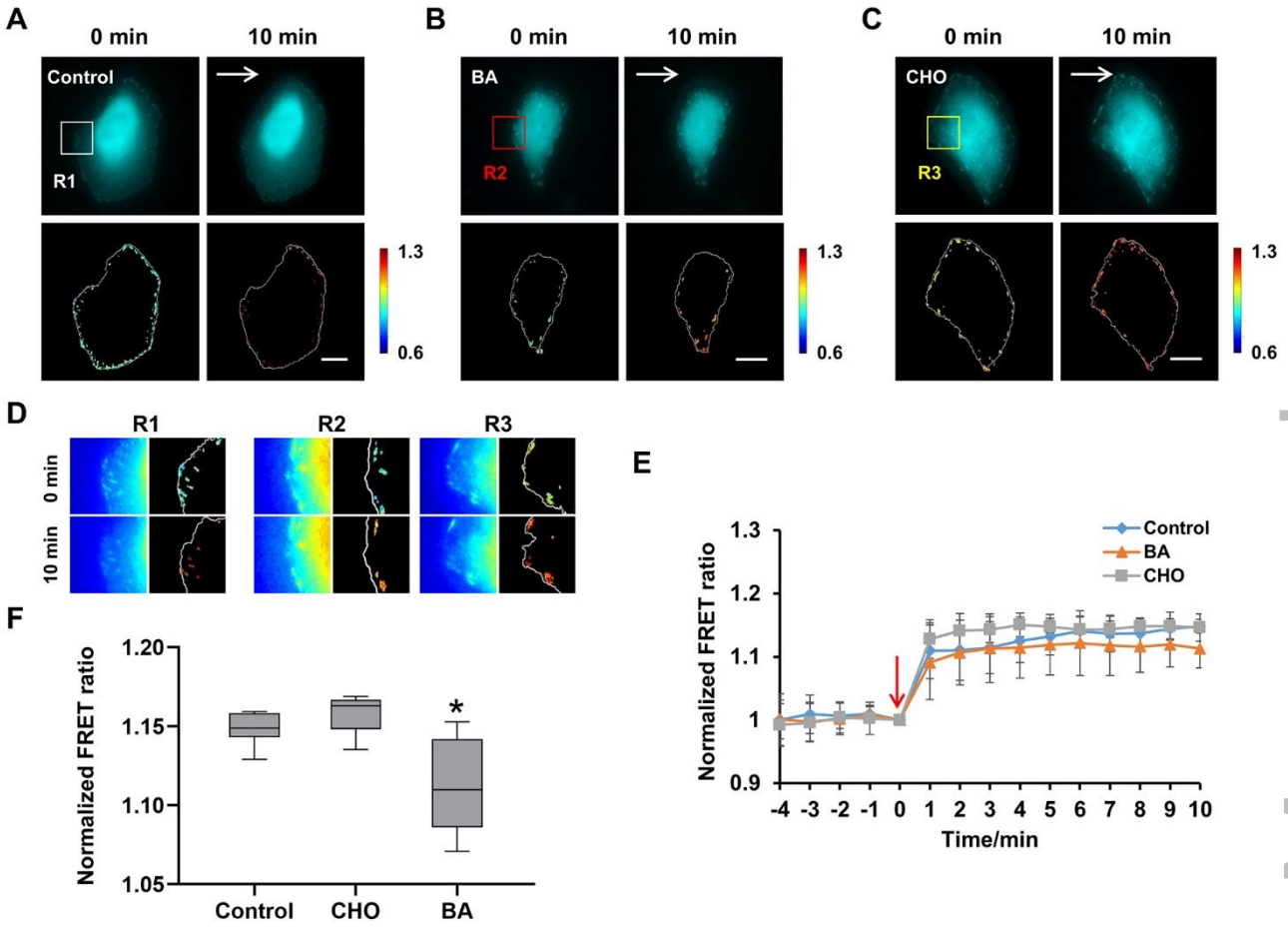

Figure 4. The tension across paxillin upon shear stress was affected by membrane fluidity. A) Live-cell images from ECFP channel of PaxTS under 20 dyn/cm^2 of shear stress without drug application and the segmentation results. Scale bar: 20 μm. B-C) Live-cell images from ECFP channel of PaxTS under 20 dyn/cm^2 of shear stress with 45 mmol/L benzol alcohol (BA) or 0.1 mmol/L of Cholesterol (CHO), and the segmentation results of FAs. The arrows showed the direction of shear stress application. Scale bar: 20μm. D) The partial enlargement of Region 1 (R1), Region 2 (R2) and Region 3 (R3) from A-C. E) The time series of FRET ratio of control group (n=6), BA group (n=5) and CHO group (n=6), after normalized. Red arrow represented shear stress applied at zero time. F) The box plot of FRET ratio in control group and BA/CHO group. * represented there was an obvious difference compared to control group.

In addition to cell membrane, paxillin is also associated with cytoskeleton, which is involved in mechanical signaling[14]. Thus, the cytoskeleton may also participate in force transfer involving paxillin. When the contractility of microfilaments was eliminated without destroying intact structure by the pre-treatment of the inhibitor of myosin light chain kinase (MLCK), ML-7, at 5 μmol/l for 1 h before applying shear stress (Fig 5A, 5B)[13], an increase of FRET ratio was observed within 1 min after the onset of shear stress, and the FRET ratio remained steadily at a higher level during flow application compared to control group (Fig 5E-5G, Supplementary Movie 8). Conversely, although destroying the microfilament by Cytochalasin D (CytoD) pre-incubation at 2 μmol/l for 1 h caused FRET ratio to increase significantly, the increment was lower than the control group and the group of ML-7 treatment ($p<0.05$, Fig 5C,5E-5G, Supplementary Movie 9). Similarly, after the application of 1 μmol/l of nocodazole (NOCO) for 1 h, which depolymerized microtubules, the change of FRET ratio was significantly lower than the control group (Fig 5D–5G, Supplementary Movie 10). These results demonstrated that the integrality of both microfilaments and microtubules was essential for force transfer mediated by paxillin.

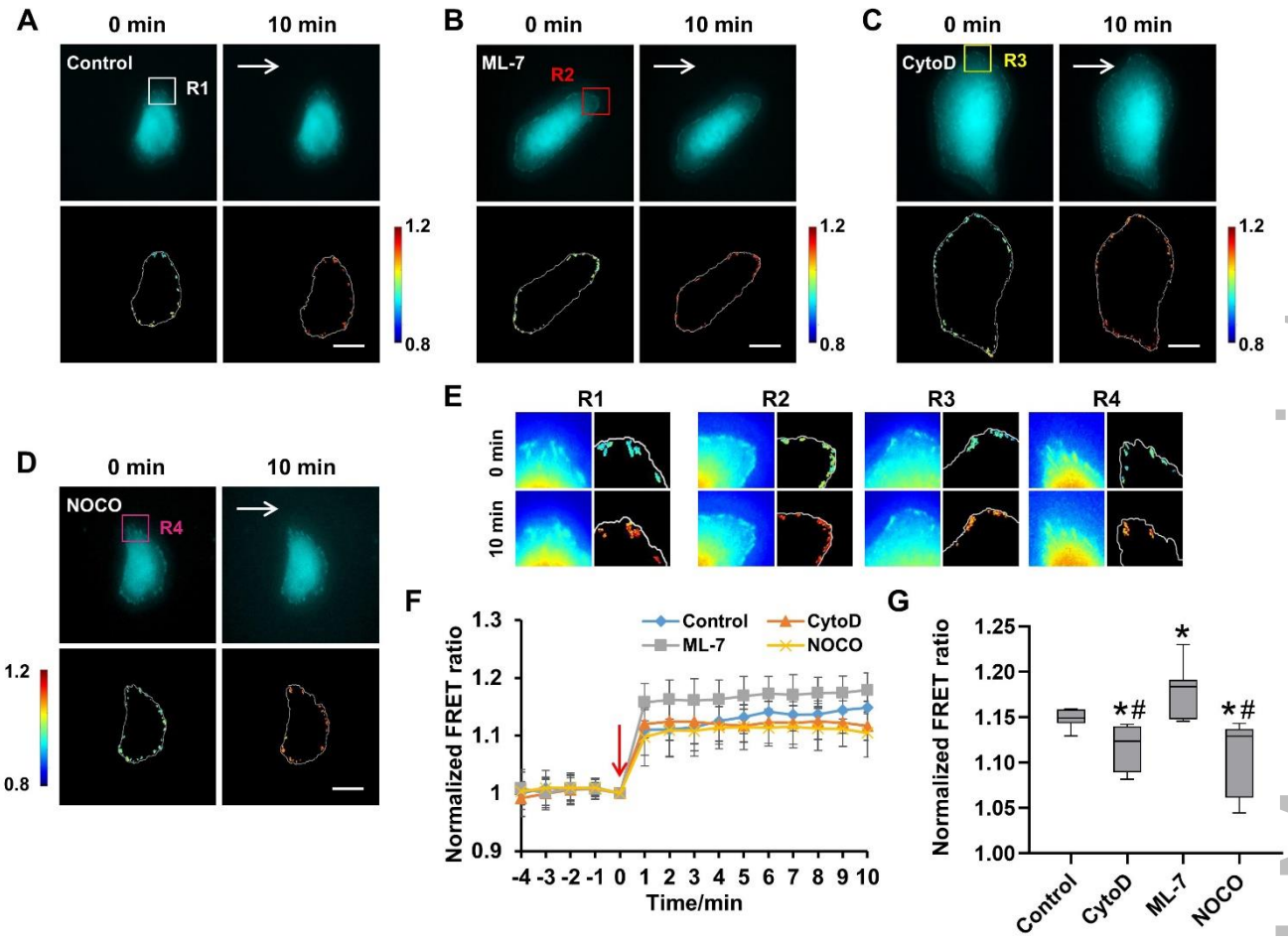

Figure 5. The tension across paxillin upon shear stress was affected by cytoskeleton. A-D) Live-cell images from ECFP channel of PaxTS under 20 dyn/cm^2 of shear stress after treatment with different drugs and the segmentation results of FAs. Fig A exhibited the control group in which cells were applied with shear stress without any drug treatment. From Fig B to Fig D, the drug treatments were 5 μmol/l of ML-7, 2 μmol/l of Cytochalasin D (CytoD) and 1 μmol/l of nocodazole (NOCO) respectively. The arrow showed the direction of shear stress application. Scale bar: 20 μm. E) The partial enlargement of Region 1 (R1), Region 2 (R2), Region 3 (R3) and Region 4 (R4) from A-D. F) The time series of FRET ratio of control group (n=6), CytoD group (n=6), ML-7 group (n=7) and NOCO group (n=5), after normalized. G) The box plot of FRET ratio in control group and CytoD/ML-7/NOCO group. * represented there was an obvious difference compared to control group. # represented there was an obvious difference compared to ML-7 group.

Based on previous studies, there should exist a force transmission pathway in cells to activate cell polarity[3c, 13]. As mentioned above, paxillin contacts several proteins related to force transmission and subsequent cell polarity, which provides a possibility that paxillin also participates in the process of force activating cell polarity directly. However, previous works focused more on the dynamics of paxillin and its interaction with other FA proteins, while the mechanical tension across paxillin and the potential force transmission pathway are still unclear probably due to lack of effective tools. The paxillin-based FRET biosensor PaxTS was designed based on the tension sensor module reported previously[11a], inserting a tension measuring module which consisted of a pair of fluorescence proteins and a nano-spring between the two domains, to visualize and measure the tension across paxillin in real time. Compared to the previous tension sensor for vinculin[11a], the FRET pairs in PaxTS was changed to ECFP/YPet and the original DNA sequence of nano-spring $(GPGGA)_8$ was improved into a series of nonredundant sequence following the degeneracy of codon (shown in Methods) to overcome the difficulties in constructing objective plasmids. All LIM domains from LIM1 to LIM4, integrally called LIM1234, were reserved in PaxTS. However, among the LD domains, LD1 and LD4 are combined with actin by actopaxin to link paxillin to cytoskeleton, while LD3 and LD5 are not related to the connection[8a]. In addition, LD4 was also removed owing to the fact that it was affected by the interaction between LIM and other proteins[15]. Only LD1 and LD2 (short as LD12) were adopted in the biosensor structure to ensure that all efficiency of energy transfer was attributed to the length changes of nano-spring in PaxTS, not the intermolecular conformation changes. Although it is possible that PaxTS cannot perform exactly the same function as endogenous paxillin protein due to its incomplete paxillin domains, the existing structure of PaxTS ensured its target to observe whether force can be transferred to the location of paxillin. The expression of PaxTS in living cells exhibited clear plaques, indicating that PaxTS replaced endogenous paxillin automatically to assemble to FAs where the biosensor should be located to as the design. It is notable that the endogenous paxillin was reserved, thus there would be a competition which could decrease the ability of PaxDL to locate to FAs and further the competitiveness with

endogenous paxillin declined. The failing in competition would lead to the fact that PaxDL showed no focal adhesions.

The module of tension measuring used in PaxTS has already been proved accurate and effective in previous study[12], thus the emphasis of evaluating PaxTS was put on whether the module could work normally. Based on the structure, the nano-spring was stretched upon force application and the FRET ratio decreased when the tension across paxillin was enhanced[11b]. The water swelling of cells caused by hypotonic treatments stretched the plasma membrane and cytoskeleton and further increased the tension across paxillin. Correspondingly, PaxTS also showed a gradually lower FRET ratio after different levels of hypotonic treatments, which implied a correspondence between the tension across paxillin and FRET ratio. After hypotonic treatment, the hypertonic treatment increased the FRET ratio after the decline caused by hypotonic treatment, due to the shrinking of cells which resulted in the relaxation of cell membrane and cytoskeleton. However, the hypertonic treatment failed to increase the FRET ratio to the ground state. It was probably owing to that the changes of intracellular ionic strength and cytoskeletal transitions triggered by hypotonicity were unable to recover to the original state with hypertonicity in the observation time. In addition, hypotonicity and hypertonicity may affect different components of cytoskeleton in different methods[16], which may also disturb the recovery of FRET ratio to ground state. With an in-depth analysis of the relationship between the FRET-proportional value and the actual force magnitude by theoretical calculation[11a, 17], the tension across paxillin measured by PaxTS was ~2 pN in cells (Fig S2), which is in the same order of magnitude as vinculin, a traditional mechanosensor[11a]. These results demonstrated that PaxTS expressed steadily in various kinds of cell, located to FA sites correctly and responded to force linearly and reversibly. In summary, PaxTS is an effective visual tool for observing tension across paxillin and exploring the force transmission between FAs and cytoskeleton.

The tension across paxillin decreased upon shear stress proving that paxillin participated in the force transmission between plasma membrane and FAs. This result is somewhat surprising considering that the tension across paxillin did not increase with shear stress application. The interesting phenomenon could be due to the cytoskeleton dynamics upon shear stress. In cytoskeleton, there is a contractile network of both branched and unbranched actin filaments and myosin underlying and being attached to the membrane, named cellular cortex[18]. Due to the close association of the actin network and the membrane, these two components should be considered as a composite material together, which means that the cytoskeleton could be affected by membrane for purely mechanical reasons[19]. When cells are pulled along the direction of flow, the force exerts on membrane and cellular cortex together, and further stretches the actin filaments which are linked to paxillin. In response to stretch, the cytoskeleton becomes softer and more fluid-like accompanying with a decrease of its prestress, while the actin filaments are the main contributors in cytoskeleton softening which is induced by stretch[20]. With the release of press stress in actin filaments, the tension across paxillin also decreases.

Plasma membrane is the barrier of the whole cell to separate cells from the external environment, and also known as the first structure to sense extracellular signals. Considering the structure of paxillin, the continuous deformation of the lipid membrane at the upper surface, where the shear stress directly acts on, stretches the cytoskeleton unavoidably, which promotes the force to affect the tension across paxillin. Interestingly, the tension across paxillin decreased less at a higher level of membrane fluidity, as revealed by the results that PaxTS was stretched more slightly when membrane fluidity was enhanced. In this process, the membrane seems to act as a 'buffer' rather than a structure merely sensing force or stretching the cytoskeleton mechanically. The function of buffer here is not offsetting or eliminating but dispersing caused by the redistribution of membrane tension upon shear stress, supported by the research that high fluidity helps to homogenize membrane tension during flow application[12]. The redistribution makes membrane tension more uniform and further causes multidirectional stretch to cytoskeleton, and hence the stretching on paxillin caused by force is attenuated even though the cytoskeleton might be stretched more acutely when fluidity is enhanced. In contrast, inhibiting membrane fluidity had no significant effect on the tension across paxillin, which is consistent with the previous report that the stiff membrane is adverse to membrane tension redistribution[12]. Besides, other mechanical changes of membrane upon shear stress application, such as the internal movements of phospholipid molecules, possibly also affect the force transmission in a direct manner. The movements of phospholipid molecules intensify with higher fluidity, which contributes to the redistribution of membrane tension.

Besides plasma membrane, paxillin is also associated with actins to establish a link from plasma membrane to cytoskeleton with the cooperation of actin-binding proteins. Since the cytoskeletal network is considered to sense and transmit force intracellularly [21], it is acceptable that cytoskeleton participates in the force transmission pathway involving paxillin. In static state, the stretch of cytoskeleton to paxillin disappeared with the destroy of cytoskeleton, which led the tension across paxillin to decrease. The measurements showed that the paxillin in FAs also endured tension which was maintained by cytoskeleton even under static state. Interestingly, inhibiting the contractility of microfilaments led to a different result compared to depolymerizing the structure, which exhibited that the cytoskeleton structure and the prestress existed in actin networks were both important to maintain the tension across paxillin in statics state, but functioned differently.

Correspondingly, our results displayed that the tension across paxillin changed after being exposed to shear stress for 10 min when microfilaments disassembled, but significantly less than control group. It indicated that microfilaments participate in the pathway of force transmission across paxillin upon shear stress in addition to maintaining the tension under static state. However, inhibiting the contractility of microfilaments performed a larger change of the tension across paxillin than the control group, while depolymerizing microfilaments led to a lesser extent. It is probably due to the inhibition of the contractility eliminates the elastic responding of microfilament system to force, and the force thus directly acts on paxillin without any cushion. As another component of cytoskeleton, microtubules were found that its destroying also decreased the tension change across paxillin caused by shear stress, which was probably due to the association of paxillin with cytoskeleton. Paxillin is linked to microfilaments by actopaxin and other actin-binding proteins directly, while microtubules are connected with paxillin through microfilament in an indirect manner[8b, 22].

Nevertheless, there existed an interesting phenomenon that the tension across paxillin still decreased slowly after the transient enhancement following the onset of flow application. However, when the microfilaments were destroyed or the contractility was inhibited, the tension across paxillin stabilized immediately and remained during the whole application. It implied that microfilaments were able to participate in the regulation of tension across paxillin indeed upon shear stress, and functioned as a 'cushion' rather than a simple transmitter. It is well known that cells show a conserved trend to counteract external tensile forces as well as to reduce the peak shear stresses when being exposed to flow and by the rearrangement of actin filaments along the direction of force[23]. Similarly, the 'cushion' would be related to the dynamics of stress fibers upon shear stress. The microfilaments network shows no clear directionality under static state. When force is sensed by plasma membrane and transmitted along actin, it is dispersed to different intracellular sites actually, not only to FAs and paxillin, to form a cushion. Meanwhile, in 2D-cultured cell, the filamentous actin depolymerizes as the earliest response of cytoskeleton to shear stress[24]. The rapid decrease in actin filaments amount results in a decline of the ability of microfilaments to disperse the cytoskeleton strain caused by membrane deformation and a sustained tension change of paxillin

in a short period of time after shear stress application, which is generalized as a cushion function. Agree with the observation in 2D cultured cells, strain softening of cytoskeleton showing decreased elasticity as well as increased hysteresivity in 3D culture, which lead the cytoskeleton to react slowly to stretch upon shear stress. It is also consistent with the definition of cushion function in the tension changes across paxillin induced by shear stress.

Conclusion

In this paper, a FRET biosensor named PaxTS was constructed to visualize the tension across paxillin, providing a useful tool for exploring how the tension across paxillin is regulated upon shear stress. The results proved that paxillin endured tension in cells and there existed a novel manner to regulate the tension across paxillin upon mechanical force. The regulation was proposed to show a relationship with the plasma membrane deformation upon shear stress and the chain reaction of cytoskeleton strain. The plasma membrane and actin network acted as cushions together to mitigate the effect of shear stress on paxillin. These results suggested that the force applied on the upper surface of the cell did affect the tension across the paxillin protein located on the sites adhered to substrate with the assistance of cytoskeleton. It also supported that there existed a potential pathway in cells to transfer force to local subcellular locations directly and probably further activate the cell polarity establishment, while aberrant cell polarity and migrating ability are recognized as main precipitating factors in various diseases[25], such as cancer invasion and metastasis. Exploring the intracellular pathway of force transmission involved with paxillin provides a new path to understand the diseases in depth. However, the distinct pathway of shear stress regulating the tension across paxillin is still incomplete. How the force is transmitted from the plasma membrane to cytoskeleton or from cytoskeleton to paxillin, and whether the actin binding proteins related to paxillin such as actopaxin participated in the regulatory pathway are interesting questions for future investigations.

Experimental Section

Design and establishment of PaxTS biosensor

The biosensor named PaxTS consisted of four sections, LD12 domain, LIM1234 domain, molecule spring and ECFP/Ypet fluorescent protein pairs for FRET. In the biosensor construction, LD12 domain was a section of LD domain which connected paxillin with cytoskeleton, while LIM1234 domain located paxillin to FA sites. The two sections were linked by an improved nano-spring (DNA sequence shown below), which could convert stress across paxillin to the distance between the fluorescent proteins pair.

5'GGTCCAGGAGGCGCAGGACCTGGCGGGGCTGGACCGG
GTGGCGCGGGACCCGGCGGAGCCGGCCCAGGTGGGGCG
GGCCCTGGTGGTGCTGGTCCGGGAGGGGCAGGGCCCGGA
GGTGCC-3'

To demonstrate the biosensor was located correctly to FA sites, a contrast biosensor without LD12 domain was designed and named as PaxDL (Fig 1B). The whole water swelling was uploaded as supplementary. The two biosensors mentioned above were constructed into pcDNA3.1(+) plasmids for expression in U-2 OS, CHO and SH-SY5Y cells, respectively.

Cell culture and transient transfection

Before transfection, U-2 OS cells were cultured with the Roswell Park Memorial Institute (RPMI-1640, Bioind) containing 10% fetal bovine serum (FBS, Bioind) and 100 unit/ml penicillin (Hyclone). CHO cells were cultured with the Ham's F 12 nutrient medium (F12, HYCLON) containing 10% FBS, 100 unit/ml penicillin and 100 mg/ml sodium pyruvate (GIBCO). SH-SY5Y cells were cultured with Dulbecco's modified Eagle medium (DMEM, HYCLON) containing 10% FBS, 100 unit/ml penicillin and 100 mg/ml sodium pyruvate (GIBCO). Different DNA plasmids were transfected into cells by the transfection reagent, Lipofectamin 3000 (Thermo Fisher Scientific). After transfection for 24 h, cells were passed onto fibronectin-coated cover slips and cultured with 0.5% FBS for 12 h before laminar flow application.

Flow systems

A classis parallel-plate flow chamber was applied to provide laminar flows, and modified to fit for dynamic observations under a FRET microscope[10a]. The glass slides seeded with separated U-2 OS cells were covered by a silicone gasket and a cover glass, and exposed to shear stress which can be calculated as equation (1):

$$\tau = \frac{6\mu Q}{bh^2} \quad (1)$$

Here τ = fluid shear stress (Pa), μ = fluid viscosity of solution (cp), Q = flow rate (cm^3/s), b = width (mm), h = height (mm). In this work, μ = 0.82 cp (dulbecco's modified eagle medium (DMEM) containing 0.5% fetal bovine serum (FBS)), b = 13 mm, h = 0.508 mm. Lamina shear stress was set to 20 dyn/cm^2 by adjusting fluid flow in the chamber[26]. The flow experiments were done 37 °C with 5% CO_2 to maintain the pH at 7.4.

Microscope image acquisition

The microscope image acquisition set-up contained an inverted microscope (Olympus, IX73) and a color camera (Olympus, DP74). The two-channel fluorescent images were taken alternatively by switching the excitation light paths through dichroic mirror. A 420DF20 filter and a 455DRLP dichroic mirror were set as excitation for ECFP, and two emission filters, 480DF30 and 535DF25, for ECFP and Ypet) All fluorescence images were collected on an isolated single cell by Software (Cellsens Dimension) with an interval of 1 min for each shoot on a single cell.

Image analysis

The software package used to analyze the stress changing of paxillin based on Matlab (Mathworks; Natick, MA, RRID:SCR_001622) contained three different sections, pretreatment, FAs identity and ratio calculation. First, all fluorescence images from different channels of a same sample were read and marked. The background of each image was set as the mean value of the fluorescence intensity from four corners and subtracted to avoid disturbance of background. The cell body was detected according to the ECFP image by a segmentation algorithm combined with Otsu's method with an adaptive detection threshold. The global threshold renewed automatically to adapt the intensity changing in ECFP images. After that, the initial segmentation result was dealt by a K-means clustering combined with a low-pass filter, to further improve the accuracy of detection at vague edges. The second section to identify FA sites was based on K-means clustering mainly. A Gaussian filter was applied to the image without background which was named ImageA, and then the original image without background was subtracted from ImageA to achieve a FA-enhanced image. After that, the enhanced image was handled with K-means clustering again to segment FA sites. Based on the current segmentation result, the distances of each FA to its nearest edge (DAE) and the distance to the cell centroid (DAC) were calculated, and the ratio of these two parameters (DAE/DAC) was set as a standard to describe positions of FAs. Cells were divided into layers according

to the standard, allowing that only the outermost FAs sites (distance ratio>0.85) were remained for further analysis. With the final segmentation results of ECFP and Ypet channel, the tension across paxillin was calculated as an averaged FRET ratio of Ypet/ECFP at FA sites (Fig S3).

Statistical analysis

All FRET ratio (YPet / ECFP) data were normalized by their basal level at zero point in the same cell. The zero point was considered as the last time point before shear stress application. Statistical analysis used in the study was Two-tailed t-test function contained in the Excel software (Microsoft) to evaluate the statistical difference between groups. The data population numbers (n) here are the number of cell samples in each group. Difference was determined as significant when the p-value was smaller than 0.05. All means involved in the manuscript were modified by standard deviation.

Data and Code Availability Statements

The MATLAB source code generated during this study are available as Supplementary Software 1.

Acknowledgements

This work was supported by National Natural Science Foundation of China (Grant No. 32071252), and the Fundamental Research Funds for the Central Universities [DUT20LAB119] in Dalian University of Technology in China. F. Cong and S. Shao are grateful to Prof. Tapani Ristaniemi for his great support to the study.

Keywords: Biosensors • focal adhesions • FRET • paxillin • shear stress

[1] M. Lintz, A. Munoz, C. A. Reinhart-King, *J. Biomech. Eng.* **2017**, *139*, 0210051-0210059.

[2] a) H. Peng, R. Qiao, B. Dong, *Front Cell Dev. Biol.* **2020**, *8*, 597446; b) P. Pandya, J. L. Orgaz, V. Sanz-Moreno, *Curr. Opin. Cell Biol.* **2017**, *48*, 87-96.

[3] a) S. Na, O. Collin, F. Chowdhury, B. Tay, M. Ouyang, Y. Wang, N. Wang, *Proc. Natl. Acad. Sci. U. S. A.* **2008**, *105*, 6626-6631; b) Y. C. Poh, S. Na, F. Chowdhury, M. Ouyang, Y. Wang, N. Wang, *PLoS One* **2009**, *4*, 0007886; c) S. Shao, C. Xiang, K. Qin, A. Ur Rehman Aziz, X. Liao, B. Liu, *PLoS One* **2017**, *12*, e0189088.

[4] a) R. E. Mott, B. P. Helmke, *Am. J. Physiol. Cell Physiol.* **2007**, *293*, C1616-1626; b) B. Sit, D. Gutmann, T. Iskratsch, *J. Muscle Res. Cell Motil.* **2019**, *40*, 197-209; c) S. Hu, Y. H. Tee, A. Kabla, R. Zaidel-Bar, A. Bershadsky, P. Hersen, *Cytoskeleton (Hoboken)* **2015**, *72*, 235-245.

[5] M. H. Ginsberg, *BMB Rep.* **2014**, *47*, 655-659.

[6] M. Morimatsu, A. H. Mekhdjian, A. C. Chang, S. J. Tan, A. R. Dunn, *Nano Lett.* **2015**, *15*, 2220-2228.

[7] C. S. Chen, J. L. Alonso, E. Ostuni, G. M. Whitesides, D. E. Ingber, *Biochem. Biophys. Res. Commun.* **2003**, *307*, 355-361.

[8] a) S. N. Nikolopoulos, C. E. Turner, *J. Cell Biol.* **2000**, *151*, 1435-1448; b) A. M. Lopez-Colome, I. Lee-Rivera, R. Benavides-Hidalgo, E. Lopez, *J. Hematol. Oncol.* **2017**, *10*, 50; c) S. Ishibe, D. Joly, Z. X. Liu, L. G. Cantley, *Mol. Cell* **2004**, *16*, 257-267.

[9] a) P. Devreotes, A. R. Horwitz, *Cold Spring Harb Perspect. Biol.* **2015**, *7*, a005959; b) Y. L. Hu, S. Lu, K. W. Szeto, J. Sun, Y. Wang, J. C. Lasheras, S. Chien, *Sci. Rep.* **2014**, *4*, 6024.

[10] a) B. Liu, S. Lu, Y. L. Hu, X. Liao, M. Ouyang, Y. Wang, *Sci. Rep.* **2014**, *4*, 7008; b) D. W. Dumbauld, T. T. Lee, A. Singh, J. Scrimgeour, C. A. Gersbach, E. A. Zamir, J. Fu, C. S. Chen, J. E. Curtis, S. W. Craig, *Proc. Natl. Acad. Sci. U. S. A.* **2013**, *110*, 9788-9793; c) T. Ueyama, *Cells* **2019**, *8*, 92; d) D. W. Zhou, T. T. Lee, S. Weng, J. Fu, A. J. García, *Mol. Biol. Cell* **2017**, *28*, 1901-1911.

[11] a) C. Grashoff, B. D. Hoffman, M. D. Brenner, R. Zhou, M. Parsons, M. T. Yang, M. A. McLean, S. G. Sligar, C. S. Chen, T. Ha, M. A. Schwartz, *Nature* **2010**, *466*, 263-266; b) A. Kumar, M. Ouyang, K. Van den Dries, E. J. McGhee, K. Tanaka, M. D. Anderson, A. Groisman, B. T. Goult, K. I. Anderson, M. A. Schwartz, *J. Cell Biol.* **2016**, *213*, 371-383.

[12] W. Li, X. Yu, F. Xie, B. Zhang, S. Shao, C. Geng, A. U. R. Aziz, X. Liao, B. Liu, *iScience* **2018**, *7*, 180-190.

[13] S. Shao, X. Liao, F. Xie, S. Deng, X. Liu, T. Ristaniemi, B. Liu, *Commun. Biol.* **2018**, *1*, 224.

[14] Y. Shafrir, G. Forgacs, *Am. J. Physiol. Cell Physiol.* **2002**, *282*, C479-486.

[15] N. O. Deakin, C. E. Turner, *J. Cell Sci.* **2008**, *121*, 2435.

[16] a) M. B. Burg, J. D. Ferraris, N. I. Dmitrieva, *Physiol. Rev.* **2007**, *87*, 1441-1474; b) P. Nunes, T. Ernandez, I. Roth, X. Qiao, D. Strebel, R. Bouley, A. Charollais, P. Ramadori, M. Foti, P. Meda, E. Feraille, D. Brown, U. Hasler, *Autophagy* **2013**, *9*, 550-567; c) L. Pan, P. Zhang, F. Hu, R. Yan, M. He, W. Li, J. Xu, K. Xu, *Adv. Sci. (Weinh)* **2019**, *6*, 1900865.

[17] M. Morimatsu, A. H. Mekhdjian, A. S. Adhikari, A. R. Dunn, *Nano Lett.* **2013**, *13*, 3985-3989.

[18] M. Bovellan, Y. Romeo, M. Biro, A. Boden, P. Chugh, A. Yonis, M. Vaghela, M. Fritzsche, D. Moulding, R. Thorogate, A. Jegou, A. J. Thrasher, G. Romet-Lemonne, P. P. Roux, E. K. Paluch, G. Charras, *Curr. Biol.* **2014**, *24*, 1628-1635.

[19] P. Sens, J. Plastino, *J. Phys. Condens. Matter* **2015**, *27*, 273103.

[20] M. Walker, P. Rizzuto, M. Godin, A. E. Pelling, *Sci. Rep.* **2020**, *10*, 7696.

[21] a) D. E. Jaalouk, J. Lammerding, *Nat. Rev. Mol. Cell Biol.* **2009**, *10*, 63-73; b) Davies, F. Peter, *Nat. Clin. Pract. Cardiovasc. Med.* **2009**, *6*, 16.

[22] R. Mohan, A. John, *IUBMB Life* **2015**, *67*, 395-403.

[23] K. Ohashi, S. Fujiwara, K. Mizuno, *J. Biochem.* **2017**, *161*, 245-254.

[24] E. A. Osborn, A. Rabodzey, C. F. Dewey, Jr., J. H. Hartwig, *Am. J. Physiol. Cell Physiol.* **2006**, *290*, C444-452.

[25] N. Jiang, J. Fan, F. Xu, X. Peng, H. Mu, J. Wang, X. Xiong, *Angew. Chem., Int. Ed. Engl.* **2015**, *54*, 2510-2514.

[26] M. Chachisvilis, Y. L. Zhang, J. A. Frangos, *Proc. Natl. Acad. Sci. U. S. A.* **2006**, *103*, 15463-15468.

10.1002/anse.202100033

Entry for the Table of Contents

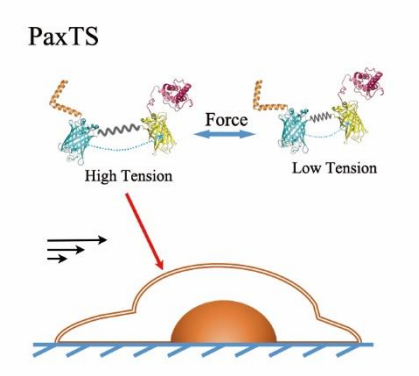

Visualizing the tension across paxillin in real time. This work provides a DNA-encoded biosensor based on Fluorescence Resonance Energy Transfer(FRET) technique to detect the tension across paxillin in living cells. The results indicate that there exists a force transmission pathway described as 'membrane-cytoskeleton-FAs' and involved with paxillin upon mechanical force.

IV

MAPPING THE DISTRIBUTION OF TENSION ACROSS PAXILLIN UPON SHEAR STRESS WITH FRET-BASED BIOSENSOR

by

Shuai Shao, Sha Deng, Fengyu Cong, Timo Tiihonen & Bo Liu 2022

Submitted to EMBO Journal.

Request a copy from author.